SCANNING PROBE OPTICAL TWEEZERS

A NEW TOOL TO STUDY DNA-PROTEIN INTERACTIONS

Jurgen Hendrikus Gerhardus Huisstede

Promotiecommissie

Prof. dr. B. Poelsema	Universiteit Twente (voorzitter)
Prof. dr. V. Subramaniam	Universiteit Twente (promotor)
Dr. M.L. Bennink	Universiteit Twente
Prof. dr. L.B. Oddershede	University of Copenhagen
Prof. dr. T. Schmidt	Universiteit Leiden
Prof. dr. W.J. Briels	Universiteit Twente
Prof. dr. G.J. Vancso	Universiteit Twente
Prof. dr. H.J.W. Zandvliet	Universiteit Twente

Acknowledgement
This research was financially supported by:
Mesa+ Institute for Nanotechnology, University of Twente

J.H.G. Huisstede,
Scanning Probe Optical Tweezers: A new tool to study DNA-protein interactions
Proefschrift Universiteit Twente, Enschede.
ISBN 90-365-2355-9

Printed by FEBODRUK BV, Enschede

SCANNING PROBE OPTICAL TWEEZERS

A NEW TOOL TO STUDY DNA-PROTEIN INTERACTIONS

PROEFSCHRIFT

ter verkrijging van
de graad van doctor aan de Universiteit Twente,
op gezag van de rector magnificus,
prof. dr. W.H.M. Zijm,
volgens besluit van het College voor Promoties
in het openbaar te verdedigen
op donderdag 20 april 2006 om 16.45 uur

door

Jurgen Hendrikus Gerhardus Huisstede
geboren op 2 augustus 1978
te Goor

Dit proefschrift is goedgekeurd door:

Prof. dr. V. Subramaniam	de promotor
Dr. M.L. Bennink	de assistent promotor

voor Chantal en mijn ouders

Contents

Chapter 1

Introduction

DNA contains the genetic instructions specifying the biological development of all cellular forms of life. DNA is replicated, transcribed, and finally translated into proteins that are the task-performing biopolymers. In this chapter we present the motivation for the development of a new single molecule microscope to study DNA-protein interactions. This microscope is based on the combination of optical tweezers and scanning probe microscopy such that it provides simultaneously force and positional information about the DNA-protein complex.

1.1 Introduction

Years of evolution brought life to what it is today. Different species adapted themselves to its surroundings in order to survive. If not or too late, it ended while others that adapted continued. This concept was proposed by Charles Darwin in the 18th century and is known as "survival of the fittest" (Darwin, 1909). The bases of this concept can be found in the development of the biological machinery. To survive for instance a disease, the defense system should find a solution to destroy the virus or bacteria.

The biological machinery is a complex system where large numbers of molecules such as proteins and nucleic acids interact. To understand life or at least a small part of it, it is important to gain insight into the details of the complex dynamic biological processes. One approach to understand these processes is the bottom-up approach, that is to start with the most elementary building blocks, the individual molecules, and make the system more and more complex while ensuring that each step is understood. Within the last decades several techniques have been developed to visualize or manipulate these individual single molecules.

One of the techniques used to visualize single molecules is fluorescence microscopy where fluorescent probes are connected to the molecules of interest. Coupling different probes to specific molecules these molecules can be distinguished based on differences in the emission spectra. This technique allows to follow the dynamics of individual proteins for example in a living cell. Furthermore mechanical techniques

such as atomic force microscopy allow manipulation and force spectroscopy of individual molecules. One of the most significant advantages of the single molecule force spectroscopy approach is that it yields new information such as the forces that hold biomolecules together, the mechanical and the dynamic behavior of individual molecules and complexes thereof. In conventional techniques these properties are masked in the ensemble average.

One of the most widely studied single molecules is DNA and more specifically its interaction with proteins since the functions of many biological processes within a cell are regulated by these specific interactions. These interactions play an important role in fundamental processes such as transcription, replication, recombination and DNA repair. In this thesis we describe the development of a new single molecule microscope combining optical tweezers (OT), which is an excellent tool for single molecule force spectroscopy, with scanning probe microscopy (SPM) that is capable of obtaining high-resolution topography images of single molecules on a surface. Combining these techniques it was possible to scan along single freely suspended DNA molecules and 'sense' the proteins that are bound to it while interacting with the DNA molecule. Simultaneously forces on the DNA molecule can be measured coinciding with the interactions between the probe and proteins, or vice versa. We can investigate the influence of tension in the DNA molecule on the protein dynamics and its function. In the next sections we introduce the principles of optical tweezers and the atomic force microscope and highlight a few examples of DNA-protein studies carried out in recent years. Subsequently we focus on the advantages of combining these two techniques into a new single molecule microscope.

1.2 Optical tweezers

Light consists of individual photons that carry momentum. If an object causes light to change direction, for instance on reflection or refraction, the change in momentum of light will exert an equal but opposite change of momentum on the object. The force acting on the bead is related to the change of momentum per time. This effect is known as radiation pressure Ashkin (1970). Forces involved in the transfer of momentum from focused light to microscopic objects are in the order of piconewtons and can move micron sized particles as indicated in Fig. 1.1.

Arthur Ashkin showed in the early 1970s that optical forces could displace and levitate micron-sized particles (Ashkin, 1970). Using transparent latex micron-sized beads it was observed that these beads did not only move in the direction of the laser caused by the reflection of light resulting in the so-called scatter force, but that they also had a tendency to move in the direction of higher intensity caused by the refraction of the light through the bead resulting in a gradient force. To create a stable three-dimensional trap this gradient force had to overcome the scattering force. To do so he used 2 counter-propagating laser beams (Ashkin and Dziedzic, 1971) and later on he developed the single-beam gradient force optical trap (Ashkin *et al.*,

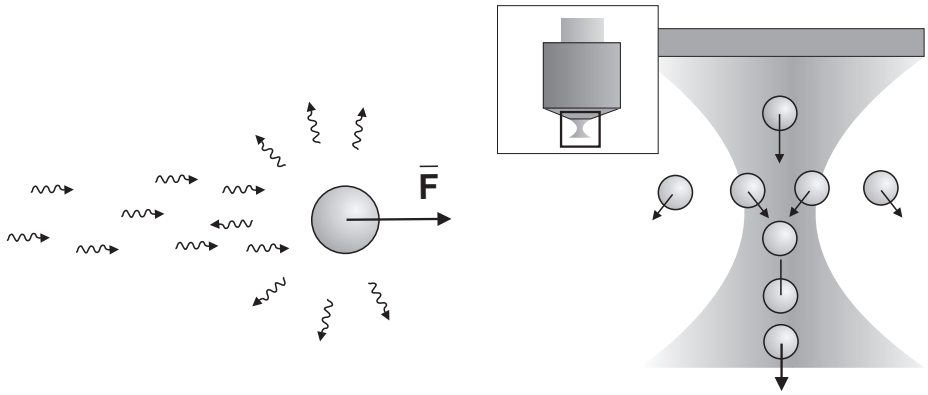

Figure 1.1. Fundamental basis of optical trapping. Light consists of photons that carry momentum. Upon reflecting off the surface of an object a part of the momentum of these photons is transferred to the object, resulting in a net force acting on this object in the direction of the light beam. Strongly focusing a light beam to a diffraction-limited spot, an intensity gradient is created where forces are exerted on transparent spherical particles and directed towards the focal point. Actually slightly behind the focal point there is a position where all the radiation forces cancel out, leading to stable trapping of these spherical beads. (Figure adapted from (Bennink, 2000))

1986) where a high-NA objective strongly focused the laser beam, creating a strong intensity gradient. Consequently the gradient force could overcome the scattering force resulting in a stable optical trap.

Although the optical trap was initially developed to cool and trap neutral atoms (Chu *et al.*, 1986) Ashkin and co-workers were able to manipulate live bacteria and viruses (Ashkin and Dziedzic, 1987; Ashkin *et al.*, 1987). At this point the optical tweezers entered the field of biophysics where the first applications were shown on molecular motors such as kinesin (Block *et al.*, 1990) using micro-spheres as handles. These spherical polystyrene beads (0.5-5 μm in diameter) provided a well-calibrated optical tweezers allowing single-molecule force measurements (Finer *et al.*, 1994; Svoboda and Block, 1994).

These properties makes optical tweezers most suitable for measuring forces with sub-piconewton resolution and displacements with angstrom-level resolution (Abbondanzieri *et al.*, 2005). Simultaneously optical tweezers can exert forces in the range of 0 to 100-200 pN which is the interesting force regime for single molecules. Optical tweezers are therefore a widely used tool involved in stretching polymers and biopolymers such as titin (Kellermayer and Bustamante, 1997), DNA and RNA (Smith *et al.*, 1996; Strick *et al.*, 1996; Wang *et al.*, 1997; Strick *et al.*, 1998; Liphardt *et al.*, 2001), and proteins or complexes thereof such as DNA-RecA (Bennink *et al.*, 1999; Shivashankar *et al.*, 1999; Hegner *et al.*, 1999), and chromatin (Cui and Bustamante, 2000; Bennink *et al.*, 2001; Pope *et al.*, 2002, 2005). Furthermore forces involved in the action of molecular motors are measured such as myosin interacting with actin

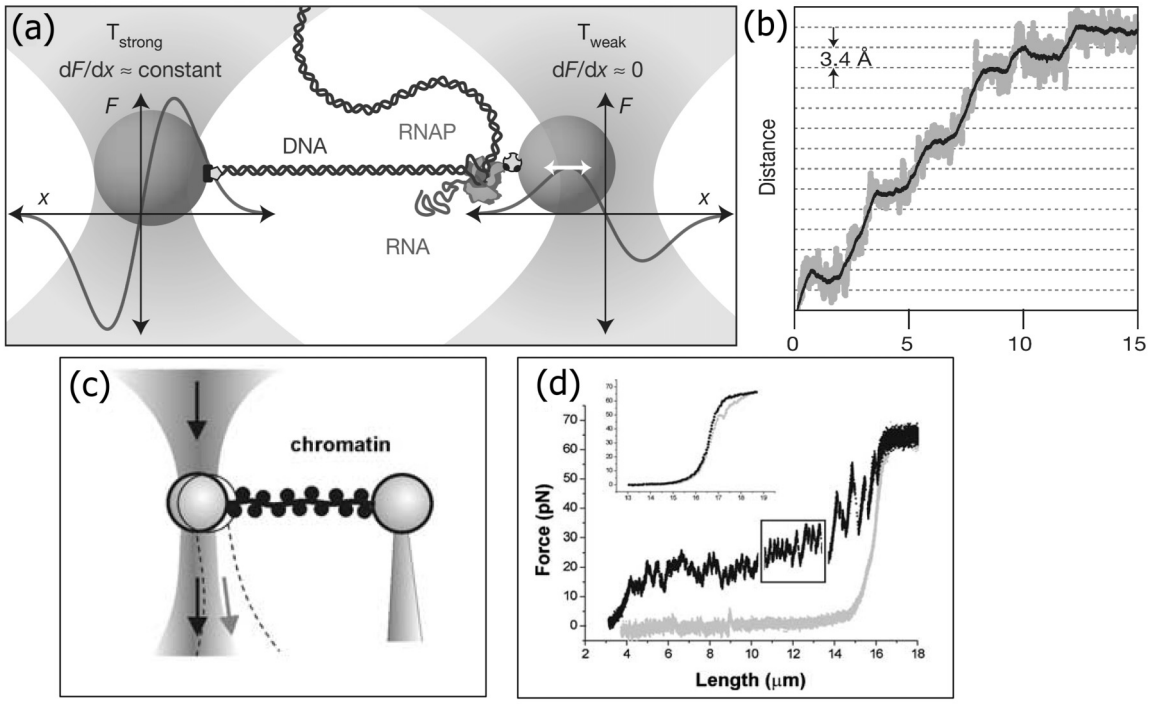

Figure 1.2. (a) Schematic layout of a dual-optical tweezers system to detect DNA-RNA polymerase interactions. (b) Steps of 3.4 *Å* (1 basepair for B-DNA) were resolved at a tension of 18 pN. (c) Schematic layout of a single optical tweezers system to stretch a single chromatin fiber while monitoring disruption interactions. (d) Comparison of a force-extension curve of the same molecule collected before and after incubation with *Xenopus laevis* egg extract containing histones leading to the formation of nucleosomes.
[Figures (a) and (b) are adapted from Abbondanzieri *et al.* (2005) by permission from Macmillan Publishers Ltd: Nature, copyright 2005; Figures (c) and (d) are adapted from Pope *et al.* (2002) with kind permission of Springer Science and Business Media].

(Finer *et al.*, 1994; Mehta *et al.*, 1997, 1999), kinesin moving along a microtubule (Svoboda *et al.*, 1993; Kojima *et al.*, 1997), and the transcriptional machines DNA and RNA polymerase (Yin *et al.*, 1995; Wuite *et al.*, 2000; Wang *et al.*, 1998; Davenport *et al.*, 2000; Abbondanzieri *et al.*, 2005). For a complete survey of the applications of optical tweezers see Lang and Block (2003).

1.2.1 Optical tweezers studies on DNA-protein interactions

OT has been widely used to study DNA-protein interactions. In this section we highlight two studies. In the first study the focus is on RNA polymerase. This transcription protein moves processively along a DNA template in steps of one basepair, which was recently shown by the group of Steven Block (Abbondanzieri *et al.*, 2005). In a dual optical tweezers configuration a single transcriptionally active molecule of

RNAP was attached to a bead held in a weak trap. Dependent on the desired direction of applied load the transcriptionally upstream or downstream end of the DNA was attached to the second bead, a configuration which is shown schematically in Fig. 1.2(a). With the addition of nucleotides and ATP (adenosine triphosphate) at optimized concentrations to control the replication rate, an elongation of approximately one base pair (bp) per second was achieved. In Fig. 1.2(b) the elongation for a tension of 18 pN is shown with an ultra-high resolution where single steps of 3.4±0.6 $\mathring{A}$ can be resolved.

Another interesting DNA-protein complex is chromatin. Within a human cell the 2 meter genome has to undergo an enormous compaction in length of a factor 10^5. The first step in this compaction process is the formation of nucleosomes. These nucleosomes are octamers of 4 different histone proteins around which DNA is wrapping itself ∼1.7 times leading to a compaction in length. In Fig. 1.2(c) a schematic is shown of a chromatin fiber in its so-called bead-on-a-string structure. This chromatin fiber is stretched between two beads in an optical tweezers apparatus leading to disruption of the individual nucleosomes. Individual opening events of 65 nm were found, indicating the individual nucleosomes being opened as is shown in the black curve in Fig. 1.2(d). The inset shows the force-extension curve of the naked DNA-molecule.

1.3 Scanning probe microscopy

Scanning probe microscopy started with the invention of the scanning tunneling microscope (STM) (Binnig *et al.*, 1982a,b). An atomically sharp probe (the tip) is moved over the surface of the material under study, and a voltage is applied between probe and the surface. Depending on the voltage electrons will "tunnel" or jump from the tip to the surface (or vice versa depending on the polarity), resulting in a weak electric current. The size of this current is exponentially dependent on the distance between probe and the surface. Keeping the tunneling current constant with a feedback loop controlling the distance between the tip and the sample, a height profile of the sample is obtained. For a current to occur the substrate being scanned must be conductive.

The atomic force microscope (AFM), a derivative of the STM, was introduced as being capable of imaging surfaces of insulators with high resolution (Binnig *et al.*, 1986). In AFM a very sharp tip located on the free end of a cantilever is scanned over the sample surface. The forces between the tip and the sample cause the cantilever to deflect. By measuring this deflection as a surface is raster-scanned a topographical image of a surface is created where atomic resolution can be achieved (Albrecht and Quate, 1987), depending on the sample and conditions.
For biological applications Marti *et al.* (1987) demonstrated that the AFM can be operated in a liquid environment after which the first demonstration of imaging a biological sample under physiological conditions was reported by Drake *et al.* (1989). Since then AFM has often been used for imaging of biomolecules including DNA (Bustamante and Keller, 1995; Rivetti *et al.*, 1996; van Noort *et al.*, 1998). Recording

consecutive AFM images under conditions that the molecules are still able to move and interact, i.e. dynamic AFM imaging, can reveal information of the dynamic aspects of the interactions between these molecules (Bennink *et al.*, 2003).

The AFM was also used for force spectroscopy studies on individual molecules by linking one end to a surface and the other end to the tip on the cantilever. Molecules such as titin (Rief *et al.*, 1997; Marszalek *et al.*, 1999) and bacteriorhodopsin (Oesterhelt *et al.*, 2000) can be extended while measuring the forces, resolving their elastic and mechanical properties. In addition the strength of bonds in ligand-receptor pairs such as streptavidin-biotin (Lee *et al.*, 1994; Hinterdorfer *et al.*, 1996) has been measured.

Besides STM and AFM there are several other scanning probe techniques developed throughout the years such as the near-field scanning optical microscope (NSOM; Dunn (1999)) and the magnetic force microscope (MFM; Martin and Wickramasinghe (1987)).

1.3.1 AFM studies on DNA-protein interactions

The chromatin fiber has been visualized with the AFM to reveal its overall structure as shown in Fig. 1.3(b). A detailed analysis of the contour length between the nucleosomes revealed two distinct nucleosomal particles, one with ∼50 nm of bound DNA and a second with ∼25 nm respectively corresponding to ∼1 wrap and ∼2 wraps of DNA around the nucleosome core particles (Nikova *et al.*, 2004).

An important protein in the repair of UV-induced DNA damage is the DNA photolyase protein. It is a protein that directly repairs DNA lesions by a light-dependent reaction known as photoreactivation. In Fig. 1.3(c) an AFM image of several DNA-photolyase complexes is shown (van Noort *et al.*, 1998). DNA lesions were created by UV-irradiation. From the position of the protein on the DNA as seen in the images a distinction could be made between non-specific and specific interactions. Specific complexes showed DNA bending of on average 36^o, whereas non-specific interactions showed no significant bending, but a slight increase in rigidity of the molecule.

In addition two more images are shown in Fig. 1.3 to give an impression of the possibilities of AFM. In Fig. 1.3(a) a phase image is shown of a Type I collagen fiber revealing the typical D-period of 65 nm. Collagen forms a connective tissue where Type I is the most abundant collagen in the human body present in scar tissue, tendons and the organic part of bones. In Fig. 1.3(d) high resolution images are shown of membranes containing the ring-shaped light-harvesting complexes LH1, LH2 and the reaction centers. These complexes form a photosynthetic system to convert light into chemical energy. The LH1 ring, consisting of 16 protomers, has a typical diameter of 12 nm and the LH2 ring, consisting of 9 protomers, has a diameter of 7 nm. With AFM even the individual protomers could be resolved (Bahatyrova *et al.*, 2004a,b).

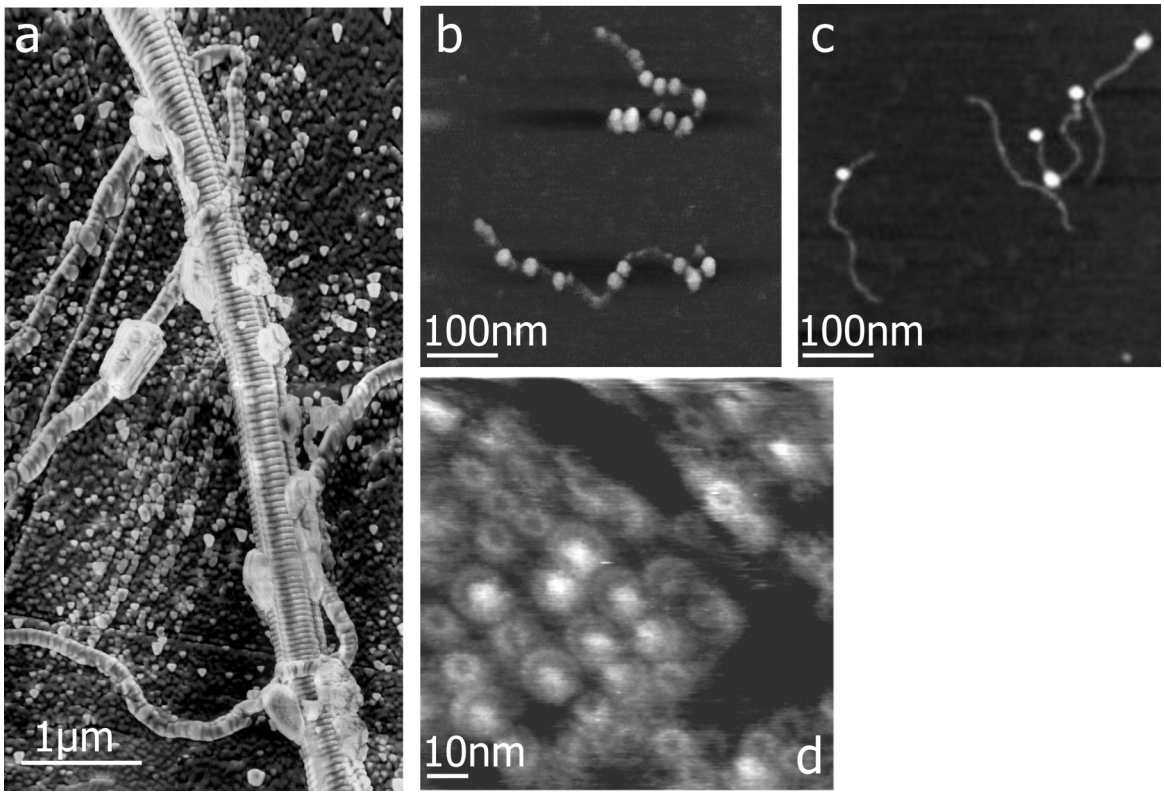

Figure 1.3. High resolution AFM images. (a) A phase image of a collagen type I fiber. Clearly visible is the D-period of 65 nm that is typical for collagen (unpublished). (b) A 208-12 reconstituted chromatin fiber (core histone : DNA ratio 1:1). DNA is thought to wrap around histone octamers forming nucleosomes leading to the 'bead-on-a-string' structure (Nikova *et al.*, 2004). (c) DNA-photolyase complexes. DNA photolyase proteins (55 kDa) bound to single DNA molecules. This enzyme directly repairs UV-induced DNA lesions using blue light (350-450 nm), a repair mechanism known as photoreactivation (van Noort *et al.*, 1998). (d) Membranes of the light harvesting complexes LH1 and LH2. For the LH1 rings its reaction center appears as a white blob (Bahatyrova *et al.*, 2004b).

As shown AFM is a high-resolution imaging technique, but a potential drawback is the surface needed for support. Often this arises questions with respect to its influence on DNA-protein complex formation and induced forces. Especially for imaging dynamic processes the influence of the surface is a point of discussion. To image dynamics it is required that the DNA molecule is not too tightly bound to the surface, but at the same time not too loosely bound to hamper imaging. To obtain the appropriate imaging conditions often salt concentrations and pH are adjusted affecting at the same time the dynamic properties of the DNA-protein complexes.

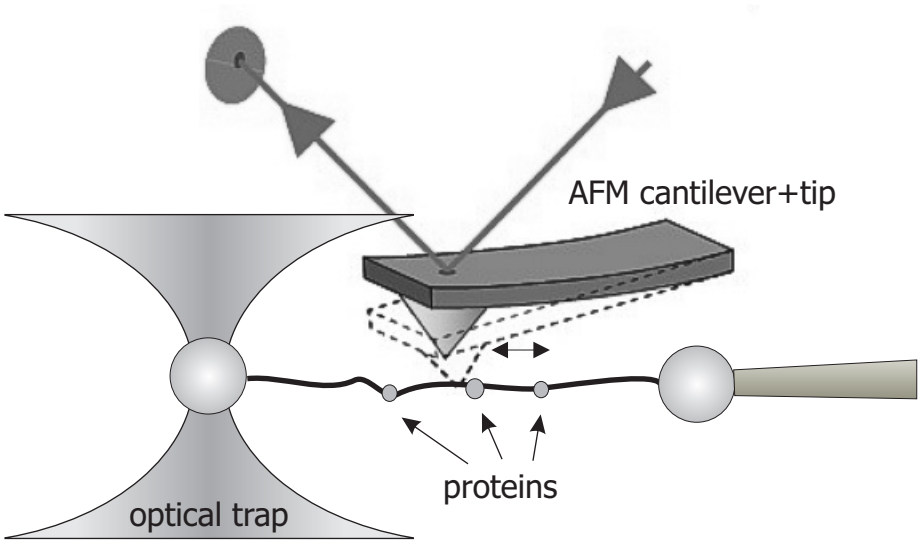

Figure 1.4. Schematic principle of localizing proteins bound to a single dsDNA molecule. A single λ-DNA molecule (16.4 μm) is suspended between two small beads (typically in the order of 1-3 μm) while allowing proteins to bind. In a next step the molecule is stretched and approached with a probe. This probe is scanning back and forth to 'feel' the individual proteins as it touches them.

1.4 Combining OT and SPM

The functions of all biological processes within the cell are regulated by specific interactions of proteins with nucleic acids or other proteins controlling processes such as transcription, translation, repair and replication that are essential for all live. To understand these processes several single molecule techniques are developed to visualize or manipulate these processes. As introduced in this chapter OT and scanning probe microscopes, and in particular the AFM, are two widely used techniques to study these DNA-protein interactions.

Both AFM and OT are tools for single molecule force spectroscopy. However due to the force resolution for AFM, typically >5 pN, and <1 pN for OT, OT is the most suitable technique to study DNA-protein interactions, but it lacks positional information on the location of these proteins on the DNA molecule. The OT as a force spectroscopy technique and AFM as a high-resolution imaging technique are complementary when combined. It allows the localization of proteins while interacting with a single DNA molecule and allows to study the influence of tension in the DNA molecule on the functional and dynamic properties of proteins. In Fig. 1.4 the concept of the combination of OT and AFM, which we will call the scanning probe optical tweezers or SPOT-microscope, is presented although the final configuration of this microscope will be different.
A single DNA molecule is stretched and free from any surface, except at both its ends where it is coupled to a bead or surface. In a next step the stretched DNA

molecule with proteins will be approached by a probe. This probe will scan back and forth (indicated in the figure with the arrow) to 'feel' the individual proteins as it touches them. In contrast to conventional SPM techniques, three dimensional diffusive processes are not obstructed by a supporting surface except by the proximity of the probe, through which the system better resembles conditions as in vivo. Yet a small stretching force is required for localization. A drawback for the experiments is the many steps that are required to attach a single DNA molecule between two beads and to start scanning with the probe, making the experiments time-consuming. Acquiring statistics is therefore a difficult and lengthy process. Nevertheless the SPOT microscope provides valuable information with several potential applications.

1.5 Outline of this thesis

This thesis describes the development of the scanning probe optical tweezers (SPOT) microscope based on the combination of optical tweezers with a scanning probe. This microscope is designed to localize proteins on a single suspended dsDNA molecule and to study the influence of tension in the DNA molecule on the functional properties of proteins.

In Chapter 2 the configuration of the SPOT microscope is presented with a description of the different aspects. First we discuss in more detail the basics of optical tweezers and atomic force microscopy. Also the elastic properties of dsDNA and present theoretical models are discussed to describe the elastic behavior of this semi-flexible polymer. Subsequently we discuss the requirements and boundary conditions of the microscope resulting in the design of a reflection-based optical tweezers apparatus. Furthermore the development of a scanning probe is discussed, pointing out its properties important for the imaging/localization accuracy. To facilitate the approach of a suspended DNA molecule by a scanning probe a new flow cell was designed, requiring modifications of a flow system used previously. Finally a complete overview of the SPOT microscope with all its components is given.

Chapter 3 treats the calibration and performance of the optical tweezers. Calibration methods necessary to measure the forces acting on and displacements of the trapped bead are presented. Properties such as the linear detection range and the noise limitations of the reflection-based optical tweezers are compared with a conventional transmission-based optical tweezers apparatus. Finally the noise limitations of the optical tweezers are discussed where we also touch upon the sensitivity of the apparatus for rotations of the trapped bead.

In Chapter 4 the detection bandwidth properties of position detectors are discussed. For optical tweezers where a near-infrared laser (1064 nm) is used the detection bandwidth can be limited to 5 kHz caused by the transparency of silicon used in position detectors. The bandwidth dependence of two types of position detectors

on bias voltage, wavelength and light power is investigated. Additionally the consequence for the force constant (stiffness) determination in AFM and OT are explored where we present corrections methods for both techniques.

Our next study, presented in Chapter 5, was undertaken to form a theoretical framework for what implications the elasticity of a single dsDNA molecule has for the measurements with the SPOT microscope. Here we focus on the expected accuracy of the microscope with which proteins can be localized and how it is influenced by the scanning probe.

In Chapter 6 we discuss the experiments done with the SPOT microscope where we focus on the interaction forces between the probe and the sample and its consequences for the resolution. As a first step we determined the friction force between the probe and naked DNA. Subsequently we localized single 450 nm polystyrene beads coupled to a DNA molecule with two different scanning probes providing us insight in the magnitude of the interaction forces and their consequences on localization. The localization results were compared with optical microscope images of the same system for validation.
As a final step towards the localization of proteins we downsized to system to individual digoxigenin sites bound to a single DNA molecule over a range of 90 nm. Scanning with an α-DIG coated pipette we were able to localize these sites due to the high binding affinity between the α-DIG/DIG antibody-antigen pair.

In Chapter 7 the main conclusions of this thesis are summarized and improvements of the instrument for future experiments are discussed.

Chapter 2

Development of the scanning probe optical tweezers

In this chapter we describe the development of the scanning probe optical tweezers. By scanning a multi-walled carbon nanotube along a stretched DNA molecule, forces are generated in the molecule due to interactions with the probe which are being monitored with the optical tweezers, allowing localization of proteins. To facilitate the approach of a suspended DNA molecule by a scanning probe we have built a reflection-based optical tweezers and designed a new flow cell.

2.1 Introduction

SPM techniques are widely used to obtain high-resolution images of samples of interest. AFM in particular, is a common technique to study DNA-protein interactions with (sub)nanometer resolution. When studying dynamic properties of such a sample an important issue is the influence of the supporting surface on for instance the motion of proteins. Combining SPM with optical tweezers could solve this problem. In this approach a single DNA molecule is suspended between two beads away from any nearby surface. Scanning with a probe allows the localization of proteins and adjusting the tension in the DNA molecule allows to study the influence of the force on the functional properties of the proteins.
In this chapter we first discuss in more detail the basic working principles and the properties of OT and AFM. Furthermore the elastic response of a single dsDNA molecule upon stretching is discussed in view of the elasticity theory applied to a thin elastic rod. With knowledge of the basics of these individual components the fundamental requirements of the combined microscope are discussed and its configuration is presented.

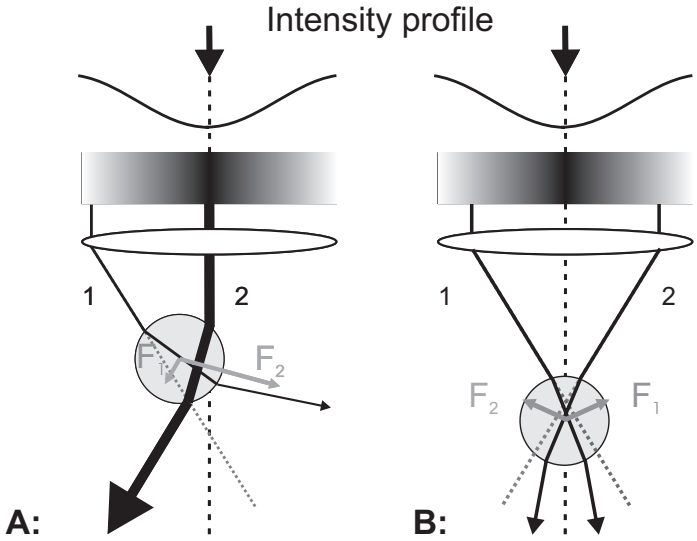

Figure 2.1. A ray optics picture of the gradient forces acting on a dielectric bead. The scattering forces due to reflection are not shown. In (a) the bead is located between the objective and the focus of the laser beam. The situation where the bead is behind the focus is shown in (b).

2.2 Optical tweezers

2.2.1 Basics of optical tweezers

Each photon has an energy of $h\upsilon = hc/\lambda$ and a momentum of $h\upsilon/c$, with υ the frequency, c the speed of light, and λ the wavelength. If an object causes light to change direction for instance on reflection or refraction, the change in momentum of light will result in an equal but opposite change of momentum on the object. The force acting on the object is related to the change of momentum per time. This effect is known as radiation pressure. Forces involved in the transfer of momentum from focused light to microscopic objects are in the order of piconewtons and can hold and move micron sized particles (Ashkin, 1970).

Basically the radiation forces can be decomposed into a 'gradient force' pointing in the direction of the intensity gradient of the light tending to pull the particle towards the focus, and into a 'scattering force' as a result of reflections directed along the optical axis, tending to push it away from the focus (Ashkin *et al.*, 1986; Svoboda and Block, 1994). In Fig. 2.1 a ray optics picture indicates the forces acting on a bead originating from two rays (1 and 2) representing parts of the beam with different intensity. The momentum changes of the light rays differ in magnitude, causing a net reaction force on the refracting medium in the direction of highest intensity. In Fig. 2.1(a) the situation is sketched for a bead located between the objective and the focal point while in Fig. 2.1(b) the bead is located behind the focal point (the focal point is indicated by the crossover point of the grey dotted lines showing the direction of the rays if they were not refracted by the bead). In these figures the reflections are not shown resulting in a scattering force pointing in the direction of the incident

light. This scattering force entails the bead to be stably trapped behind the focus where this force is compensated by the gradient force.
The calculation of optical forces on a particle is relatively straightforward in the regimes where a particle is much smaller (Rayleigh) or much larger (ray optics) than the wavelength used for trapping (Svoboda and Block, 1994). Most OT applications involve particles whose size is comparable to the wavelength. In this situation, also called the Mie regime, exact solutions for the force field are more difficult. Fortunately there are several straightforward methods for empirically measuring the force exerted by the OT on an object, discussed in Chapter 3. Right here we shortly discuss the ray-optics regime to point out the important parameters in optical trapping.

In the ray optics regime ($R \gg \lambda$, where R is the bead radius) the optical gradient force F_g and scattering force F_s for a single ray with power P and incident momentum per second of $n_1 P/c$ can be written as

$$F_s = Q_s \frac{n_0 P}{c} \qquad\qquad F_g = Q_g \frac{n_0 P}{c} \tag{2.1}$$

where P is the incident power, c is the speed of light in vacuum and n_0 is the refractive index of the surrounding medium. Q_s and Q_g are the dimensionless scattering and gradient efficiency factors. The total force can be calculated by the sum of contributions of each ray composing the total light beam as has been done by Roosen and co-workers (Roosen and Imbert, 1976; Roosen, 1979). It can be seen from the above equations that to a achieve a stronger trapping force one can increase n_0, P or the total efficiency factor $Q = \sqrt{Q_g^2 + Q_s^2}$.
Generally the trapping efficiency factor for the whole beam depends on the laser beam characteristics such as wavelength, spot size, convergence angle and the corresponding incidence angle, polarization, and beam profile. It also depends on the optical properties of the particle including size, shape and the relative refractive index ($n = n_1/n_0$) with respect to the surrounding medium (n_0), where n_1 is the refractive index of the bead.

2.2.2 Optical tweezers as force transducer

Initially optical tweezers were used as a tool to manipulate viruses, bacteria and complete cells (Ashkin and Dziedzic, 1987). However when trapping spherical beads, it was shown that a single beam gradient trap could be used to accurately measure forces within the range of piconewtons (Ghislain *et al.*, 1994). In the center of the optical trap the optical forces are cancelled out, but when the bead is slightly displaced, a net gradient force tends to drive the bead back to its center position. It was shown that the amplitude of this force is linear with the distance over which the bead is displaced. Conceptually this relation can be considered a Hookean spring as indicated in Fig. 2.2(a), where the force F_{tr} needed to displace a trapped bead by a distance Δx with respect to its center position is

$$F_{tr} = k_{tr} x \tag{2.2}$$

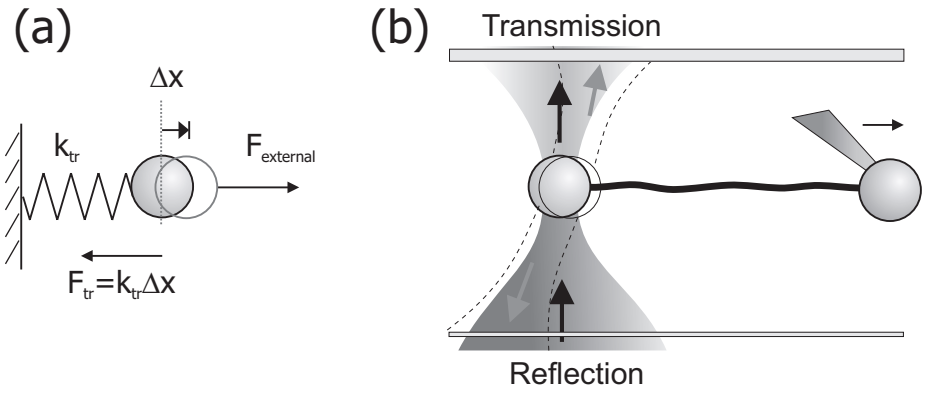

Figure 2.2. Optical tweezers measuring forces within a stretched DNA molecule. (a) When an external force $F_{external}$ is applied to the bead it is balanced with a counteracting trapping force F_{tr}, achieved for a bead displacement Δx with respect to its center position. (b) Attaching a single DNA molecule to the trapped bead and a second bead immobilized on a μ-pipette the forces in the molecule upon extension can be measured. The bead size is typically in the order of 1-3 μm and the length of a single dsDNA molecule (λ-phage DNA) is 16.4 μm.

where k_{tr} denotes the trap stiffness, expressed in pN/μm. From this equation it is clear that in order to measure forces the position of the bead and the trap stiffness are required. The stiffness can be determined using the intrinsic properties of the optical trap as we will discuss in Chapter 3. The actual position of the bead is acquired by measuring the deflection of the laser trapping light that is transmitted through or reflected off the trapped bead surface using a position detector. With typical bead sizes of 1-3 μm the trap stiffness is in the order of 50-500 pN/μm and can be controlled by the trapping laser power. Coupling a (bio)polymer at both its extremities to the trapped bead and another bead immobilized on a μ-pipette, enables measurement of the force within the individual molecule as for instance dsDNA (Fig. 2.2(b)).

2.3 Atomic force microscopy

The heart of an atomic force microscope (AFM) consists of a cantilever with a sharp tip at its end, typically composed of silicon or silicon nitride with tip sizes in the order of nanometers. The tip is brought into contact with or in close proximity to a sample surface. Interaction forces as the Van der Waals forces between the tip and the sample lead to a deflection of the cantilever according to Hooke's law, where the spring constant of the cantilever is in the order of 0.01-100 N/m or 10^4-10^8 pN/μm for comparison with the trap stiffness of an optical trap. The deflection is measured using a laser beam reflected from the top of the cantilever onto a position detector, schematically represented in Fig. 2.3. For biological applications this optical deflection method enables the operation of the AFM in liquid environments (Meyer and Amer, 1988; Drake *et al.*, 1989). In many cases constant force mode is used in which a feedback mechanism is employed to adjust the tip-to-sample distance to keep the force

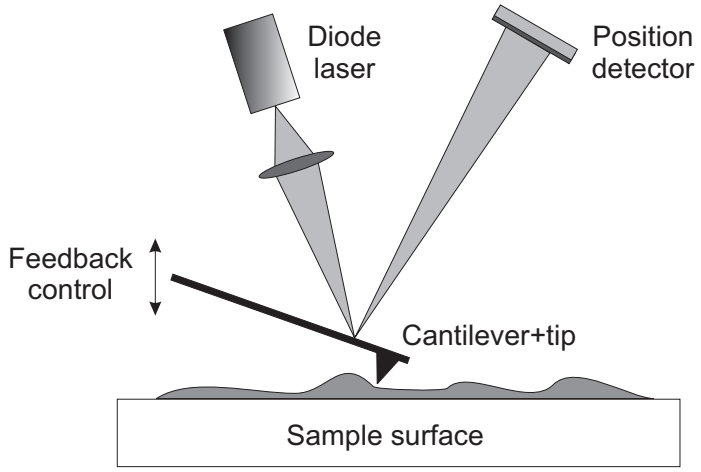

Figure 2.3. Measure principle of an atomic force microscope (AFM). The deflection signal measured by a position detector is used in a feedback loop in order to maintain a constant deflection and consequently a constant imaging force.

between the tip and the sample constant and thus preserving a constant deflection of the cantilever. Generally, the sample is mounted on a piezoelectric tube, which can move the sample in the z direction for maintaining a constant force, and the x and y directions for scanning the sample. The resulting map represents a high-resolution image of the topography of the sample.

In this contact mode AFM imaging the tip is in continuous contact with the sample surface during scanning. Imaging of soft or weakly immobilized samples with this mode easily leads to disruption or removal of the sample due to the high lateral forces. In order to reduce these lateral forces the tapping mode is used (Hansma *et al.*, 1994; Putman *et al.*, 1994). Modulating the amplitude at or near its resonance frequency, changes in the oscillation amplitude yield topographic information about the sample. Additionally, changes in the phase of oscillation can be used to discriminate between different types of materials based on properties such as adhesion and compliance.

In AFM the cantilever acts as the force transducer converting the forces acting on the tip at its end to a bending of the lever. Cantilevers are available in many different shapes such as triangles or rectangles leading to a different lateral and torsional stiffness. The width of a typical rectangular cantilever is $\sim$20 μm and the length is in the order of 100-500 μm.

2.4 Mechanical and elastic properties of dsDNA

In this section we first introduce important parameters such as Young's modulus, bending constant, persistence length and stretching modulus by considering elasticity theory (Landau *et al.*, 1986) applied to a thin elastic rod. Subsequently we discuss the worm-like chain model that is used to describe the elastic properties of a DNA molecule upon stretching.

Stretching an elastic rod

For an elastic rod with radius r and length L_0 that is stretched (or compressed) by a force F the force per area applied to the interior of the rod is $\sigma = F/(\pi r^2)$ where σ is called the stress. Assuming the linear stretching law we can formulate

$$\sigma = \frac{F}{\pi r^2} = Y \cdot \varepsilon = Y \frac{\Delta L}{L_0}$$

$$F = \pi r^2 Y \frac{\Delta L}{L_0} = S \frac{\Delta L}{L_0} \tag{2.3}$$

where Y is the Youngs modulus (N/m^2=Pa=J/m^3), a material-related parameter of the rod, ε the strain and ΔL the extension of the rod. The stretching modulus (or force constant) $S = \pi r^2 Y$ indicates the force required to stretch a rod to double its length in equilibrium.

For dsDNA Smith *et al.* (1996) measured a Youngs modulus of $3 \cdot 10^8$ Pa. Assuming dsDNA having a diameter of $\sim$2 nm the stretching modulus is 1000 pN.

Thermal fluctuations of an elastic rod

The equipartition theorem states that a system in thermal equilibrium has an average kinetic energy of $\frac{1}{2}k_bT$ per degree of freedom. Calculating the elastic energy stored in the rod we are able to determine the fluctuations in length of the rod.
The elastic energy stored in the rod can be derived by integrating the force to compute the work done for stretching:

$$E_{stretch} = \int_0^{\Delta L} F d(\Delta L) = \int_0^{\Delta L} \frac{S \Delta L}{L_0} d(\Delta L) = \frac{S(\Delta L)^2}{2L_0}$$

When putting this term equal to $\frac{1}{2}k_bT$ the typical fluctuation of length as a result of thermal fluctuations can be calculated as

$$\sqrt{< \Delta L >^2} = \sqrt{\frac{k_b T L_0}{S}} = \sqrt{\frac{k_b T}{k_{rod}}} \tag{2.4}$$

with $k_{rod} = S/L_0$ the stiffness of the rod. For a dsDNA molecule with a contour length L_0 of 16.4 μm and a stretching modulus of 1087 pN the stiffness is 66 pN/μm and consequently the end-to-end fluctuations are 8 nm when forces between 20-50 pN are applied.

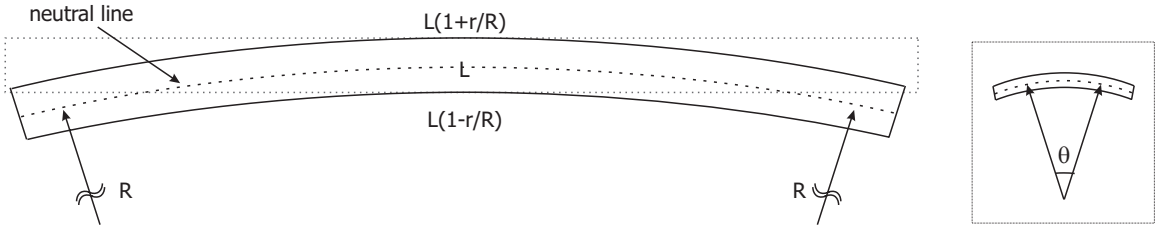

Figure 2.4. Geometry of a bent rod with the neutral line that exhibits no stretching nor compression indicated by the dotted line.

Bending energy of a thin rod

Consider the configuration as sketched in Fig. 2.4. A thin rod with radius r and length L is bent slightly ($R \gg r$) to have a radius of curvature R. Due to bending the upper convex side of the rod is stretched to $L(1 + r/R)$, whereas the lower concave side is compressed to $L(1 - r/R)$. In between there is a neutral surface, which is neither stretched nor compressed. Since bending involves stretching and compression the bending energy is again a function of the Youngs modulus Y. The elastic bending energy can be derived as

$$E_{bend} = \frac{BL_0}{2}\frac{1}{R^2} = \frac{B}{2}\kappa^2 \tag{2.5}$$

where $\kappa = 1/R$ indicates the curvature. B is the bending constant or flexural rigidity ($\mathrm{J \cdot m}$ or $\mathrm{N \cdot m^2}$) that can be written as

$$B = YI = \frac{\pi}{4}Yr^4 \tag{2.6}$$

for a rod with a circular cross-section. I is the moment of inertia. Eq. 2.5 can be expressed in terms of the angle θ reflecting the angle of bending indicated in Fig. 2.4. Substituting $R = L_0/\theta$ yields

$$E_{bend} = \frac{B}{2L_0}\theta^2 \tag{2.7}$$

and equalling this to $\frac{1}{2}k_bT$ the fluctuations of θ can be written as

$$\sqrt{\langle\theta^2\rangle} = \sqrt{\frac{k_bTL_0}{B}} = \sqrt{\frac{L_0}{L_p}} \tag{2.8}$$

where L_p is called the persistence length of the rod which equals $B/(k_bT)$ and is a measure of the rigidity expressed as a distance. Rods much smaller than the persistence length are essentially straight. For rods much longer than the persistence length many bends occur in random direction. The persistence length therefore indicates the length scale over which the rod loses its orientational order. In this case the rod cannot simply be described by a single curvature as is done above, but is parameterized

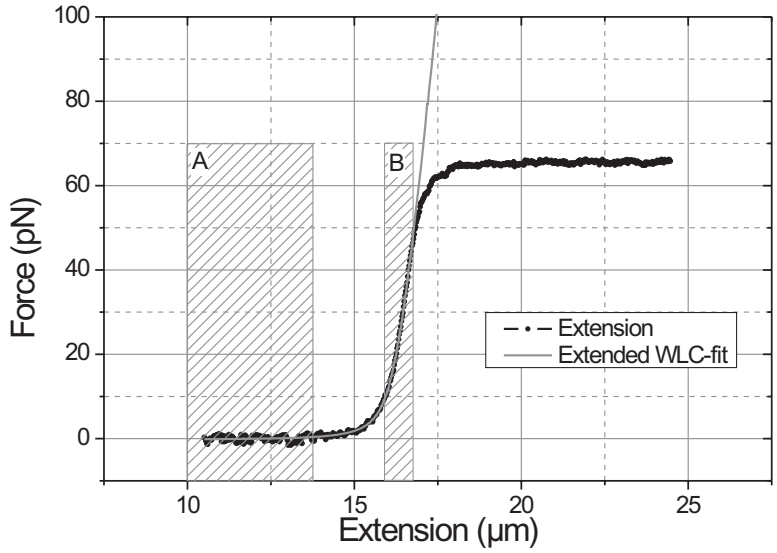

Figure 2.5. A typical force-extension curve of dsDNA in a TE-buffer supplemented with 150 mM NaCl, 0.05% BSA and 0.01% NaN_3 (pH 7.5). In addition the resulting curve-fit up to a force of 50 pN for the extended WLC model (Eq. 2.13) is shown. The contour length L_0 found was 16.4 µm, the stretching modulus S=1002 pN and the persistence length L_p=52 nm. Area A indicates the linear entropic regime and area B the enthalpic regime.

by a tangent vector describing the local curvature along the rod. For this tangent vector the correlation function follows an exponential decay and can be written as

$$\langle cos(\theta) \rangle = e^{-s/L_p} \tag{2.9}$$

where s indicates the position along the rod and θ is the angle of the tangent vector indicating its orientation. Actually this equation holds for a semi-flexible polymer such as dsDNA that can be described as a worm-like chain, which we will discuss in the following section. For dsDNA the persistence length is in the order of 50 nm (Smith *et al.*, 1996).

2.4.1 The Worm-like Chain Model

In the past decade several groups acquired high-resolution force-extension curves of single dsDNA molecules over a large force range using OT (Smith *et al.*, 1996; Cluzel *et al.*, 1996; Wang *et al.*, 1997). This allowed the determination of parameters such as the Youngs modulus, the persistence length, and the stretching modulus. In Fig. 2.5 the force-extension curve is shown for a single dsDNA molecule with a length of 16.4 µm. At this point we only focus on the part of the force-extension curve till 50 pN. In the theoretical analysis of the force-extension behavior of a dsDNA molecule a distinction can be made for different force regimes as discussed by Marko and Siggia (1995).

- ***Low-force entropic elastic response***
  If the flexible polymer is not too strongly stretched ($x \ll L_0$) or equivalently

$F \ll k_bT/L_p$ the force response is dominated by the polymer entropic flexibility and its thermal motion and can be expressed as a flexible polymer formula

$$F = \frac{3k_bT}{2L_p}\frac{x}{L_0} \tag{2.10}$$

where x is the end-to-end extension. For dsDNA this equation holds till approximately $k_bT/L_p \approx 0.1$ pN. In Fig. 2.5 this regime is indicated as area A.

- ***High-force elastic response***
  At higher forces (1-10 pN) the filament obviously gets straightened out. A detailed calculation gives

$$F = \frac{k_bT}{L_p}\frac{1}{4(1-x/L_0)^2} \tag{2.11}$$

  In this high-force regime the energy of a stretched DNA molecule is calculated as the summation of the bending and the stretching energy. These energies exhibit a similar pattern as for a thin rod as discussed in section 2.4. The main difference is that since the length of the molecule is much larger than the persistence length the shape of the molecule is described by a space vector.

- ***Interpolation formula: the Worm-Like Chain Model***
  A useful interpolation formula (Marko and Siggia, 1995) to connect these two regimes is

$$F = \frac{k_bT}{L_p}\left[\frac{x}{L_0} + \frac{1}{4(1-x/L_0)^2} - \frac{1}{4}\right] \tag{2.12}$$

  This expression diverges as $x/L_0 \to 1$ indicating that the length of the molecule can never exceed its contour length. For forces <10 pN this formula well fits the force-extension behavior of dsDNA.

- ***Extensible Worm-like Chain Model***
  For even higher forces (10-50 pN) the effective contour length of the DNA molecule is increased. In this regime, indicated in Fig. 2.5 as area B, the force response behaves as an enthalpic (Hookean) spring and can thus be described by the linear stretching law given by Eq. 2.3. To include the increase in the effective contour length in the WLC-model x/L_0 has to be replaced by $x/L_0 - F/S$ (Odijk, 1995; Wang *et al.*, 1997). Consequently Eq. 2.12 becomes

$$F = \frac{k_bT}{L_p}\left[\frac{1}{4(1-x/L_0-F/S)^2} - \frac{1}{4} + \frac{x}{L_0} - \frac{F}{S}\right] \tag{2.13}$$

  also called the extensible WLC model that describes the force-extension response up to 50 pN. Several other interpolation formulas are derived for different force ranges. A good overview of these models is given by Bouchiat *et al.* (1999). In Fig. 2.5 the curve-fit to the the force-extension curve till 50 pN is shown for this model. The contour length L_0 was found to be 16.4 μm, the stretching modulus S 1002 pN, and the persistence length L_p 52 nm.

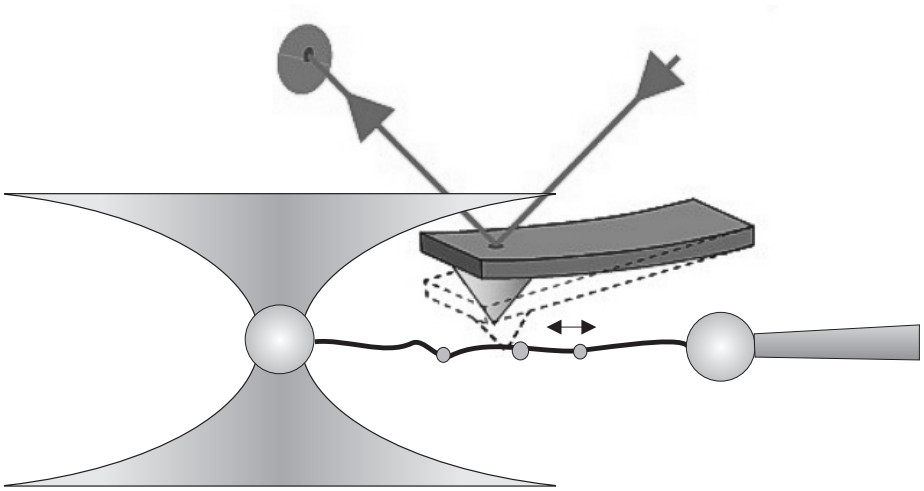

Figure 2.6. Schematic representation of the principle of localizing proteins bound to a single dsDNA molecule, stretched with optical tweezers.

2.5 Combining OT and SPM

The rationale for combining optical tweezers and scanning probe microscopy is to localize individual proteins on a single stretched DNA molecule as depicted in Fig. 2.6. In this section we discuss the fundamental scales at which DNA-protein interactions occur and the consequences for the configuration of the combination microscope.

2.5.1 Fundamental scales and requirements

In the world of molecular biology and especially at the level of single molecules the fundamental length scale is the nanometer. Proteins are typically 1-10 nm in size. According to the equipartition theorem (Reif, 1965) each system in thermal equilibrium has an average kinetic energy of $\frac{1}{2}\mathrm{k}_b\mathrm{T}$ per degree of freedom. Since most biological systems operate at room temperature the random (thermal) force acting on components is in the order of 1 $\mathrm{k}_b\mathrm{T/nm}$=4.1 $\times$ 10^{-12} J/m=4.1 pN, where k_b is Boltzmann's constant and T the absolute temperature in Kelvin. For proteins bound to DNA we can therefore expect the typical forces to be at least 4 pN otherwise proteins would diffuse away as a result of thermal motion.

When we want to localize proteins on a DNA molecule this molecule has to be stretched to the enthalpic regime (10-50 pN, see Fig. 2.5). In this regime the slope of the force extension curve is the highest for which the maximum detection accuracy is achieved as we will show in Chapter 5 and 6.

2.5.2 Configuration of the combined microscope

As discussed above the combined microscope should be capable of measuring forces in the (sub)piconewton range and simultaneously detect nanometer displacements.

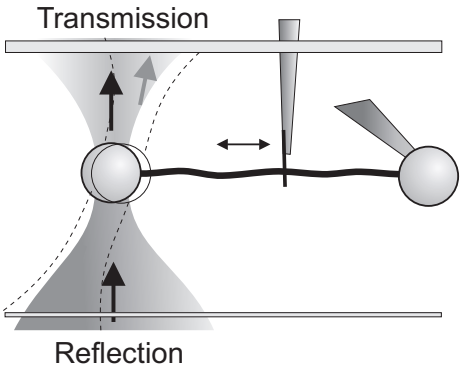

Figure 2.7. Schematic overview of the optical tweezers and scanning probe configuration. A single dsDNA molecule is stretched between two micron-sized polystyrene beads. A probe is scanned along the molecule initiating forces dependent on the local structure. By relating the position of the probe to the forces measured simultaneously with the optical tweezers the position of proteins are revealed.

Although there are several SPM techniques as discussed in Chapter 1 the AFM is most widely used for imaging DNA-protein interactions with (sub)nanometer resolution. Both the AFM and OT are force transducers where a difference in the probe stiffness (or force constant) is the most important parameter to be considered in combining these two techniques. Both the position and force resolution in these two techniques are limited by the thermal motion of the probe induced by thermal collisions of the surrounding medium. This thermal motion is a function of the probe stiffness.

Referring back to the equipartition theorem we can write for both the OT and the AFM $\frac{1}{2}k_bT = \frac{1}{2}k_{pr}\langle x^2\rangle$ where k_{pr} is the stiffness of the probe and $\langle x^2\rangle$ the variance in the probe position x. Actually for AFM this equation holds for each vibration mode of the cantilever and is only valid for a freely moving cantilever, which is the case in our situation as shown in Fig. 2.6. Both the stiffness of the DNA molecule (66 pN/μm) and the trap stiffness (50-500 pN/μm) are much lower than the stiffness of the cantilever (10^4 pN/μm) such that the latter determines the effective stiffness. Based on equipartition we can thus write

$$x_{rms} = \sqrt{< x^2 >} = \sqrt{\frac{k_bT}{k_{pr}}} \qquad F_{rms} = k_{pr}x_{rms} = \sqrt{k_{pr}k_bT} \tag{2.14}$$

Assuming a trap stiffness of 100 pN/μm for OT x_{rms}=6.4 nm and F_{rms}=0.64 pN whereas for AFM assuming a stiffness of 10^4 pN/μm, x_{rms}=0.64 nm and F_{rms}=6.4 pN. As can be seen the force fluctuations for OT are much lower than for AFM. When OT and AFM are combined in a way as sketched in Fig. 2.6 the induced forces by an AFM tip are already detected by the OT before the AFM itself detects a change in force. Instead of using an AFM for the localization of proteins, a scanning probe is thus sufficient to initiate forces within the molecule related to its interactions with proteins where the OT is used as sensor. With the OT as sensor the scanning probe should be stiff to minimize its thermal vibrations and thin in the scanning direction (along the DNA molecule) to minimize convolution. In Fig. 2.7 this idea is schematically presented.

This figure also nicely illustrates which parts of the apparatus have to be movable. First of all we need to acquire a force-extension curve of the DNA molecule to verify if a single molecule is suspended between the two beads, requiring one of the beads

to be moved with respect to the other. In a next step we want to localize the proteins on the molecule, which requires that the DNA molecule is stretched to the enthalpic linear regime (10-50 pN). While keeping the extension constant the scanning probe has to scan independently along the molecule inducing forces in the DNA molecule dependent on its interaction with the molecule and the proteins. These forces are sensed by the OT and related to the position of the probe making it possible to determine the position of proteins.

Another important issue is the configuration of the optical trap. Optical trapping requires a strongly converging beam that is created with a high NA objective (typically 1.2-1.4). Consequently the convergence/divergence angle of the trapping laser light is about 65 degrees. Considering these high angles the proximity of a scanning probe close to the optical trap will lead to refraction, reflection and absorption of the laser light transmitted by the trapped bead. In this case the force detection using the transmitted light is disturbed and thus requires a reflection-based deflection detection scheme. For such a detection scheme it was estimated that the backscattered light power is in the order of 0.1% of the input power at the back aperture of the objective.

In the final design of the combined OT and SPM microscope we have chosen for a fixed single beam gradient optical trap in combination with a flow cell design in which a μ-pipette was integrated for the immobilization of the second bead (a configuration with which our lab has experience (Bennink *et al.*, 1999)). A fixed trap requires thus a movable flow cell to displace the immobilized bead with respect to the trap and an independent position-controlled scanning probe. In the next sections we will discuss the design of the reflection-based optical tweezers, the scanning probe and a new flow cell design that facilitates the approach of a single stretched DNA molecule with the scanning probe. Finally we discuss the complete design of the combined microscope, which we will call the scanning probe optical tweezers (SPOT-microscope) throughout this thesis.

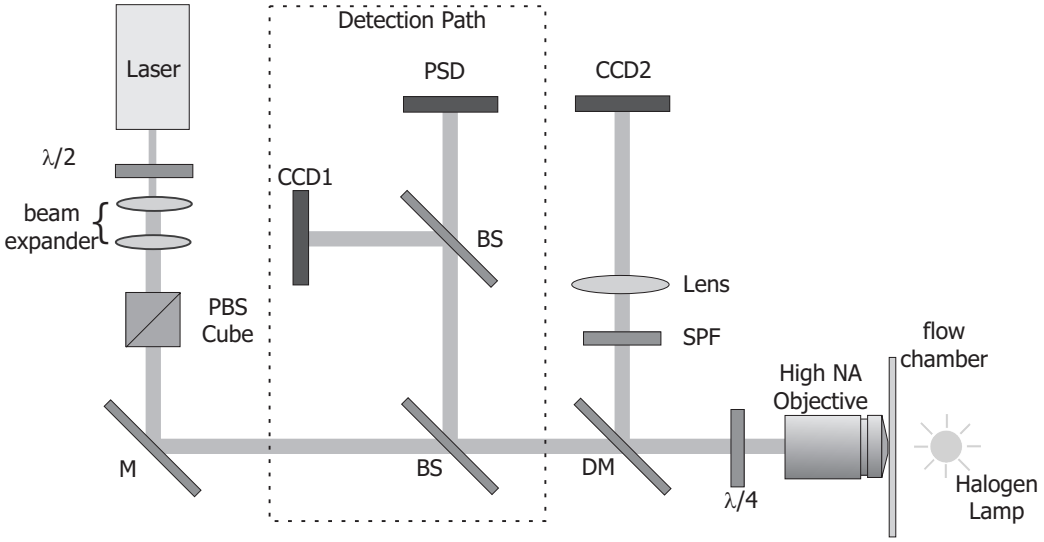

Figure 2.8. Schematic representation of the reflection-based optical tweezers apparatus. A beam expander provides overfilling of the back-aperture of a high NA objective. The laser power at this aperture is controlled by combining a half-wave plate and a polarizing beam splitter cube. A quarter-wave plate just in front of the objective provides circularly polarized light for the trap. A beam splitter (BS) directs the backscattered light onto a position sensitive detector (PSD) where a second beam splitter in the detection path (indicated with the dotted line) enables visualizing the reflection pattern on a CCD camera (CCD1). A halogen lamp provides white light illumination for optical microscopy imaging the trapped bead via a dichroic mirror (DM) on a second CCD camera (CCD2). A short-pass filter (SPF) blocks the 1064 nm laser light.

2.6 The optical tweezers[1]

We designed and constructed a reflection-based OT to facilitate the approach of a scanning probe without obstructing the force detection of the OT.

2.6.1 Design of the reflection-based OT

A diode-pumped Nd:YAG (CrystaLaser IRCL-2W-1064) laser with an output power of 2 W at $\lambda = 1064$ nm (TEM_{00}) serves as the trapping laser. A beam expander, consisting of two lenses, is used to overfill the objective entrance in order to optimize the optical tweezers efficiency (Ghislain *et al.*, 1994). A combination of a half-wave plate and a polarizing beam splitter cube was added to control the laser power at this entrance as shown in Fig. 2.8. A 100x, infinity-corrected, water-immersion objective (Leica N PLAN) with a NA of 1.20 yields a steep gradient in the electric field to trap small dielectric particles. This objective simultaneously collects the backscattered

[1]The contents of this section are based on Huisstede *et al.* (2005),
[Huisstede J. H. G., van der Werf K. O., Bennink M. L., and Subramaniam V., "Force detection in optical tweezers using backscattered light", *Optics Express*, **13**(4), 1113–1123. 2005].

light from the trapped particle, directing the light onto a position sensitive detector (DL100-7-KER, Pacific Silicon Sensors) using a 90/10 beam splitter for 1064 nm (CVI Laser, BS1-1064-10-1037-45-P). A second 90/10 beam splitter (CVI Laser, BS1-1064-10-1012-45-P) in the detection path is used to visualize the backscattered light with a charge coupled device camera (Panasonic F15) with an active area of 8.5x6.4 mm^2 (CCD1 in Fig. 2.8). A quarter-wave plate placed in front of the objective converts the incident p-polarized laser light into circularly polarized light, providing an equal trap stiffness in both lateral directions (Wohland *et al.*, 1996). Upon reflection the circularly polarized light changes direction and after passing the quarter-wave plate the light becomes s-polarized. For the 90/10 beam splitter (defined for p-polarized light at 1064 nm; 90% transmission, 10% reflection) the reflectance is 20% for s-polarized light. Measuring the reflected light power impinging on the position sensitive detector from a 2.6 μm bead with and without the quarter-wave plate a factor 2 in light power was gained using the quarter-wave plate. Due to reflection at the front and back surfaces of the beam splitter a ghost image is created. An anti-reflection coating on the back surface provides a 40 times lower reflection intensity of this ghost reflection. Furthermore the 1 cm thickness of the beam splitter spatially separates the two beams by a distance of 1.4 cm. The maximum trapping laser power at the back aperture of the objective is 550 mW. In this case the power of the collected backscattered light at the position sensitive detector is in the range of 100-500 μW dependent on bead size. A halogen lamp is used as light source for the white light detection. Using a dichroic mirror an image is formed on a second charge coupled device camera (CCD2 in Fig. 2.8) with an active area of 6.4x4.8 mm^2.

2.7 The scanning probe

In the configuration presented here, and in contrast to SPM techniques, the probe is not used as a sensor. In this section we discuss in detail the scanning probe configurations that we investigated.

2.7.1 The canti(c)lever

In contrast to SPM techniques the SPOT microscope requires a probe that achieves a high resolution in only dimension (i.e. along the DNA). In other words, instead of a point probe such as the tip in AFM, a blade or pillar can be used with the resolution determined by the thickness and the thermal fluctuations of the probe. A probe that satisfies these conditions is the recently developed canticlever for magnetic force microscopy (MFM) applications (van den Bos *et al.*, 2002). In Fig. 2.9(a) a SEM image of the canticlever is shown. The triangular shaped blade (indicated with an arrow) has a thickness of ∼50 nm and is partially thicker to increase the stiffness of the blade.

The canticlever is analogous in shape to an AFM cantilever. Instead of a point probe connected to a lever a blade is connected to a lever with dimensions similar to

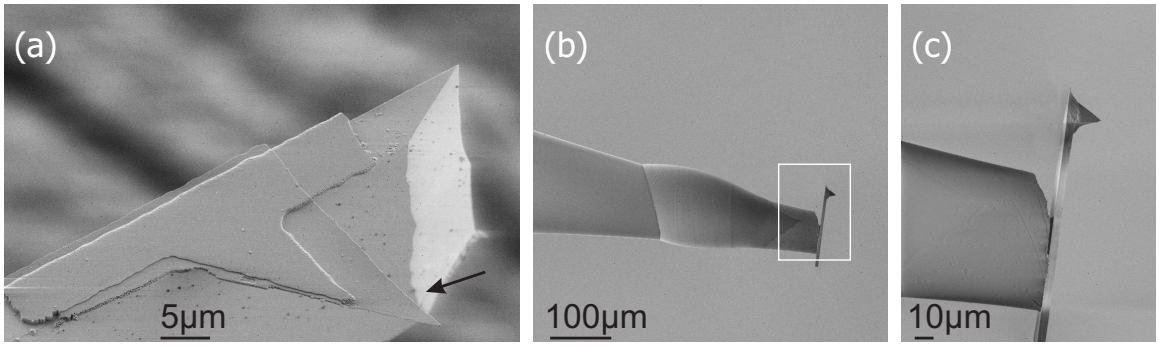

Figure 2.9. SEM images of a canticlever designed for MFM (a) and an AFM cantilever fixed to a borosilicate µpipette using UV glue shown in (b) and (c). In (a) the blade with a thickness of 50 nm is indicated with the arrow.

those of the standalone AFM cantilever. Due to the limited availability of the canticlever, normal AFM cantilevers were used for testing. A µ-pipette with an ending diameter of 40 µm was dipped in a droplet of UV glue (Norland, Cranbury, NJ). A small amount of UV glue was sucked into the pipette using a syringe connected to its end. The AFM cantilever was placed with its supporting base on top of a microscope glass and visualized in a bright field microscope. Subsequently the pipette was brought in contact with the cantilever in a way as shown in the SEM images in Fig. 2.9(b) and (c). Applying pressure with the syringe the UV glue was slightly pressed out of the pipette until a connection with the AFM cantilever was visible. The pipette was pushed downwards to bend and break the cantilever off its supporting base. The presence of the UV glue prevented the cantilever to leap away from the pipette. Using an UV lamp the UV glue was cured for 15 minutes providing a rigid fixation. In Fig. 2.9(c) the connection of some glue at the inner side of the pipette (dark) to the cantilever is visible. Furthermore one can see that at the outer side of the pipette some additional UV glue is spread out over the surface due to the surface tension.

Approaching the optical trap with a canti(c)lever fixed to a µ-pipette, several problems were encountered. The main problem was the size of the lever, typically 20 µm in width and 100 µm in length and huge in comparison with the micron-sized beads that were trapped. The size of the probe system resulted in a strong backscattering of the trapping laser light, where the total intensity was at least in the order of the backscattered light power of the trapped bead (>100-500 µW). Furthermore the high trapping power resulted in most of the cases to heating of the probe, leading to bubble formation presumably caused by dirt particles on the probe. Another disadvantage of the dimensions of the lever was that it strongly reduced the visibility of the trapped bead in the optical microscope due to blocking of the illumination.

2.7.2 Carbon nanotubes as a probe

Nowadays a lot of research is done on carbon nanotubes (CNT) as a sharp probe in AFM applications to improve the spatial resolution (Hafner *et al.*, 2001). Due to their small diameter, high aspect ratio, large Young's modulus, their ability to buckle elastically under large loads, well-defined structure, and unique chemical properties they represent ideal AFM tips. They consist of seamless cylinders made from sp^2-bonded carbon (graphene sheets wrapped into a cylinder). There are two basic structural classes of carbon nanotubes. Single-walled carbon nanotubes (SWNT) consist of a single cylinder with a radius of 0.4-3 nm. Multi-walled carbon nanotubes (MWNT) are consisting of multiple SWNTs nested coaxially within one another typically having a radius ranging from 3 to over 100 nm (Hafner *et al.*, 2001). Length scales are in the order of 1 to 100 μm. Calculations of the Young's moduli suggest that both classes have a modulus in the order of 1 TPa (Lu, 1997). Experimental results for MWNT's made by direct bending with AFM revealed a Young's modulus of 1.3 TPa (Wong *et al.*, 1997). Studies of individual 1.0 nm diameter SWNT found a similar Young's modulus of 1.25 TPa (Krishnan *et al.*, 1998).

The first carbon AFM tips were produced by manually attaching MWNTs to the tip, while viewing in an optical microscope (Dai *et al.*, 1996). Using micro manipulators for the independent position control of an AFM tip a MWNT was connected to a tip covered with a thin layer of adhesive. More recently a similar strategy was used under the view of a SEM that allows assembly of about 10 nm diameter tips (Akita *et al.*, 1999). An important limitation of the manual assembly method of producing tips is the fact that it is time-consuming. Additionally the procedure inherently leads to selection of the thicker CNTs since these are the easiest to observe. These problems are solved by directly growing CNTs on the tip using chemical vapor deposition (CVD). This provides higher resolution probes and allows mass production (Hafner *et al.*, 1998). Better control of nanotube properties is achieved through optimization of the reaction parameters.

We used a manual assembly method to connect a MWNT to a borosilicate μ-pipette. Borosilicate μ-pipettes were pulled from 1.2 mm outer diameter and 0.94 mm inner diameter capillaries (Harvard Apparatus GC120TF-15, Holliston, MA) using a Sutter P-87 micropipette puller (Novato, CA). Freshly pulled pipettes are hydrophilic due to the density of surface hydroxyl groups (≈4.6 free OH groups per 10 nm^2). Silanization of these charged surfaces produces a molecular hydrophobic finish (Smith *et al.*, 1999). This hydrophobic layer provides a sticky surface for the hydrophobic MWNTs.

Silanization of pipettes

Freshly pulled pipettes were placed upright in a glass beaker, which was placed on a glass Petri dish. The pipettes were covered under a 100 ml glass beaker and baked in an oven at 200^{o}C for at least 4 hours. All glassware (except the pipettes) was pre-silanized by placing them in a 2% APTES (3-aminopropyltriethoxysilane, Sigma)

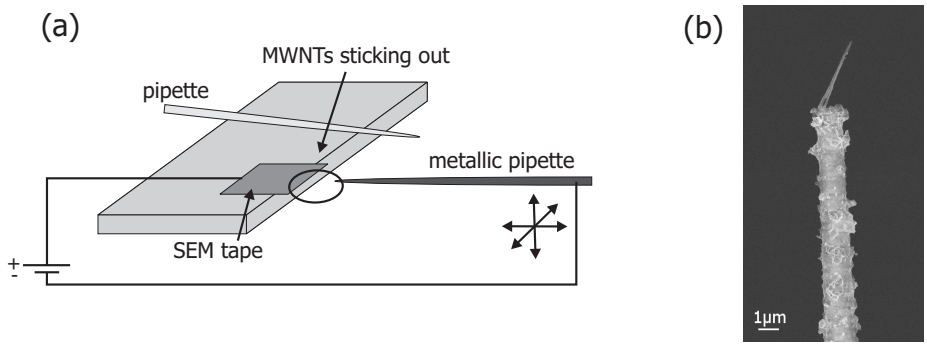

Figure 2.10. (a) A metal-coated pipette was used to pull a MWNT out of a conducting tape (SEM) tape. The interaction force was controlled by applying a DC voltage. Next the MWNT was transferred to a silanized µ-pipette. (b) A SEM image of a bundle of MWNTs connected to a ∼2 µm borosilicate pipette. This particular pipette was not silanized.

solution in 95% aqueous acetone for 1 hour. If the pipettes were not freshly pulled they were cleaned by placing them in a solution of 65% HNO_3 (nitric acid) for at least a few hours and rinsed several times with acetone.
After the oven was cooled TMSDMA (N,N-dimethyltrimethylsilyamine, Fluka) was injected under the 100 ml beaker through a syringe. The TMSDMA almost immediately vaporized and the vapor produced a homogeneous hydrophobic silane coating on the pipettes. After 30 minutes the beaker was opened for a short period of time to allow any residual vapor to escape. The silanized pipettes were baked at 200^oC overnight. Another silanization procedure placing the pipettes in 2% APTES in 95% aqueous acetone for 1 hour resulted in an inhomogeneous coating clearly visible in the optical microscope.

Connection of MWNT to pipettes

MWNTs were pulled out of an array of nanotubes aligned perpendicular to its supporting surface (Nanolab, Newton, MA) by gently touching the adhesive side of conducting adhesive tape (SEM tape) to the nanotubes. These MWNTs have a typical diameter of 40-90 nm and an average length of 5 µm. A metal-coated µ-pipette (TIP01F12S40, WPI) was brought within a few microns to a MWNT protruding out of the tape. A DC voltage difference (tens of Volts) was applied between the MWNT and the metallic pipette to control the strength of the electrostatic interactions (Stevens *et al.*, 2000). When the MWNT started to align towards the pipette it was touched by the pipette and pulled out of the tape. Next the MWNT was transferred from the metallic pipette to the silanized µ-pipette without applying a DC field. Schematically the principle is shown in Fig. 2.10 together with a SEM image of a MWNT connected to a µ-pipette.

We were able to connect a MWNT from the adhesive to a borosilicate pipette directly using electrostatic interactions, but a much lower throughput was achieved due to lower forces. Furthermore using the metallic pipette as an intermediate step, the end of the MWNT used for scanning will be free of SEM tape remnants.

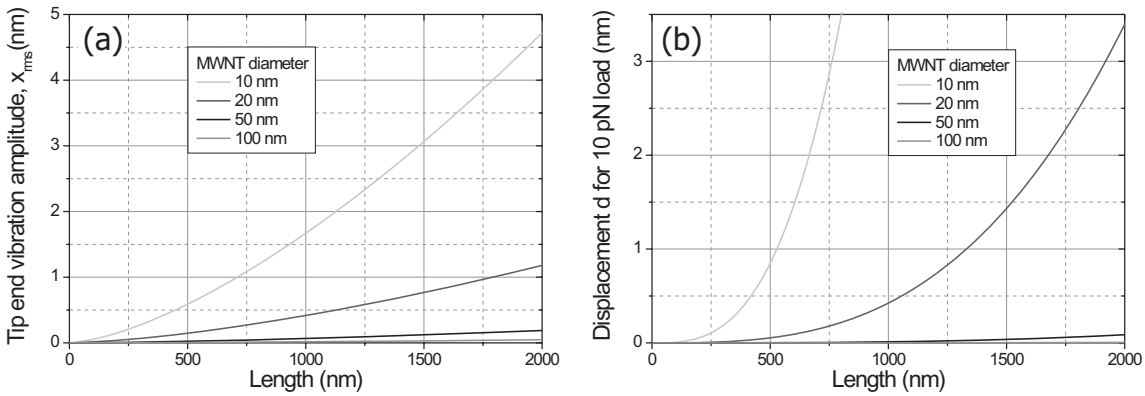

Figure 2.11. (a) The vibration amplitude of the end of a MWNT clamped at one side for different lengths and diameters. (b) The displacement of the end of the MWNT under a load of F=10 pN.

Direct use of a metallic pipette with a MWNT close to the optical trap (100-300 mW) resulted in bubble formation presumably caused by heating up of the metallic layer or of dirt present due to the absorption of photons.

MWNTs as a scanning probe for imaging

The vibration amplitude at the end of the MWNT is a result of thermal motion. For the first vibration mode the amplitude is the largest. With a thermal energy $\frac{1}{2}k_bT$ for each mode the vibration amplitude x_{rms} can be readily estimated from

$$x_{rms} = \sqrt{\frac{k_bT}{k_{nt}}} = \sqrt{\frac{4k_bTL^3}{3\pi Yr^4}} \qquad k_{nt} = \frac{3\pi Yr^4}{4L^3} \tag{2.15}$$

where k_b is Boltzmann's constant, T is the temperature in Kelvin, L is the length, Y is the Young's modulus, r is the radius of the nanotube and k_{nt} the stiffness (Hafner *et al.*, 2001). This estimate of the vibration amplitude works well for both individual and bundle nanotube tips (Lu, 1997). In Fig. 2.11(a) the vibration amplitude as function of the length of the MWNT is shown for diameters corresponding to our system, where we assumed a Young's modulus of 1 TPa. For a 2 μm long MWNT with a diameter ≥50 nm clamped at one side the vibration amplitude is less than 0.5 nm. Besides the thermal vibration of the probe it is important to know the bending of the MWNT under a certain load (i.e. stiffness). When a force F normal to the end of the probe is applied, the probe will bend over a distance d (see Fig. 2.11(b)) according to

$$d = \frac{F}{k_{nt}} = \frac{4FL^3}{3\pi r^4 Y} \tag{2.16}$$

The deflection d under a certain force is strongly dependent on the radius r and the length L of the MWNT. In the case a force of 10 pN is applied, a MWNT of 2 μm

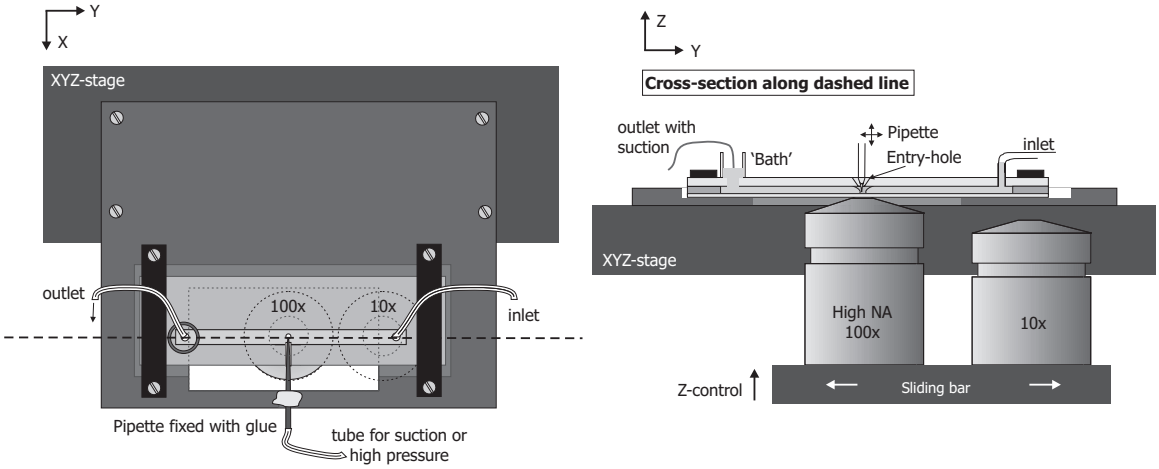

Figure 2.12. A schematic representation of the flow cell, the holder and its fixation to a XYZ-stage (the complete system is positioned in the horizontal plane). In addition the two objectives are shown that are mounted on a sliding bar.

and a diameter of 20 nm will bend a distance of ∼3.3 nm. If the diameter is 50 nm d will be <0.2 nm. It was verified that the binding strength between the MWNT and the silanized μm-pipette was high enough such that the MWNT is not displaced by indenting the DNA molecule with the MWNT and the pipette itself.

In contrast to the AFM where the end of a SWNT or MWNT is used as a probe in the SPOT microscope the side of the CNT is used. Touching the DNA molecule at a point closer to where the nanotube is attached, will shorten the effective length of the probe.

2.8 The flow cell

A new flow cell was designed in order to approach a stretched DNA molecule with the scanning probe system as shown in Fig. 2.12. The flow cell consisted of two layers of parafilm sandwiched between a precleaned microscope glass and a coverslip (170μm). A channel was cut out of the parafilm providing a flow channel with a height of ∼200 μm and a width of ∼5 mm. In the microscope glass three holes were powder-blasted (Wensink *et al.*, 2000). Two holes (ø2 mm) at the end of the flow channel act as entry and exit points for the flow channel. An additional entry-hole in the middle of the cell was created to enable the injection of the scanning probe. Due to the powder-blasting the entry-hole has a conical shape with a smaller diameter of 200 μm at the bottom side as indicated in Fig. 2.12. The other two holes are drilled after powder-blasting with a diamond drill to provide a cylindrical hole. A square glass capillary with an inner diameter of 50x50 μm^2 (VitroCom, Mountain Lakes, NJ) was aligned in between the coverslip and the microscope glass such that a μ-pipette for the bead immobilization can be injected into the flow cell with its end located below the entry-hole (stiffness approximately 4 nN/μm; Leuba *et al.* (2004)). This complete

sandwich was heated up shortly to 60 ^{o}C using a heating plate to provide a waterproof sealing. To prevent leakage through the center entry-hole a small reservoir was placed on top of the outlet hole. Because the size of the outlet was 10 times larger than the center entry-hole the highest fluid resistance is at this hole such that fluid leaves the flow cell through the outlet first. A small tube placed in the reservoir is actively sucking away fluid whenever it reaches the tube (see Fig. 2.12).

2.8.1 The flow cell holder

The flow cell is fixed to an aluminum holder using two plastic bars. Two objectives are mounted on a sliding bar. The high NA objective is required for the optical trap. The objective with a 10 times magnification is necessary to visualize the probe-pipette system for injection into the flow cell. The thickness of the holder is minimized at the position of the flow cell to be able to reach the upper side of the flow cell with the 10 times objective. The pipette for the bead immobilization is fixed to the holder using a rapid curing two component glue (Leuba *et al.*, 2004). An XYZ-stage (P-509, Physik Instrumente, Karlsruhe, Germany) operated in closed-loop mode, enables the accurate positioning of the bead immobilized on the pipette with respect to the optical trap by moving the holder and the flow cell. Movement of the objectives in the z-direction is controlled manually with a resolution of $\sim$1-5 μm.

2.9 The flow system

A flow system as shown in Fig. 2.13, was designed to be able to introduce the desired solutions in the flow cell. Using a 6-way selector valve (Upchurch Scientific, Oak Harbor, WA, USA) different solutions (buffer, beads, DNA, proteins, washing buffer) were introduced in the flow cell through a fluid line (Intramedic Polyethylene tubing, non-sterile, PE10, ID=0.28 mm, OD=0.61 mm Becton Dickinson, Franklin Lakes, NJ, USA). The flow rate was controlled by the pressure in a container in which the liquid containers are placed. The pressure in this container is measured with a sensor

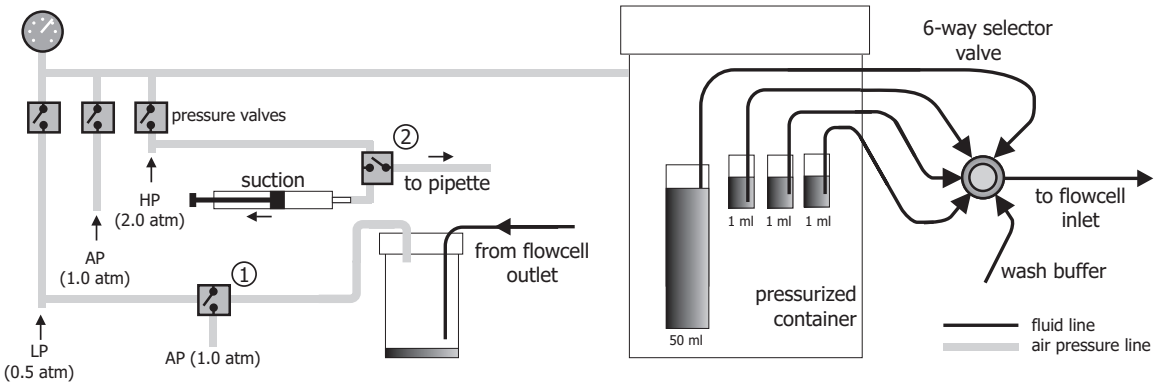

Figure 2.13. Schematic representation of the flow system.

and regulated to the desired pressure using three computer-controlled pressure valves that are connected to a high pressure (2.0 atm), an atmospheric, and a low pressure (0.5 atm) line respectively. Furthermore the low pressure line is used to achieve a low pressure in a second container that is connected to the outlet fluid line of the flow cell shown in Fig. 2.12. In this way fluid is actively sucked away and stored in this container. Pressure valve 1 allows the control of the suction by selecting atmospheric or low pressure. A high or low pressure, controlled by pressure valve 2, can be applied to the μ-pipette used to immobilize a bead. A syringe allows the application of a controlled suction. After each experiment the valve is switched to the high pressure line, which starts to flow air through the pipette. In this way the μ-pipette is prevented from being blocked by dirt present in the flow cell when it is not in use.

2.10 Combining SPM and OT: The SPOT

The experimental configuration of the scanning probe optical tweezers microscope is shown in Fig. 2.14. The pipette with the scanning probe is mounted on a piezo tube

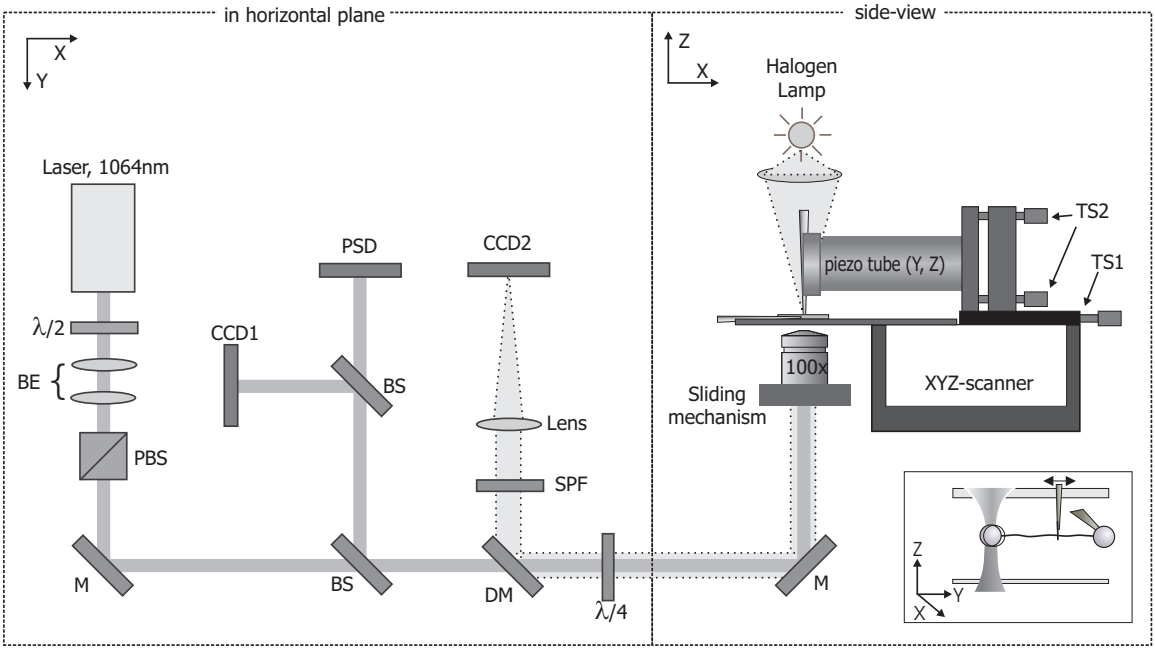

BE	Beam expander	**PSD**	Position sensitive detector
BS	Beam splitter	**SPF**	Short-pass filter
CCD	Charged coupled device	**TS**	Translation stage (TS1 with piezo stack)
DM	Dichroic mirror	**λ/2**	Half-wave plate at 1064nm
M	Mirror	**λ/4**	Quarter-wave plate at 1064nm
PBS	Polarizing beam splitter cube		

Figure 2.14. Schematic layout of the scanning probe optical tweezers (SPOT). The inset indicates the scanning direction of the probe (in Y).

that controls its position. This piezo tube is mounted on manual translation stages (TS). Due to the configuration of these two components the position of the probe can be controlled in all 3 dimensions with ∼5 μm accuracy.
During experiments a DNA molecule is scanned in the Y-direction (see inset figure). The hysteresis that a piezo tube exhibits is among other things a function of the scan range, scan speed and its position in the three dimensional volume within which it can move. An additional piezo stack has been integrated in the x-translation stage (TS1), which allows accurate positioning of the tip independently of the piezo tube. This preserves a constant hysteresis of the end of the piezo tube. The piezo tube system together with the flow cell holder are mounted on a linearized XYZ-scanner (P561, Physik Instrumente, Karlsruhe, Germany) required to control the position of the bead immobilized on the μ-pipette. Due to the mass of the tube and the holder, the resonance frequency of the stage is ∼40 Hz. Force-extension curves of a single DNA molecule are typically acquired at a speed <10 μm/s corresponding to frequencies in the range of 1-5 Hz. Whenever the flow cell is displaced with respect to the optical trap the probe moves with it, keeping the position of the probe within the entry-hole fixed.

Both the piezo tube and the XYZ stage are adressed by a multifunction data acquisition (DAQ) card. For most experiments described in this thesis a 12-bit DAQ card (PCI-MIO-16E4, National Instruments) was used if not mentioned. The scan range is 100 x 100 x 20 μm for the XYZ-stage and 20 x 20 x 7 μm for the piezo-tube. The piezo stack has a range of 8 μm. Images acquired with the CCD camera are digitized using an image acquisition (IMAQ) framegrabber card (PCI-1407, National Instruments). The IMAQ card is synchronized with the DAQ card using a programmable function interface (PFI) line of the DAQ card. Labview-written software controls the data and image acquisition as well as the position of the XYZ-scanner, the piezo tube and the piezo stack, dependent on the type of experiment.

2.11 Modes of operation

In the current configuration of the SPOT microscope there are 2 different operation modes available that are depicted in Fig. 2.15. Using the first mode (Fig. 2.15(a)) a 1D scan is made in the y-direction. In this case the indentation of the molecule is controlled manually by applying an offset voltage to the piezo stack responsible for the x-position of the probe. This mode can be used to detect individual proteins on the DNA or to measure friction between probe and DNA. The second mode (Fig. 2.15(b)) is a 2D scanning mode analogous to the force distance mode in SPM. The fast scanning direction is in the x-direction. Trace and retraces are acquired for the same y-position. After each completed cycle the probe is moved one step in the y-direction. One of the parameters that can be deduced using this mode is the adhesion force.

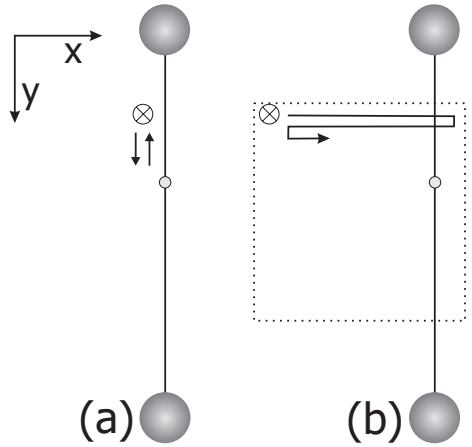

Figure 2.15. Operation modes of the SPOT. (a) A 1 dimensional scan mode where the indentation of the DNA molecule (in the x-direction) is controlled by an offset voltage applied to the piezo stack. This modes allows among other things mapping of the friction force. (b) A mode analogous to the force distance mode in SPM that can be used to measure for instance the adhesion force between the probe and the DNA molecule

2.12 Conclusions

The SPOT-microscope presented in this chapter is based on the combination of a reflection-based optical tweezers apparatus and a MWNT-functionalized μ-pipette as scanning probe. This microscope allows the localization of particles bound to a single stretched DNA molecule. The flow cell design in which an entry-hole facilitates the approach of a DNA molecule by a scanning probe offers flexibility in the type of scanning probe used. An important advantage of the SPOT-microscope in comparison with conventional SPM techniques such as AFM, NSOM and STM is the absence of a supporting surface for imaging dynamic processes. Since there is no surface nearby, proteins or other type of particles are not obstructed in their motion. Due to the stretching of a single DNA molecule with the optical tweezers a one dimensional scan is sufficient in order to obtain the location of a protein. This allows the determination of the 'instantaneous' position of particles at a much higher rate as in conventional SPM techniques where a two dimensional scan has to be performed.
However, in the current configuration where the optical tweezers is used as sensor, a stretching force of ∼10-50 pN is required to obtain a relevant signal. Besides topographical information, friction and adhesion forces can be measured using different modes of operation.

Chapter 3

Calibration of reflection-based OT

Optical tweezers are a sensitive force-measuring technique that allow force spectroscopy studies on the single molecule level. In this chapter we discuss the most commonly used calibration techniques required to measure forces with OT. For a bead size of 2.50 μm we found that the linear detection range of the apparatus was 0.57 μm, achieved with a position sensitive detector whereas this range was found a factor of 2 lower using a quadrant detector. For a transmission-based OT apparatus the difference in detection range for the position sensitive detector and the quadrant detector was not found. For the characterization of a single dsDNA molecule it is important to be able to measure forces up to at least 75 pN. To reach this force level within the linear detection range a minimum bead size of 1 μm must be used. The resolution of the reflection-based OT apparatus is limited by the thermal motion of the bead, but not only by the translational movements but also by rotational movements of the bead. The rotational movement is found to appear as 1/f-noise in the power spectral density of the deflection signal decreasing the resolution with which the position of the trapped bead can be determined.

3.1 Introduction

The basis of OT to be able to measure forces is the fact that the optical tweezers creates a harmonic potential well in which a bead is trapped. In the first section we present the physical equations. To measure forces the apparatus needs to be calibrated by determining the deflection sensitivity and the trap stiffness. However there are also limitations as the maximum detectable force and the resolution with which the position of the trapped can be determined that are discussed in Section 3.4 and 3.5 together with their dependence on the bead size. In Section 3.5 we discuss the sensitivity of the reflection-based OT apparatus for bead rotations.

3.2 Optical tweezers as force transducer

The optical tweezers creates a three-dimensional potential well for a trapped micron-sized bead that can be approximated by three independent harmonic oscillators, one

each for the x, y, and z direction. The potential energy of such an oscillator for one direction can be written as

$$U(x) = \frac{1}{2} k_{tr} (x - x_0)^2 \tag{3.1}$$

where k_{tr} is the trap stiffness typically expressed in pN/μm, x the position of the trapped bead, and x_0 its center position within the trap. The force needed to displace a trapped bead by a distance x is thus

$$F_{tr} = \frac{dU}{dx} = k_{tr} x \tag{3.2}$$

If the optics are well aligned, the x and y spring constants will be roughly the same; for a single-beam optical tweezers configuration the z spring constant is typically smaller by a factor of ∼5 (Neuman and Block, 2004).

In order to measure forces acting on the bead, both the trap stiffness in the desired direction and the position of the bead should be determined. The latter is obtained by measuring the deflection of the backscattered laser light using a position sensitive detector, resulting in a voltage according to

$$V_{det}(t) = \beta \cdot x(t) \tag{3.3}$$

where $V_{det}(t)$ is the time dependent detector response in Volt, β is the deflection sensitivity of the detector expressed as Volt/μm and $x(t)$ is the position of the trapped bead in time. In order to determine the force acting on the bead, the trap stiffness and the deflection sensitivity of the position sensitive detector were calibrated. In the following section calibration techniques determining these two parameters are discussed.

3.3 Calibration OT

Before discussing the various calibration techniques we look in more detail to the dynamical behavior of a trapped bead. Besides an inertial force $\mathbf{F_{inert}}$ indicating the resistance of the bead to an acceleration, the bead is subjected to a drag force $\mathbf{F_{dr}}$ resulting from the viscous medium around it, a force $\mathbf{F_{tr}}$ resulting from the optical trap and the so-called (thermal) Langevin force $\mathbf{F_{rand}}$ that represents the random Brownian forces originating from the thermal activity of the surrounding medium, a random Gaussian process. The governing equation of motion is

$$\begin{aligned} \mathbf{F_{inert}} + \mathbf{F_{dr}} + \mathbf{F_{tr}} &= \mathbf{F_{rand}} \\ m\ddot{x} + \gamma_0 \dot{x} + k_{tr} x &= F_{rand}(t) \end{aligned} \tag{3.4}$$

with m the mass of the bead and γ_0 the hydrodynamic drag coefficient (N · s/m). This equation can be simplified if we acknowledge that a micron-sized trapped bead

in water behaves as an extremely overdamped oscillator permitting to neglect $\mathbf{F_{inert}}$ since its effect is only just noticed for frequencies beyond 100 kHz. The hydrodynamic drag coefficient γ_0 can be calculated by Stokes' law (Reif, 1965) as

$$\gamma_0 = 6\pi\eta r_{bead} = 6\pi\rho\nu r_{bead} \tag{3.5}$$

where η is the fluid's dynamic viscosity (for water 10^{-3} N $\cdot$ s/m^2), ρ is the mass density of the fluid (water 10^3 kg/m^3) and ν is the kinematic viscosity (water 1 cSt=10^{-6} m^2/s) and r_{bead} the radius of the bead. All the experiments are done around 50 μm away from any surface where corrections to Stokes' law can be neglected (Gittes and Schmidt, 1998). This equation holds only for low Reynolds numbers (Rouzina and Bloomfield, 2001; Anselmi *et al.*, 1999) and for frequencies below 1 kHz. For higher frequencies hydrodynamic corrections should be taken into account since the fluid's velocity field around the sphere cannot be considered constant anymore and becomes frequency dependent (Landau and Lifshiftz, 1987; Berg-Sorensen and Flyvbjerg, 2004) as discussed in more detail in Section 3.3.2 and the Appendix.

Several calibration methods are available to determine the deflection sensitivity β and the trap stiffness k_{tr} necessary to convert the detector signal to a force. In Table 3.1 an overview of the calibration methods is presented.

Table 3.1. Overview of the calibration methods.

Methods	**Technique**	**Calibration parameters**
Flow	Continuous flow	Determines β
	Sawtooth modulation	Determines β and k_{tr}
	Sinusoidal modulation	Determines k_{tr}, requires β
Thermal motion	Equipartition	Determines k_{tr}, requires β
	Power spectral density	Determines k_{tr}
Force plateau dsDNA		Determines β

The flow methods are based on modulation of the drag force to initiate a displacement of the bead where a range of ±0.7 μm can be achieved dependent on bead size and trap stiffness. The thermal motion methods are based on analysis of bead displacements resulting from the thermal collisions of the surrounding medium that are in the order of 1-10 nm. A third calibration method (not mentioned in literature to our knowledge) is the determination of the deflection sensitivity by extending a single dsDNA molecule that exhibits a force plateau at 60-70 pN, initiating displacements of the trapped bead corresponding to $x_{bead} = F/k_{tr}$. In the next section we discuss these calibration methods in more detail where a division was made according to their ability to determine β or k_{tr}. Although the sawtooth modulation method also can be used to determine k_{tr}, it was only applied to acquire β.

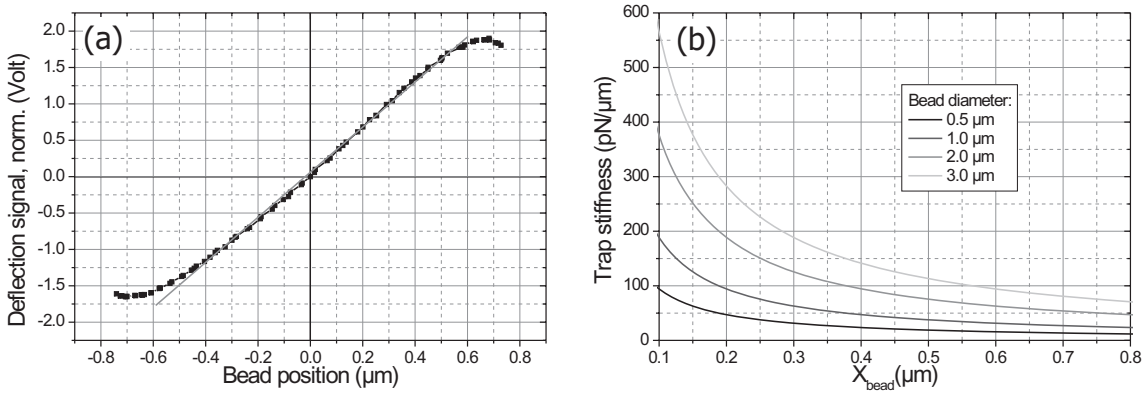

Figure 3.1. (a) A deflection curve for a 2.67 µm bead. (b) The (theoretically calculated) trap stiffness required to achieve a certain bead displacement using the sawtooth modulation method shown for different bead sizes. The scan range of the stage is 100 µm and the maximum driving frequency is 12.5 Hz, limited by video microscopy.

3.3.1 Deflection sensitivity

To determine the deflection sensitivity β the detector signal was related to the position of the bead, which in all cases was determined by applying a centroid method algorithm (Wuite *et al.*, 2000) to the optical microscope images. The conversion from pixels to nanometers in these images was achieved by imaging a calibration slide with a micrometer ruler, with lines spaced 10 µm from one another. In our microscope the typical conversion factor was 60 nm/pixel.

Continuous flow

The drag force acting on a trapped bead is increased stepwise by adjusting the flow rate within the flow cell, controlled by the pressure in the flow system. For each step it is ensured that the flow rate is constant; simultaneously optical images of the trapped bead and the position detector signals are recorded. In this way the detector output is related to the position of the bead. In Fig. 3.1(a) a typical deflection curve is shown for a 2.67 µm bead. The deflection sensitivity β is deduced from the slope of this curve around its zero position. Due to the S-shape of the curve the linear detection range is limited.

Sawtooth modulation

The flow around a trapped bead can be controlled by modulating the position of the flow cell using the XYZ stage since the trap is fixed with respect to the outer world (i.e. optical table). The flow velocity is identical in magnitude to the velocity of the stage. Modulation of the stage with a sawtooth function with amplitude A and frequency f results in a block wave response of the flow speed with amplitude $4Af$. As a result the drag force, linearly related to the flow speed, will cause a bead

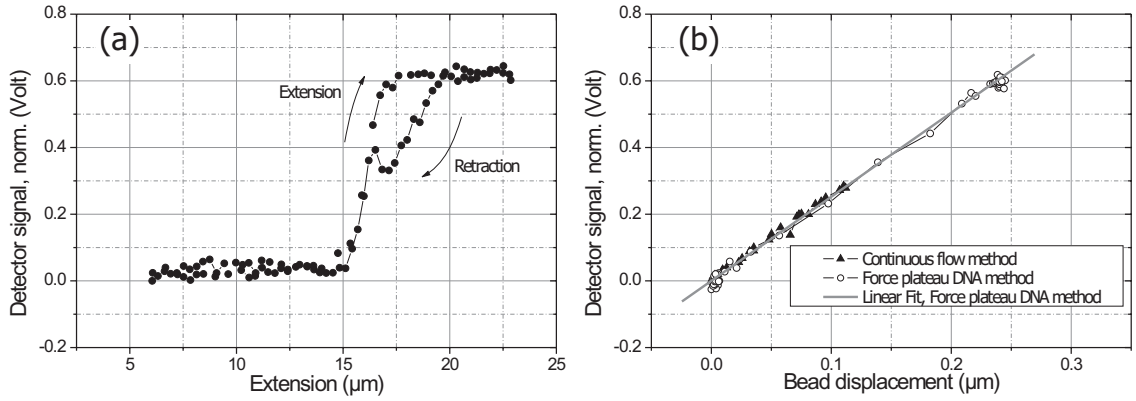

Figure 3.2. (a) A force-extension curve of a single dsDNA molecule used to determine the deflection sensitivity. (b) The deflection signal upon stretching the DNA molecule as function of the actual bead position determined from the optical images.

displacement $x_{bead}(t)$ according to

$$x_{bead}(t) = \frac{4Af\gamma_0}{k_{tr}}[1 - exp(-\frac{k_{tr}}{\gamma_0}t)] \tag{3.6}$$

with the term between the square brackets taking into account the relaxation time ($\gamma_0/k_{tr} \approx$ 0.2-1 ms) of the system. To determine the position of the bead using video microscopy, the bead should have a constant position during 1 video frame of 40 ms (25 Hz). This limits the driving frequency of the stage to 12.5 Hz.
By moving the stage at different constant velocities the same deflection curve can be acquired as with the continuous flow method, shown in Fig. 3.1(a). However to achieve a displacement extending the linear detection range, the trap stiffness had to be lowered. In Fig. 3.1(b) the trap stiffness required to achieve a certain bead displacement is depicted for various bead sizes. For the amplitude A we considered a maximum scan range of 100 µm and a maximum driving frequency of 12.5 Hz.

Plateau DNA molecule

Another method to determine the deflection sensitivity is by acquiring a force-extension curve of a single dsDNA molecule. As a single DNA molecule is stretched, both the deflection signal and the position of the trapped bead are recorded. Applying the centroid method algorithm to the images the displacement of the bead was related to the detector signal. In Fig. 3.2(a) a typical force-extension curve obtained in this way is shown. The extension of the molecule is determined by the distance between the beads corrected for the radii of both beads. The force-extension curve of a single dsDNA molecule exhibits a constant force plateau. Consequently the bead position is nearly constant at this plateau. In Fig. 3.2(b) the detector signal (Volt) during the extension of the molecule is plotted as function of the bead displacement as determined from the optical microscope images showing a linear relation. The slope of a

linear fit obtains the deflection sensitivity β. Since there is a typical hysteresis visible during retraction of the DNA molecule this part of the curve is not included in the determination of β.

For the same bead a deflection curve was obtained using the continuous flow method. This curve is also plotted in Fig. 3.2(b) (solid triangles). The maximum displacement achieved was 0.12 μm after which the bead was pushed out of the trap by a passing bead. Nevertheless the obtained data is in good agreement with the data acquired with the force-extension curve.

3.3.2 Trap stiffness

Equipartition method

A trapped bead is in thermal equilibrium with a much larger system (the surrounding fluid). An important result of statistical mechanics is the equipartition theorem that states that a system has an average energy of $\frac{1}{2}k_bT$ for each quadratic term appearing in its Hamiltonian. Thus each rotational or translational component of the random thermal motion of a molecule has an average kinetic energy of $\frac{1}{2}k_bT$. For a harmonic potential well the average potential energy $\langle U(x)\rangle$ can be described as

$$\langle U(x)\rangle = \frac{1}{2}k_{tr}\left\langle (x-x_0)^2\right\rangle = \frac{1}{2}k_bT \tag{3.7}$$

where x_0 is the mean (equilibrium) position. The brackets denote the time-averaged quantity

$$\left\langle (x-x_0)^2\right\rangle = x_{rms}^2 = \lim_{T\to\infty}\frac{1}{T}\sum_{i=1}^{N}(x_i-\bar{x})^2\cdot\Delta t \tag{3.8}$$

which is actually the statistical variance of the bead x-coordinate with T being the total observation time, Δt being the time interval between observations, and $\bar{x}$ being the sample mean. Thus if we can accurately estimate the statistical variance we can deduce the spring constant, k_{tr}. In Fig. 3.3(a) time signals are shown for a 2.67 μm bead acquired at different trap stiffnesses with a sample frequency of 100 kHz. A higher trap stiffness results in a stronger confinement of the bead and therefore a smaller variation of the position.

Another way of determining the trap stiffness based upon the equipartition theorem is fitting a Boltzmann distribution to the position histogram of the bead. The probability density $\rho(x)$ of finding the bead at a certain position can be described by

$$\rho(x) = \frac{1}{Z}e^{-U(x)/k_bT} = \frac{1}{Z}e^{-\frac{1}{2}k_{tr}(x-x_0)^2/k_bT} \qquad = \frac{1}{\sigma\sqrt{2\pi}}e^{-\frac{-(x-x_0)^2}{2\sigma^2}} \tag{3.9}$$

where Z is the partition function normalizing the probability density function. Actually the Boltzmann distribution can be represented by a Gaussian function that

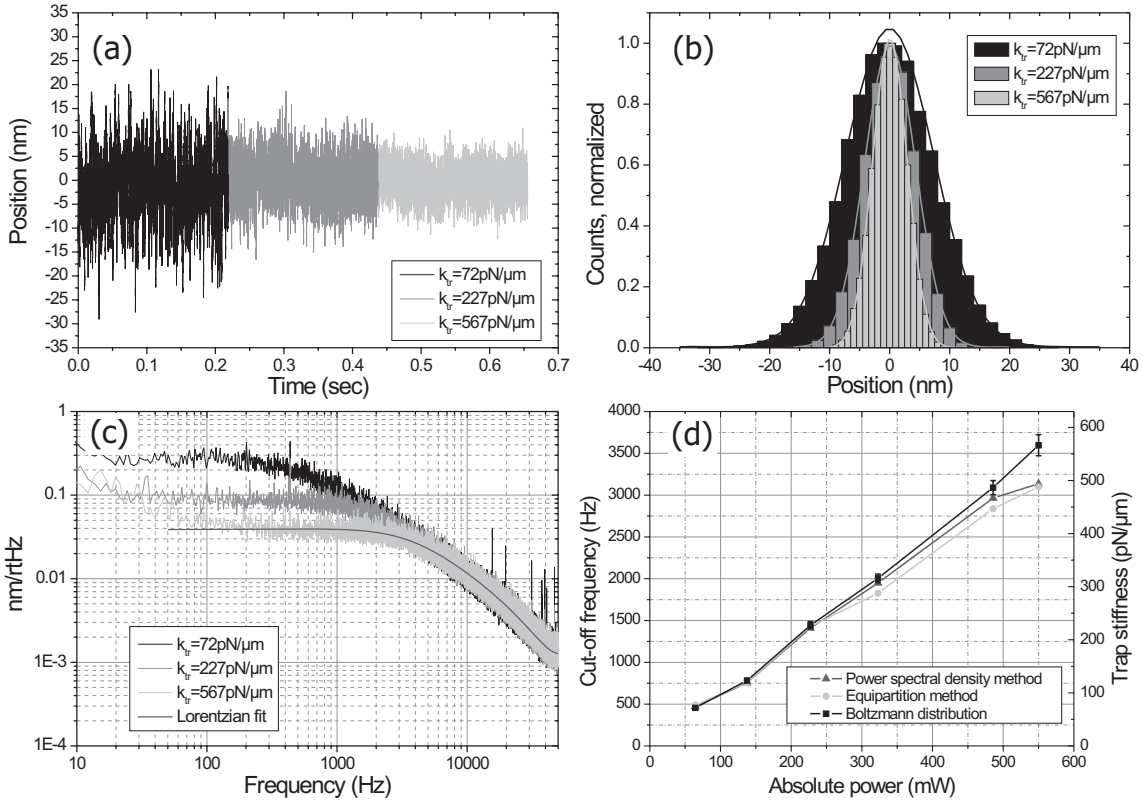

Figure 3.3. (a) Position of a 2.67 μm bead as a function of time acquired at different trap stiffnesses. (b) Histogram presenting the position distribution of the bead for the position signals shown in (a). (c) Power spectral densities calculated from the position signals shown in (a). A Lorentzian fit for the highest trap stiffness is shown with a solid line. (d) The cut-off frequency (and therefore the trap stiffness) as function of the trapping power (at the back-aperture of the objective) as determined with the equipartition method and the power spectral density method.

expresses the distribution as a function of statistical parameters given by the latter part of Eq. 3.9 with σ the standard deviation and σ^2 the variance. Fitting the probability density function, with parameters Z and k_{tr} to a histogram of the position's ensemble obtains the trap stiffness k_{tr} (Fig. 3.3(b)).

Power spectrum method

Fourier transforming the equation of motion Eq. 3.4 yields the power spectral density of the position of the bead, where the thermal white-noise force magnitude can be expressed as

$$S_F(f) = 4\gamma_0 k_b T \tag{3.10}$$

and therefore the power spectral density reflects the transfer function of the optical tweezers. For such a Brownian harmonic oscillator, where motion takes place at small

Reynolds numbers, one can show that the power spectral density of the bead position is (Gittes and Schmidt, 1998)

$$S_x(f) = \frac{k_b T}{\gamma_0 \pi^2 (f_c^2 + f^2)} \tag{3.11}$$

where k_b is Boltzmann's constant, T is the absolute temperature and γ_0 the hydrodynamic coefficient. The corner-frequency f_c of this Lorentzian function is a function of the trap stiffness k_{tr} related as $k_{tr} = 2\pi\gamma_0 f_c$. The units of $S_x(f)$ are nm^2/Hz. In Fig. 3.3(c) the power spectral density is given for different trap stiffnesses. At low frequencies the power spectrum is approximately constant, given by

$$f \ll f_c \Rightarrow S_x(0) \approx \frac{k_b T}{\gamma_0 \pi^2 f_c^2} = \frac{4\gamma_0 k_b T}{k_{tr}^2}$$

Note that the thermal white-noise force magnitude is reflected by $S_F(f) = 4\gamma_0 k_b T$ and $S_x(0)$ thus reflects the confinement of the bead, dependent on the trap stiffness. For frequencies $f \gg f_c$ the power spectrum drops off like $1/f^2$, indicating free diffusion. Integrating the power spectral density of the whole frequency range the position variance is obtained

$$x_{rms}^2 = \int S_x(f) df = \frac{k_b T}{k_{tr}} \tag{3.12}$$

The trap stiffness can be deduced by fitting the Lorentzian function given by Eq. 3.11 to the measured power spectral density. Introducing Einstein's equation $D = k_b T/\gamma_0$, which relates the diffusion constant D (m^2/s) to the Boltzmann energy and the drag coefficient, the fit parameters are f_c and D. In Fig. 3.3(c) a Lorentzian fit is shown for the highest trap stiffness, corrected for the effects of a finite sampling frequency, the anti-aliasing filter and hydrodynamic effects discussed in detail in the Appendix.

First we compare the power spectrum method, the equipartition method and the trap stiffness obtained by fitting the Boltzmann distribution. For different laser trap powers the stiffness is determined using these methods. In Fig. 3.3(d) the results are shown where the deduced trap stiffness is plotted versus the absolute power at the back aperture of the objective. Using the power spectrum method a linear relation between the power and the trap stiffness was found as expected. For both the equipartition method and the Boltzmann distribution fit method a deviation is found at higher powers. Referring back to the power spectra shown in Fig. 3.3(c) one can see that for this particular bead at a high trap stiffness '1/f-noise' is visible for frequencies <100 Hz (origin of this noise will be discussed in Section 3.5.1). The integral of this power spectral density, reflecting $\langle x^2 \rangle$ includes this 1/f-noise resulting in an underestimation of the trap stiffness. In contrast, the power spectrum method allows selection of a fit range beyond 100 Hz and is therefore unaffected by this 1/f-noise resulting in an appropriate determination of the trap stiffness.

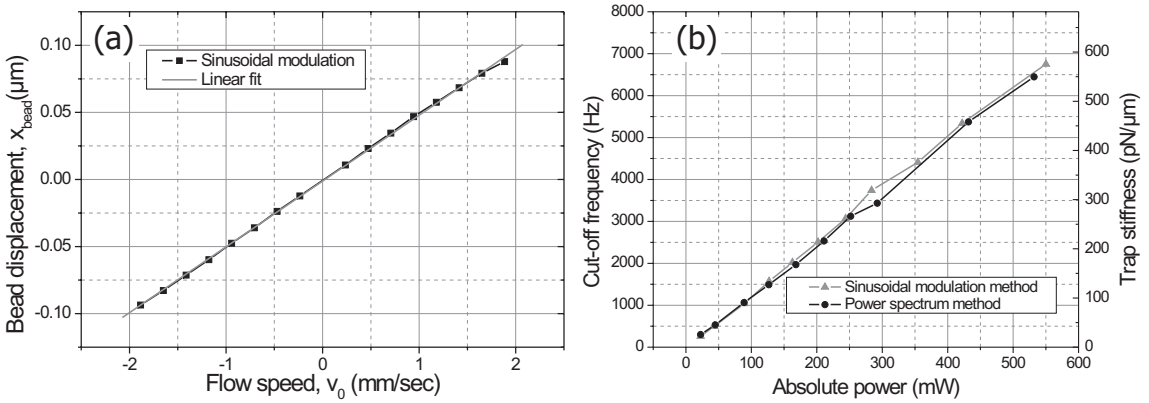

Figure 3.4. (a) Trap stiffness calibration for a 1.44 µm bead using sinusoidal modulation of the flow speed. Plotted is the amplitude x_{bead} versus the corresponding velocity v_0 obtained at the maximum trap stiffness. (b) The cut-off frequency and therefore the trap stiffness for different laser trap powers as determined with the power spectrum method and the sinusoidal method, both applied to the same 1.44 µm bead.

Sinusoidal modulation

Similar to the sawtooth modulation method the position of the flow cell can be modulated with a sinusoidal function. The flow speed that equals the velocity of the stage, can be derived as

$$v_{st} = \frac{d}{dt}x_{st} = \frac{d}{dt}[Asin(2\pi ft)] = 2\pi fAcos(2\pi ft) = v_0 cos(2\pi ft) \tag{3.13}$$

with x_{st} and v_{st} respectively the position and the velocity of the stage. The applied scan range of the stage is indicated with A and the driving frequency with f. The bead displacement x_{bead} as a result of this is

$$x_{bead} = \frac{F_{drag}}{k_{tr}} = \frac{\gamma_0 v_0}{k_{tr}} cos(2\pi ft) \tag{3.14}$$

that holds for $f < f_{cut}$. For driving frequencies beyond the corner frequency the bead will not be able to follow the applied motion anymore, resulting in a phase delay. Determining the amplitude of the sinusoidal movement of the bead the factor γ_0/k_{tr} can be calculated as

$$\frac{\gamma_0}{k_{tr}} = \frac{x_{bead}}{v_0} \tag{3.15}$$

Increasing v_0 stepwise by increasing the driving amplitude A or the frequency f, x_{bead} can be determined as a function of v_0 as shown in Fig. 3.4 for a 1.44 µm bead. The slope of this curve gives an accurate value for γ_0/k_{tr}. Note that for this method the deflection sensitivity must be known. Whereas the driving frequency for the stage in the sawtooth modulation method must be limited to 12.5 Hz due to the video

microscopy, here the driving frequency is limited by the resonance frequency of the stage. The unloaded resonance frequency of the stage is 190 Hz, but due to the mass of all the mounted components the driving frequency is limited to 40 Hz. In Fig. 3.4(b) this method is compared with the power spectrum method where the discussed corrections are included. Where the power spectrum method relies on the thermal fluctuations of the bead around its center position (typically 1-10 nm), the sinusoidal modulation method displaces the bead over a much larger range (0.3-0.6 μm at a trap stiffness of 500 pN/μm and a bead size of 2.50 μm). Both methods are in good agreement with each other.

3.4 Linear detection range

Besides determining the trap stiffness k_{tr} and the deflection sensitivity β it is important to know the maximum measurable force. In this section we discuss the dependence of the linear detection range on the type of position detector used for both a reflection and transmission-based optical tweezers apparatus. For the reflection-based apparatus we furthermore discuss the influence of the bead size on the detection range and consequently the maximum measurable force.

3.4.1 PSD versus QD

In order to measure the deflection of a light beam two types of position detectors are commonly used. The first type is a quadrant detector (QD) that measures differences in signals from the quadrant segments, schematically depicted in Fig. 3.5(a). The second type is a position sensitive detector (PSD). A light beam impinging on the detector surface creates a photocurrent that is split between the two electrodes connected to the n-type layer according to ohmic laws as shown in Fig. 3.5(b). This yields positional information about the center of energy of the light spot. Both detector types were tested in the reflection-based OT apparatus and a transmission-based

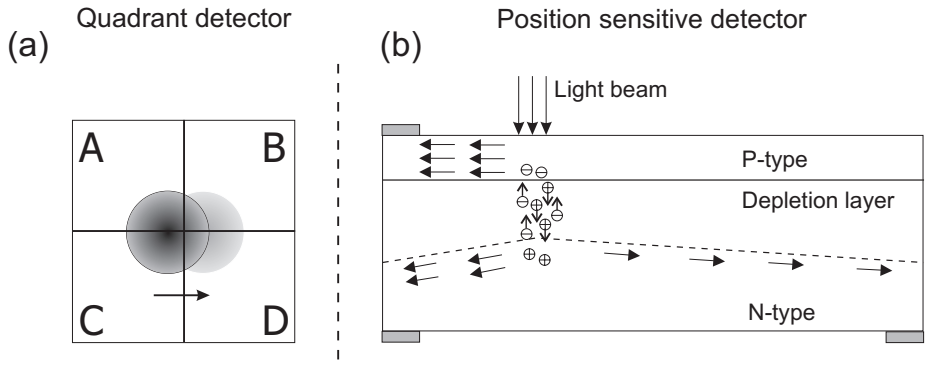

Figure 3.5. A schematic drawing representing the operation of the quadrant detector (a) and the position sensitive detector (b).

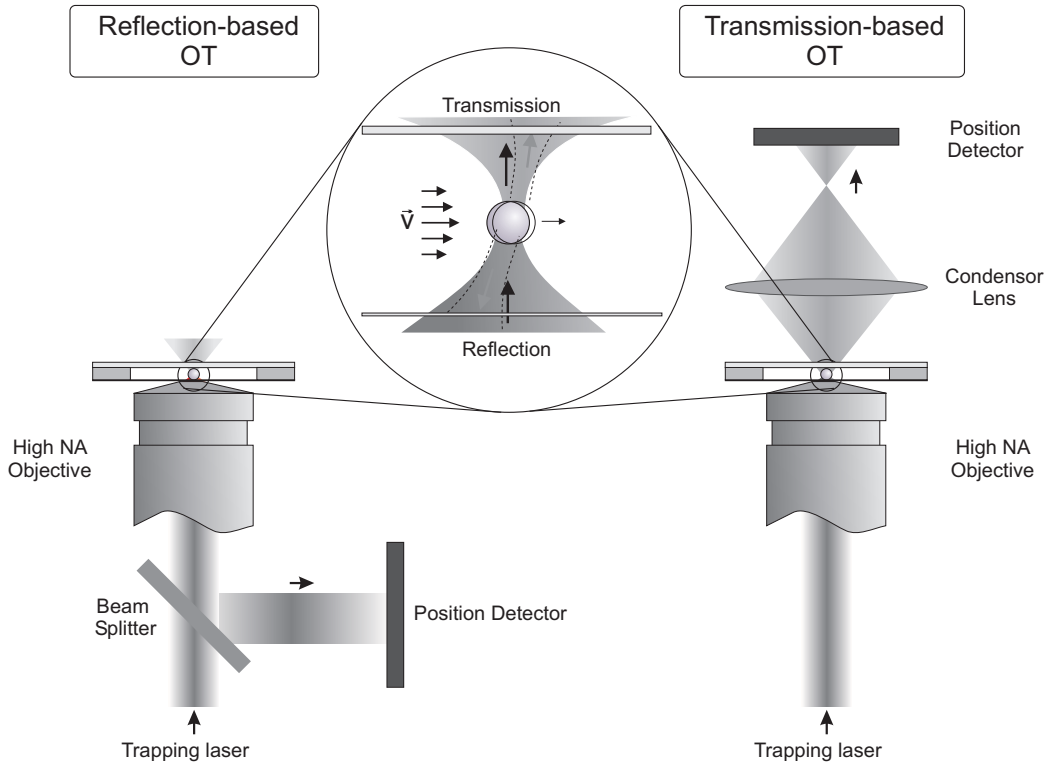

Figure 3.6. Detection principles for the reflection-based and transmission-based OT apparatus.

OT apparatus (Bennink *et al.*, 2001). In both microscopes the optical trap layout was similar and in addition the laser, the objective and the beam expander were from the same manufacturer and the same types. The detection part of the two microscopes is shown in Fig. 3.6. For the transmission detection a condenser lens (NA 0.9) collected a part of the light transmitted by the trapped bead and directed it onto the position detector, which was positioned behind the conjugate back focal plane of the condenser lens. As in the reflection-based apparatus, a quarter-wave plate was incorporated just in front of the objective (not shown in Fig. 3.6). A polarizing beam splitter was placed in between the condenser lens and the position detector to direct 50% of the transmitted light onto a CCD camera (Panasonic F15) for visualization of the transmission pattern. We used a neutral density filter in front of this beam splitter to decrease the laser intensity to measurable levels. Using the continuous flow method we determined deflection curves for 2.50 μm polystyrene beads (Polysciences) using the DLS10 PSD (UDT, Hawthorne, CA, USA) and the S5891 QD (Hamamatsu, Japan). Moreover we acquired images of the deflection pattern as 'seen' by the detector using the CCD camera.

For the reflection-based apparatus the deflection curves acquired with the PSD and the QD on the same 2.50 μm bead are shown in Fig. 3.7(a). Also the reflection images acquired at a bead position of -0.6 μm, 0.0 μm, and +0.6 μm are given,

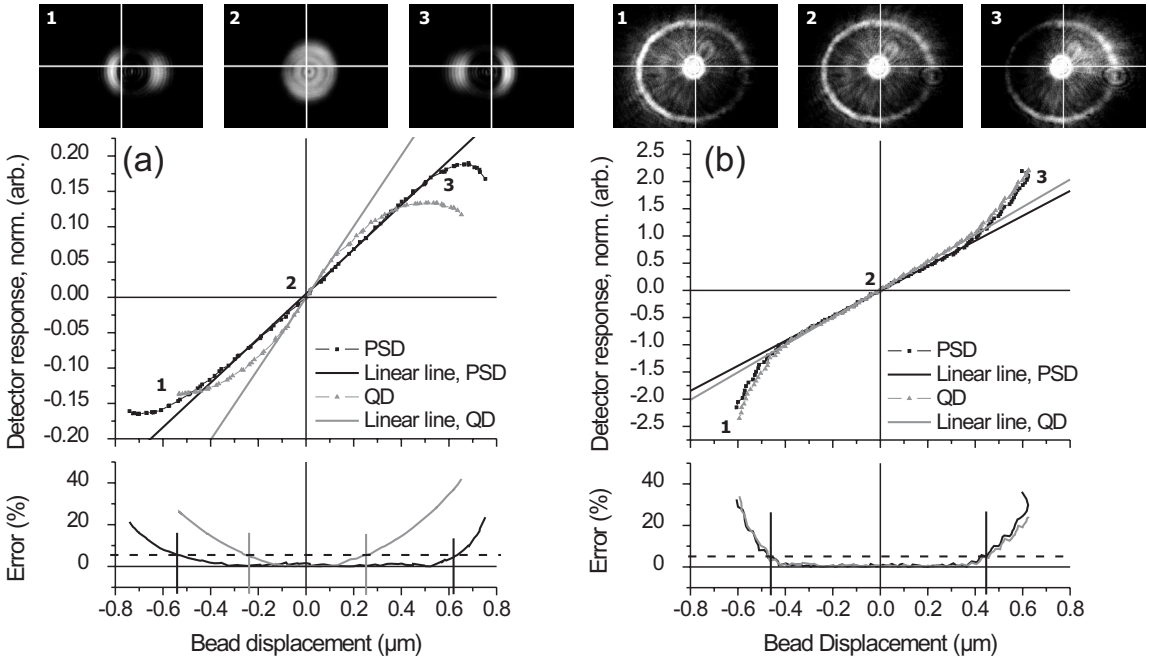

Figure 3.7. Deflection curves for a 2.50 μm bead acquired in (a) the reflection-based OT apparatus integrated in the SPOT microscope and (b) a transmission-based OT apparatus. The CCD images visualizing the deflection pattern are acquired for a bead position of -0.6, 0, and +0.6 μm indicated with the numbers 1,2, and 3 respectively in both the images and the deflection curves.

where the positions are indicated in the deflection curve with the numbers 1, 2, and 3 respectively. The slope of the curve around the center position of the bead was determined. In a next step the difference between the experimental data and a linear line having this slope was calculated. Subsequently the difference was divided by the value of the linear line at 1.0 μm and expressed as a percentage, shown in Fig. 3.7. The linear range was defined as the region in which this deviation was less than 5% and expressed as a range with respect to the center position of the bead. As a result the linear detection range for a 2.50 μm bead measured with a QD is 0.25 μm whereas the range measured with a PSD is 0.57 μm. The backscattered reflection pattern of a trapped bead (see Fig. 3.7(a)) not only shifts for a displacement of the bead, but also changes shape, especially for larger displacements. In the reflection image for a displacement of -0.6 and +0.6 μm the pattern exhibits two high intensity regions. The QD, which measures the intensity difference across a border indicated in the reflection images as a white cross will not measure a movement of the spot at higher bead displacements, because there is no light intensity transferred across this border due to the black region. Only a relative change in intensity of the two distinct high intensity regions will be detected. The PSD on the other hand determines the center of intensity of the incident spot and circumvents this problem. Another property of the QD is that the deflection sensitivity is dependent on spot size. The smaller the

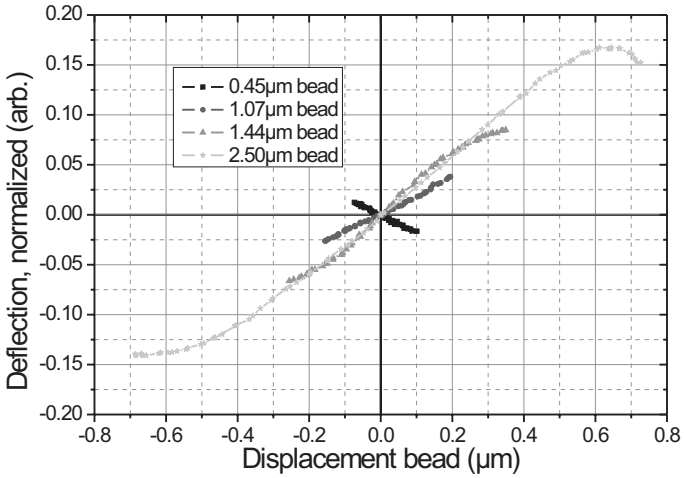

Figure 3.8. Position sensitive detector signal as a function of the bead position for different bead sizes in a reflection-based instrument.

spot the higher the deflection sensitivity. Because the PSD determines the center of energy we found that it is insensitive for spot size as expected.

For the transmission-based apparatus the typical deflection curves for the PSD and the QD are presented in Fig. 3.7(b). The images of the transmission pattern are recorded for a bead position of -0.6 µm, 0.0 µm, and +0.6 µm. The deflection curves are somewhat noisier when compared to the ones for the reflection-based apparatus, induced by small flow instabilities originating from the pressure system controlling the flow speed. For both position detectors the linear range is 0.45 µm, accepting a maximum error of 5% as deduced from the error graph. Outside the linear range the deflection sensitivity increases. Moving the condenser lens to another position did not change this behavior qualitatively.

3.4.2 Different bead sizes

Using the PSD (UDT-DLS10) as position detector the influence of the bead size on the deflection sensitivity and the linear detection range was investigated. Deflection curves were acquired for four different bead sizes of 0.45, 1.07, 1.44, and 2.50 µm as shown in Fig. 3.8. For each bead size we recorded deflection curves of multiple beads and corresponding power spectral densities with a sampling rate of 100 kHz for a period of 21 seconds. From these results we determined parameters such as the deflection sensitivity, the linear range and the trap stiffness. These were averaged over a number of beads with the same size and the results are shown in Table 3.2. Both the values for the light power at the position sensitive detector and the trap stiffness are given for the maximum achievable laser power in our microscope, which was 550 mW at the back aperture of the objective.

For the 1.07 µm beads the highest trap stiffness was found, which is in agreement with previous results shown by Simmons *et al.* (1996) also for a laser wavelength of λ=1064 nm. According to Ashkin (1992), for Rayleigh particles ($r \ll \lambda$) the trapping force depends on r^3. On the other hand, for large particles ($r \gg \lambda$), where the ray

Table 3.2. Experimental results for different bead sizes.

Bead size (μm)	**Reflected Light power** (μW)	**Trap stiffness** (pN/μm)	**Deflection sensitivity** (V/μm)	**Linear range** (μm)	**Force range** (pN)	**Limitation**
0.45	76 ± 2	334 ± 48	-0.16 ± 0.02	0.10	33	Escape Force
1.07	418 ± 22	511 ± 31	0.17 ± 0.01	0.15	77	Escape Force
1.44	464 ± 37	310 ± 18	0.32 ± 0.03	0.24	74	Reflection pattern
2.50	235 ± 59	242 ± 7	0.28 ± 0.02	0.57	138	Reflection pattern

optic regime holds, the trap stiffness is decreasing for increasing bead diameter. Our results, which are for sizes of particles in between these regimes, are consistent with these predictions. For the 1.44 and 2.50 μm beads we found the highest deflection sensitivities, $\sim$ 0.28 V/μm, whereas for the 1.07 and 0.45 μm beads this was a factor of 2 lower. A remarkable result is the change in sign of the deflection sensitivity for the 0.45 μm beads.

For the 1.44 μm and 2.50 μm beads the linear range is limited by the shape of the reflection pattern at large displacements, whereas for the 1.07 μm and 0.45 μm beads the maximum displacement is limited by the escape force, which is the maximum force that can be applied on the bead just before it is pushed out of the trap. The linear detection range determines the maximum measurable force in the OT apparatus via the trap stiffness. For DNA force spectroscopy experiments a minimum force range of 75 pN is needed in order to identify a single dsDNA molecule with its unique force plateau at 60-70 pN. For the trap stiffness values given in Table 4.1 the force range for the 2.50 μm bead with a value of 138 pN is the largest. For both the 1.44 μm and 1.07 μm beads the maximum force that can be measured is $\sim$75 pN. Although the linear range for the 1.44 μm bead is higher, the force ranges are similar due to the higher trap stiffness of the 1.44 μm beads. The maximum force that can be measured with 0.45 μm beads was found to be 33 pN.

For our application of force spectroscopy of single dsDNA molecules beads with sizes >1 μm are preferable. The use of smaller bead sizes is currently limited by the maximum achievable trap stiffness for these beads. Another important parameter is the light power impinging on the detector. A higher light power results in a higher signal-to-noise ratio making the 1.07 and 1.44 μm preferable with respect to the 2.50 μm bead. However larger beads makes it easier to catch a single DNA molecule when they are introduced in the flow cell due to their size and the higher amount of available streptavidin sites. Therefore we used 2.67 μm beads that are streptavidin coated (the 2.50 μm were not coated).

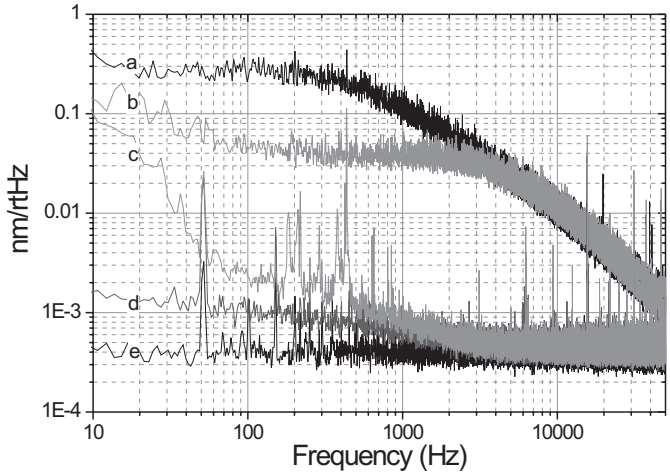

Figure 3.9. Noise levels of the reflection-based OT apparatus. The Brownian motion of a 2.67 μm bead is shown for a low (a) and a high (b) trap stiffness. The total noise is given by curve (c) containing electronic noise (curve (d)), laser noise and noise originating from air convection, mechanical vibrations and acoustics. Curve (e) is the electronic noise of the 16-bits DAQ card.

3.5 Noise limitations reflection-based OT

In a well-designed optical tweezers apparatus the limiting noise source determining the resolution is the thermal noise of the trapped bead. To characterize the instrument and thermal noise power spectral densities were acquired. In Fig. 3.9 the power spectral densities for a 2.67 μm bead at two trapping laser powers are shown. Additional spectra indicate the instrument noise sources. The basic noise level indicated by curve (e), is the electronic noise from the 16-bit DAQ card (PCI-6052E, National Instruments) used to digitize the analog deflection signals, in this case $3 \cdot 10^{-4}$ nm/$\sqrt{Hz}$. Although the electronic noise is measured as a voltage it attains a meaningful value when converted to nanometers using the deflection sensitivity for the 2.67 μm bead, in this case 3.07 V/μm. The dark current from the position sensitive detector (DL100-7-KER, Pacific Silicon Sensors) is shown in curve (d) and is a result of created electron-hole pairs in the absence of any light through thermal agitation. PSDs when compared to QDs generally have a higher dark current. For comparison the dark current of the DL100-7-KER (PSD) is typically 80 nA at a bias voltage of -10 Volt whereas the dark current for the S5981 (Hamamatsu; QD) is 0.60 nA for a bias of -15 Volt. The maximum level is $2 \cdot 10^{-3}$ nm/$\sqrt{Hz}$, which is far below the thermal motion of the trapped bead. Finally the total noise in the system is shown in curve (c) that has been acquired in a similar way as the power spectral density of the trapped bead with the difference that nothing was trapped. Contributions to the total noise (besides the electronic and dark current noise) are laser noise in the form of pointing instability and power fluctuations, and air convection leading to fluctuations in the air density and thereby variations in the refractive index, which in turn results in pointing instabilities of the laser. Acoustical noise and mechanical vibrations can

lead to displacements and fluctuations of optical components leading to positional noise. Vibrational isolation of the microscope was therefore performed by placing the optical table on rubber tyres. To prevent air convection as much as possible the laser path was shielded as it travels through air. The total noise slightly influences the spectrum of the trapped bead at a trap stiffnesses >300 pN/μm in the low frequency regime (<200 Hz).

For a system where the noise level is determined by the thermal motion of the bead the position variation is given by Equation 3.12. The resolution can be improved by low-pass filtering the deflection signal with a roll-off frequency B below the corner-frequency f_c of the optical trap. In this case the remaining variation x_{rms}^2 is approximated by the integrated power below B and equals

$$x_{rms} = \sqrt{\frac{4\gamma_0 k_b T B}{k_{eff}^2}} \tag{3.16}$$

where k_{eff} is the effective stiffness. A stretched DNA molecule attached to a trapped bead will effectively increase the spring constant that the bead experiences ($k_{eff} = k_{tr} + k_{dna}$), resulting in a reduced variation of the bead position. For a trap stiffness of 100 pN/μm the positional fluctuations, x_{rms}, are 6.4 nm and for a trap stiffness of 500 pN/μm 1.3 nm in the case the bandwidth B is limited to 1 kHz. At a high trap stiffness (curve (b)) it can be seen that the power spectral density for this bead shows 1/f-noise for frequencies <200 Hz. In the next section we focus on the origin of this noise.

3.5.1 Rotation of the bead

To measure the position of the bead, backscattered trapping laser light was used. Considering ray optics and tracking a single reflected light ray, the (fresnel) reflection coefficient is dependent on the incoming angle of the ray. This causes the total backscattered intensity profile to be sensitive for any irregularities or dirt particles present on the bead surface. If the backscattered pattern is not symmetric its center of energy will not coincide with the center of rotation of the bead. As a result the detection system becomes sensitive for rotations of the bead. This is demonstrated in Fig. 3.10. Rotation of a trapped bead is induced by approaching it with a μ-pipette causing asymmetry in the flow profile, which drives rotation of the bead. During a period of 2.5 sec the deflection signal and images of the reflection pattern (using CCD2 in Fig. 2.8) were recorded. The amplitude of the variation observed for this rotation is ∼4% of the maximum deflection amplitude obtained during the recording of a force-extension curve of a single dsDNA molecule. When expressed as a force the amplitude of this rotation is in the order of ∼2 pN.

A centroid method was applied to the images to determine the center of energy as indicated with the black cross-hair in the image shown in Fig. 3.10. The center of energy determined from the images is plotted together with the deflection signal

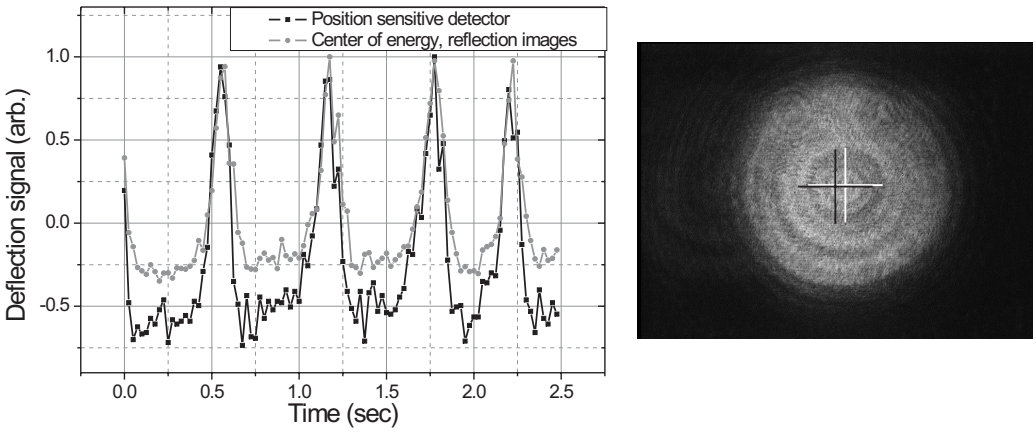

Figure 3.10. The deflection signal for induced rotations of the bead. Dissimilarities in the shape of the bead results in a slightly asymmetric reflection pattern. Consequently the center of energy of the reflection pattern (indicated with a black cross-hair in the right picture) is not overlapping with the center of rotation (indicated with the white cross-hair). In this case the detection system is sensitive for rotations of the bead as shown in the left figure where a time signal is shown.

where both signals are normalized to 1, showing the effect of the rotation of the bead. The working principles of a PSD and the center of energy method applied on the reflection images are similar and therefore show the same characteristics.

For rotation a similar equation of motion can be formulated as for translation (see Eq. 3.4).

$$\sum M = J \cdot \ddot{\theta} \qquad\qquad J\ddot{\theta} + \gamma_{rot}\dot{\theta} + k_{rot}\theta = M_{rand}(t) \tag{3.17}$$

where θ is the angle of rotation, $J = 2/5mr_{bead}^2$ the rotational mass , γ_{rot} the rotational Stokes drag for a sphere, k_{rot} the rotational stiffness, and $M_{rand}(t)$ the thermal (white) noise term. Following the same considerations as for the translational movement the first term can be neglected since it is an overdamped system (La Porta and Wang, 2004). For a sphere the rotational stiffness can be considered zero such that the final equation of motion yields

$$\gamma_{rot}\dot{\theta} = M_{rand}(t) \tag{3.18}$$

where $\gamma_{rot} = 8\pi\eta r^3 = \pi\eta d_{bead}^3$ (Romano *et al.*, 2003). As a consequence the power spectral density for pure rotation will only show the drag component which appears with a '-1' slope (1 order of magnitude per decade). We have shown that we are sensitive for rotations of the bead, experimentally however, it is not possible to separate the translational and rotational movement of the bead. The power spectral density of the deflection signal will therefore show both the rotational and translational properties. Although for the translational movement the deflection sensitivity of the detector is known this is not the case for rotational sensitivity. The appearance of the 1/f characteristics of the rotation in the power spectral density of the signal is dependent on

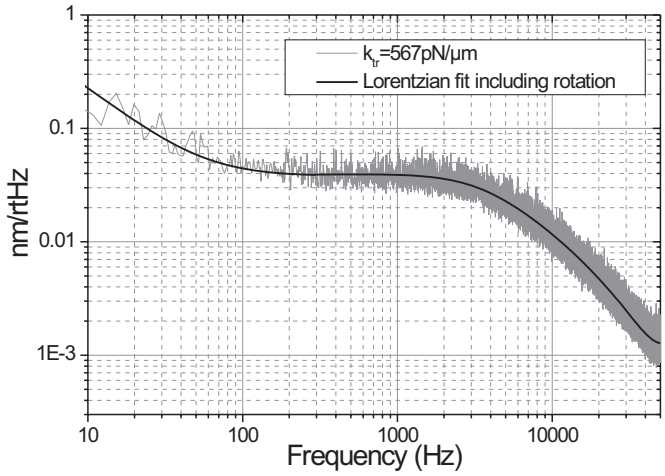

Figure 3.11. Power spectral density of a 2.67 µm bead showing 1/f-noise in the low-frequency part. A Lorentzian was fitted that included a model for the rotational movement of the bead according to Eq. 3.19.

the relative translational and rotational sensitivity. In Fig. 3.11 the power spectral density of a 2.67 µm bead is shown showing where we fitted a Lorentzian including Eq. 3.18 according to

$$S_{tot} = S_{trans} + S_{rot} = \frac{D_x/\pi^2}{f_c^2 + f^2} + A\frac{D_\theta/\pi^2}{f^2} \tag{3.19}$$

where S_{trans} and S_{rot} reflects resp. the translational and rotational power spectral density and A takes into account the unknown rotational sensitivity. D_x and D_θ are resp. the translational and rotational diffusion constants. For the fit shown in Fig. 3.11 we actually included all the corrections for the translational movement discussed in the previous sections. As can be seen the model describes the power spectral density very well. Lowering the trap stiffness the plateau of the translation power spectral density at lower frequencies is increasing, whereas the 1/f characteristics related the rotational drag are unaffected and therefore do not change as can be seen in Fig. 3.3 and Fig. 3.9.

3.6 Conclusions

A force-measuring OT apparatus needs to be calibrated to obtain the deflection sensitivity relating the trapped bead position with the measured voltage and the trap stiffness, required to convert this position to a force signal. Although various calibration methods for the deflection sensitivity are discussed and lead to the same results, the easiest calibration method when using the microscope for single dsDNA molecule force spectroscopy is making use of the distinct force plateau of a single dsDNA molecule at 60-70 pN in its force-extension curve. Since this curve already needs to be acquired to identify if a single DNA molecule is stretched, no extra calibration step

is required. Furthermore the deflection sensitivity is acquired at the appropriate trap stiffness and for the relevant positional range, which does not necessarily have to be the case for the other methods.

The power spectral density method and the sinusoidal modulation method are the preferable calibration methods for the trap stiffness where we have shown that both methods are in good agreement. The sinusoidal modulation moves the bead over much larger distances, such that it is not dependent on the noise limitations of the instrument. On the other hand a well-calibrated detector is required, leading to additional errors in the trap stiffness. Advantage of the power spectral density method is that the detector has not to be calibrated, but in contrast with the sinusoidal modulation method it considers bead displacements in the order of 1-10 nm as a result of the thermal motion. Nevertheless the power spectral density method allows discrimination of noise sources appearing in certain frequency ranges as 1/f-noise, which are not noticed by other calibration methods, considering the thermal motion of the bead. However, corrections for the frequency dependence of the friction force, aliasing effects, and electronic low-pass filters should be taken into account.

Finally we have shown that the reflection-based OT is sensitive for rotations of a trapped bead presumably caused by irregularities in shape. This can lead to the appearance of 1/f-noise in the power spectral density decreasing the positional resolution. Because the rotational sensitivity varies for different beads, the appropriate bead can be selected based on the appearance of 1/f-noise.

Chapter 4

Silicon position detector bandwidth limitations for near-infrared light [1]

Silicon-based position detectors become transparent for wavelengths above 850 nm limiting the detection bandwidth. To characterize this low-pass effect for several quadrant detectors (QD) and position sensitive detectors (PSD) we have developed a two-LED wobbler system generating a spatial displacement of total light intensity on a detector surface, facilitating the acquisition of frequency responses of the detector up to 600 kHz with high accuracy as a function of wavelength, applied bias voltage, and total light power.
In AFM and OT applications the low-pass effect of the commonly used silicon detectors leads to serious errors in the force constant determination of the probe. We show that this low-pass effect can be compensated for using the frequency response of the detector as determined with the LED-wobbler applicable for both AFM and OT. Furthermore for OT a second method is available based on fitting an expression in which the low-pass characteristics of the detector are already accounted for.

4.1 Introduction

In atomic force microscopy (AFM) and optical tweezers (OT) the optical beam deflection method is used to accurately measure the position of the probe. For both techniques the power spectral density of the deflection signal of the probe (i.e., AFM tip or bead) is widely used to calibrate the stiffness of the probe (Meyer and Amer, 1988; Svoboda and Block, 1994). For these applications it is important to obtain the frequency response of the detector and other electronics to be able to apply appropriate corrections if necessary. In OT applications in which near infrared lasers are often used it was noticed that the frequency response was unexpectedly attenuated above $\sim$5 kHz, caused by a low-pass effect of the silicon position detector (Berg-Sorensen *et al.*, 2003). This results in an incorrect determination of the stiffness.

[1] The contents of this section are based on Huisstede *et al.* (2006), [Huisstede J.H.G., van Rooijen B.D., van der Werf K.O., Bennink M. L., and Subramaniam V., "Dependence of silicon position-detector bandwidth on wavelength, power, and bias", *Optics Letters*, **31**(5), 610–612. 2006]

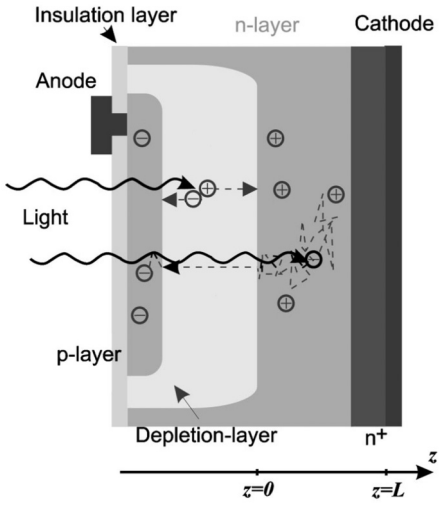

Figure 4.1. A schematic cross-section of a typical photodiode. Electron-hole pairs created outside the deflection layer first have to diffuse into the depletion region before going to the electrodes [adapted from Berg-Sorensen *et al.* (2003)].

First we present the LED-wobbler that is developed to characterize the low-pass effect of position detectors and the dependence of the low-pass effect on the wavelength, bias voltage, and impinging light power. After the characterization of several position sensitive detectors (PSD) and quadrant detectors (QD) the consequences of the low-pass effect for the probe stiffness calibration are investigated for both AFM and OT applications. We show that for these applications we can correct for the low-pass effect by determining the frequency response of the detector with the LED-wobbler at the appropriate wavelength, bias voltage and light power. For OT an additional correction method is discussed based on including a model for the low-pass effect within the Lorentzian function curve-fitting.

4.2 Dependence of silicon position detector bandwidth on wavelength, power and bias

The electrical response of a typical silicon photodiode to infrared light consists of both a fast and a slow component. The fast component results from optical absorption in the depletion layer, whereas the slow component results from absorption beyond this layer owing to the transparency of silicon in the near infrared schematically depicted in Fig. 4.1. In the depletion layer the electron hole pairs created are rapidly swept to the electrodes, whereas electron-hole pairs created outside the depletion layer first diffuse into the depletion region before going to the electrodes. As a result the bandwidth of the detector is limited dramatically (Berg-Sorensen *et al.*, 2003). For OT, although several groups of researchers have investigated this phenomenon (Berg-Sorensen *et al.*, 2003; Peterman *et al.*, 2003; Neuman and Block, 2004), the experimental configurations used had inherent limitations and the low-pass effect was shown only for a limited bandwidth measured indirectly or for only one wavelength.

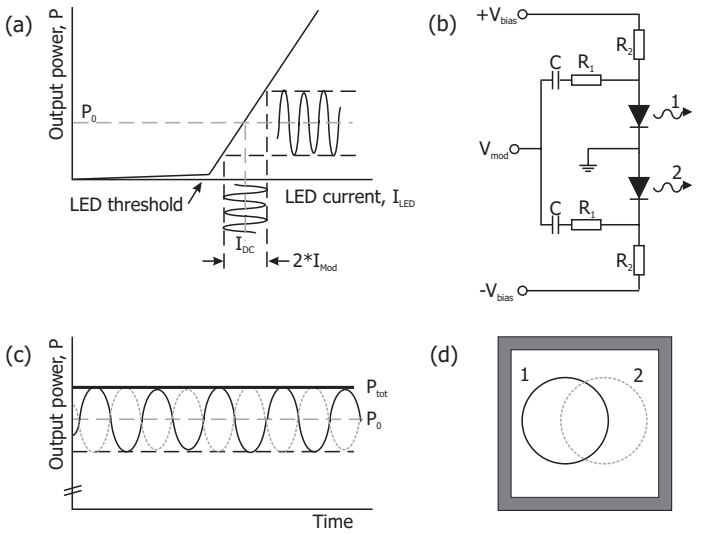

Figure 4.2. (a) Principle of frequency modulation of a LED. (b) Schematic of the LED wobbler circuit used to superimpose the frequency modulation on the dc current: R_1=50 Ω, R_2=1 kΩ, C=100 μF. (c) Light intensity of both LEDs in time. The phase difference between the two LEDs is 180^o. The darker curve corresponds to LED1, the lighter curve to LED2. (d) Schematic drawing of the light impinging on a detector. The solid circle corresponds to LED1, the dotted circle to LED2.

4.2.1 The LED wobbler

In order to determine the frequency response of both QDs and PSDs up to high frequencies a spatial deflection of light power up to those high frequencies has to be generated. For this purpose we developed a two-LED wobbling system (the LED wobbler) as depicted in Fig. 4.2. With this system a spatial deflection of light power is simulated, analogous to the experimental situation in AFM and OT. Each of the two LEDs is frequency modulated above the LEDs threshold current level, one with $\sin(\omega t)$ and the other with $-\sin(\omega t)$, resulting in a 180^o phase difference (Fig. 4.2(c)). The LED wobbler allows us to measure the frequency response of both QDs and PSDs up to a frequency of 600 kHz over a dynamic range of 18 dB with high accuracy. A modulation depth in the deflection signal of 10% of the total light intensity was used. The resultant variation in total intensity was found to be less than 0.5%, showing a good match in characteristics of the two LEDs used. We used LEDs in the range 405-1070 nm (Roithner Lasertechnik LEDs; 405, 505, 605, 700, 830, 850, 910, 970, and 1070 nm). All LEDs except the 910 and 970 nm LEDs, had a response time of $\leq$25 ns, resulting in a bandwidth of at least 6 MHz. The response time for the 910 and 970 nm LEDs was approximately 1 μs, resulting in a bandwidth of $\sim$150 kHz. The frequency responses of the detectors at these two wavelengths were corrected for the transfer function of the individual LEDs, determined by use of a UDT-PIN H040 (UDT) photodiode with a bandwidth of >1 MHz. The custom-built electronics used to acquire the detector signals were optimized to suppress gain peaking. Frequency responses were acquired with a gain-phase analyzer (Hewlett-Packard HP 4194A, Palo Alto, CA, USA) and transferred to a PC using custom Labview software. The frequency responses shown here were corrected for the response of the electronic hardware.

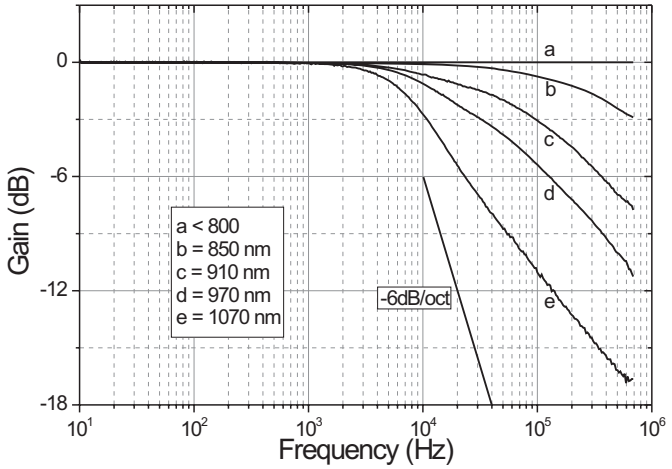

Figure 4.3. Frequency response of a quadrant detector (S5891, Hamamatsu) operating at no bias for several wavelengths with a light power of 500 μW. Curves a-e show the frequency response for wavelengths ≤800, 850, 910, 970, and 1070 nm.

We investigated two types of silicon position detectors: the quadrant detector (QD) and the position sensitive detector (lateral effect diode, PSD) as a function of wavelength, applied bias voltage, and total incident light power. A QD works by measuring the difference in light power incident on its four quadrants. A PSD measures the center of energy of a spot. A direct consequence is that a PSD is insensitive to the spot size, which is not the case for a QD. Furthermore the detection range and the deflection sensitivity of a QD can be restricted more by the shape and size of the spot than can those of a PSD (Chapter 3).

4.2.2 Wavelength dependence

We first investigated the low-pass behavior of a silicon position detector as a function of wavelength. The typical frequency response of a standard QD (S5891, Hamamatsu) operating at no bias is shown in Fig. 4.3 for wavelengths ranging from 850 to 1070 nm. For wavelengths of ≤800 nm we found that the bandwidth is limited by the electronics (600 kHz). Above 800 nm, silicon becomes increasingly transparent for higher wavelengths. The output of the diode becomes effectively low-pass filtered ($f_{3dB} \approx$ 10-12 kHz at 1070 nm), where the attenuation is less than 6 dB/octave and strongly dependent on the wavelength. In Fig. 4.3 the solid line indicates the slope of a first-order low-pass filter (-6 dB/octave).

4.2.3 Bias voltage dependence

Applying a bias voltage will increase the thickness of the depletion layer of the silicon-based detector and therefore increase the bandwidth of the detector; in Fig. 4.4 we demonstrate this by showing the frequency response of three QDs operating with and without a bias voltage. The curves are acquired at a wavelength of 1070 nm with a light power of 500 μW. All three detectors show an increase in bandwidth where a bias voltage is applied. Beyond 10 kHz, where all detectors already show the low-pass

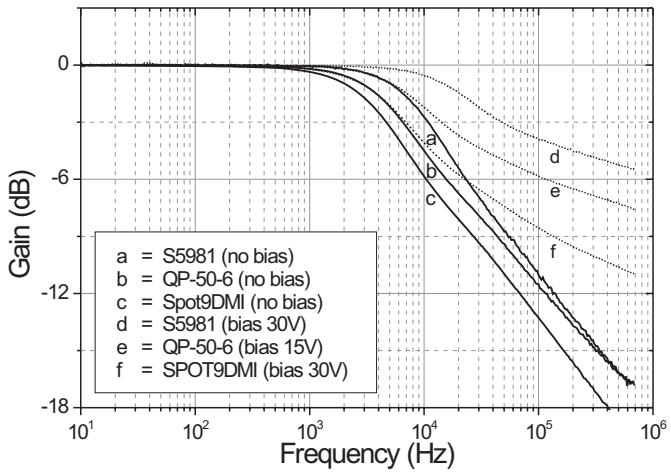

Figure 4.4. Frequency response of the S5981 (Hamamatsu), the QP-50-6 (Pacific Silicon Sensor) and the SPOT9DMI (UDT) operating with and without bias (all QDs), measured at a wavelength of 1070 nm and a light power of 500 μW. Curves a-c were acquired with no bias. Curves d-f correspond to the same detectors but operating with bias (S5891, bias 30 V; SPOT9DMI, bias 30 V; QP-50-6, bias 15 V).

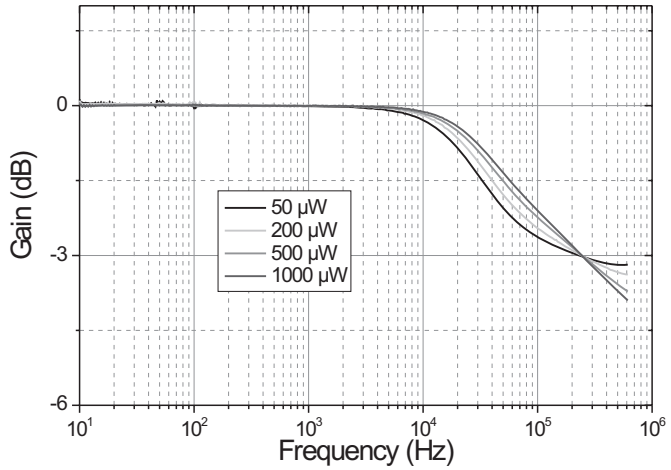

Figure 4.5. Frequency response of the DL100-7-KER (Pacific Silicon Sensor) PSD for four total intensities (the wavelength used was 1070 nm). Compare the vertical scale with those of the previous figures.

effect, a small nick in the curves is visible, after which the attenuation further exhibits a smaller slope.

4.2.4 Light power dependence

The influence of the incident light power on the frequency response of the detectors is demonstrated for the DL100-7-KER PSD in Fig. 4.5. The responses were acquired at light powers of 50, 200, 500, and 1000 μW at a wavelength of 1070 nm. An increase in light power resulted in an increase in bandwidth. For this detector we found that at a frequency near 230 kHz the curves are crossing each other, after which a smaller attenuation was found at lower light powers with respect to higher powers. Other detectors showed a similar response to a change in light power, and a crossing of the curves for different powers was observed. For detectors with a larger low-pass effect the crossing of the curves was found at lower frequencies. In Table 4.1 the bandwidth

Table 4.1. Influence of light power on the bandwidth of detectors

Detector	Light Power	
	50 μW	500 μW
DL100-7-KER	230	244
DLS10	10.9	15.4
SPOT9DMI	6.3	6.9

the DL100-7-KER and the DLS10 (UDT) (both PSDs) and the SPOT9DMI (UDT; a QD) are given for light powers of 50 and 500 μW. For all detectors an increase in bandwidth is found for increasing light power. The DL100-7-KER exhibits a notably higher bandwidth with respect to the other detectors (shown previously by Neuman and Block (Neuman and Block, 2004)). The effect of light power on the low-pass effect up to the crossing region suggests a saturation effect of the electron-hole pairs created outside the depletion layer caused by their relatively slow diffusion. If this effect indeed can be explained by saturation, it will be dependent on the local intensity and therefore also on the spot size, a factor that has not been investigated in this work.

4.2.5 Bandwidth results for various detectors

Finally we show in Fig. 4.6 the bandwidth as a function of wavelength for the various detectors used in the measurements at a light power of 500 μW and at operating bias voltages indicated in the figure. At 850 nm the first detectors become bandwidth limited by the low-pass effect of the detector. Remarkable is the high bandwidth of the DL100-7-KER PSD for all wavelengths.

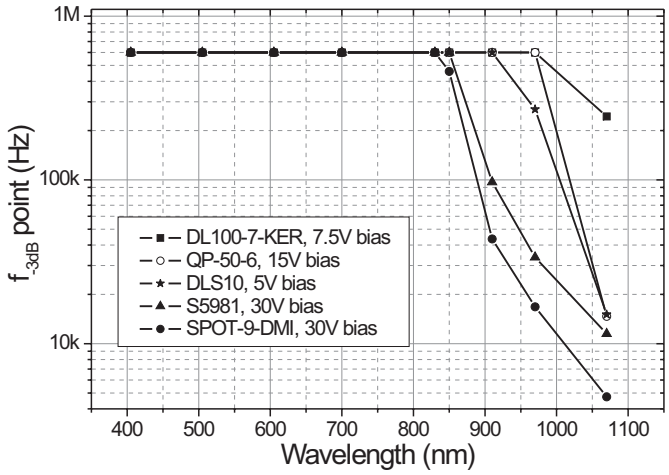

Figure 4.6. Bandwidth as a function of wavelength for several detectors. The maximum bandwidth of 600 kHz is the bandwidth of the electronics.

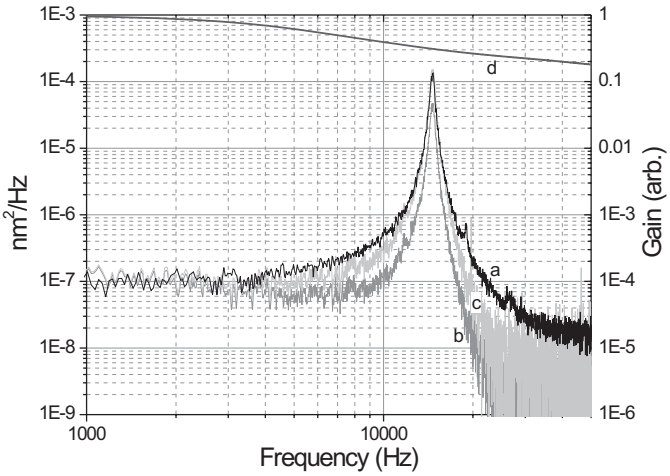

Figure 4.7. Power spectral densities of a cantilever measured in an AFM with a laserdiode operating at 785 nm (a) and a hybrid AFM/optical microscope with a laserdiode operating at 1050 nm (b). For the latter one the curve is corrected for the low-pass effect of the detector (c). The gain of the detector used for correction is depicted in curve (d).

4.3 Corrections for the force constant determination in OT and AFM

The accurate calibration of the force constant of the probe in AFM and OT applications is extremely important for force spectroscopy applications. The low-pass effect of the commonly used silicon detectors leads to serious errors in the force constant determination of the probe. We show that this low-pass effect can be compensated for using the frequency response of the detector as determined with the LED-wobbler for both AFM and OT. For OT an additional correction method is discussed based on including a model for the low-pass effect in the Lorentzian function curve-fitting.

4.3.1 Force constant corrections in AFM

The frequency response of the Brownian motion of a cantilever (tipB, Veeco, NY, USA) was measured in air in a custom-built AFM (van der Werf *et al.*, 1993) using a 785 nm laser diode. The same cantilever was transferred to a hybrid AFM-confocal optical microscope (Kassies *et al.*, 2005) that uses a 1050 nm laser diode to prevent induced photo bleaching during simultaneous fluorescence (at 800 nm) and topography measurements. In both microscopes the same type of detector has been used (UDT, Spot9-DMI). To convert the detector signal to nanometers calibration of the position detectors was carried out in the range of 10-100 Hz. In Fig. 4.7 we show a typical power spectral density function (S_x) for the same cantilever as acquired in both microscopes ((a) and (b)) and corrected for background noise that was determined by blocking the laser. The S_x at 1050 nm was corrected for the frequency response of the detector and presented in (c). In addition the detector response (gain versus frequency) that has been used for this correction is depicted in (d).
According to the equipartition theorem (Reif, 1965) in AFM each mode of vibration of the cantilever equals an energy $\frac{1}{2}k_bT$ and therefore for the first mode of vibration,

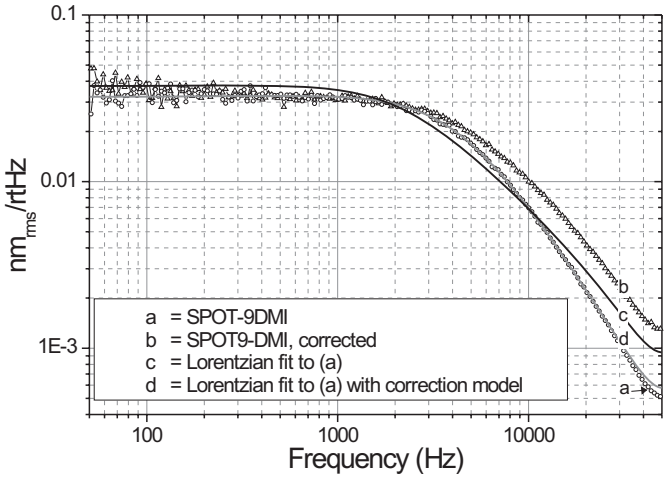

Figure 4.8. Power spectral density of the deflection signal of a 2.67 μm polystyrene bead in an optical trap recorded with the SPOT9DMI (a). The spectrum corrected for the detector response is also plotted (b). Furthermore the Lorentzian fit to (a) including the model described by Eq. 4.2 (d) and without the model (c) is shown.

the energy equals $\frac{1}{2}k_{pr}\langle x^2\rangle$. For a high Q-factor $\langle x^2\rangle$ can be approximated by integrating around the first resonance peak. Integrating the spectra (Fig. 4.7) within the range of 6-21 kHz we found a stiffness of $(3.8\pm0.2)\cdot10^{-2}$ N/m for the probe acquired at a wavelength of 785 nm. However at a wavelength of 1050 nm a stiffness of $(11.1\pm0.6)\cdot10^{-2}$ N/m was calculated indicating that due to the low-pass effect the stiffness was overestimated with a factor 3. After correcting S_x for the response of the detector the stiffness was found to be $(3.5\pm0.2)\cdot10^{-2}$ N/m, within 10% of the value at 785 nm. Small differences just next to the peak of the spectrum acquired at 785 nm and the corrected spectrum at 1050 nm are expected to be caused by background noise corrections.

4.3.2 Force constant corrections in OT

In contrast to AFM in OT applications the power spectral density S_x looks different (see Fig. 4.8, curve (a)) due to the fact that in this case the damping forces are dominating. The same method of integrating S_x can be applied, but in this case it is also possible to fit this spectrum using a Lorentzian function not requiring a calibrated position detector as discussed in Chapter 3. From the cut-off frequency found here the trap stiffness can be deduced, even when the detector is not calibrated. The Lorentzian function is given by

$$S_x = \frac{D/\pi^2}{f^2 + f_c^2} \tag{4.1}$$

where D is the diffusion constant (with an additional factor if the detector is not calibrated), f the frequency and f_c the cut-off frequency. The trap stiffness is calculated according to $k_{tr} = 2\pi\gamma_0 f_c$ with γ_0 the Stokes friction coefficient for a sphere (Svoboda and Block, 1994).

We used three different position detectors in an optical tweezers apparatus (Bennink *et al.*, 2001) to acquire spectra for a trapped 2.67 μm polystyrene bead (Bangs

Table 4.2. Optical trap stiffness values determined by curve-fitting the power spectral density with a Lorentzian function. The power spectra for all detectors were obtained for the same 2.67 μm polystyrene bead. Two corrections methods for the low-pass effect of a silicon detector were investigated and compared with the situation where no corrections were applied.

Detector	Lorentzian, no corrections k_{trap} (pN/μm)	Lorentzian, corrected spectra k_{trap} (pN/μm)	Lorentzian with model low-pass effect		
			f_{diode} (kHz)	α	k_{trap} (pN/μm)
DL100-7-KER 500μW	566	577	47.1 [2]		593
DL100-7-KER 150μW	566	575	17.3	0.83	599
DLS10 500μW	419	595	12.8	0.45	572
DLS10 150μW	401	595	10	0.48	590
SPOT9DMI 500μW	337	591	8.1	0.40	569
SPOT9DMI 150μW	323	574	6.7	0.38	599

Labs, Fishers, IN, USA) using a 2.5 W Nd:YAG laser (Coherent, Compass 1064-2500MN, Santa Clara, CA, USA) operating at a wavelength of 1064 nm. In contrast to AFM, where the light power can be adjusted manually without affecting the probe stiffness, the light power on the detector in OT applications can differ for various trapped beads and therefore the low-pass effect can vary. In transmission-based OT the variation in intensity is approximately 10-20% and for a reflection-based apparatus it can be up to a factor of 2 (Chapter 3). To investigate the effect of light power, spectra were recorded at light powers of 500 and 150 μW. Reduction of the light power was achieved by using a neutral density filter in front of the detector. In this way the optical trap was not affected and only the effect of light power on the detector was investigated. The detectors used were the DL100-7-KER (Pacific Silicon Sensor), the DLS10 (UDT) and the SPOT-9DMI (UDT).

Fig. 4.8 shows the power spectral density of a trapped bead acquired with the SPOT9-DMI (curve (a)). First we demonstrate the influence of applying no corrections on the trap stiffness determination by fitting directly the Lorentzian function given by Eq. 4.1 to the acquired spectra. The resulting Lorentzian fit is shown in Fig. 4.8, curve (c). Hydrodynamic and aliasing corrections were included in the Lorentzian curve-fitting (Berg-Sorensen and Flyvbjerg, 2004). The fit results for the uncorrected S_x for all three detectors at the two light powers are given in the second column of Table 4.2. If a detector that reveals a low-pass effect starting at lower frequencies was used a lower value for the trap stiffness was found.

As for AFM applications S_x can be corrected using the frequency response of the detector as measured with the LED wobbler (at 1070 nm and the same light powers). After correction S_x is curve-fitted with the Lorentzian function. For all spectra the fit-range was 110 Hz - 15 kHz. The resulting optical trap stiffness values are given in the third column of Table 4.2 showing that the trap stiffness values deduced are in good agreement with a variation of <2%.

For OT a second method is available based on fitting an expression included in the Lorentzian function to account for the low-pass effect. Actually this expression for the low-pass effect, given by Eq. 4.2, is derived by Berg-Sorensen *et al.* (2003) to account for the low-pass effect and to circumvent the requirement to determine the total light power. Before discussing this correction method we validate the expression by fitting it to the frequency response of the detector as measured with the LED wobbler. The expression is given by

$$S_{diode} = \alpha^2 + \frac{1-\alpha^2}{1+(f/f_{diode})^2} \tag{4.2}$$

In this equation α describes the fraction of light absorbed in the depletion layer, which is a function of the effective thickness of the depletion layer and therefore a function of wavelength, bias voltage and light power. Since the fraction of light absorbed outside the depletion layer has to diffuse towards the depletion layer it is low-pass filtered with a characteristic frequency f_{diode}. Depending on the detector f_{diode} is in the order of 5 kHz. In Fig. 4.9 we show frequency responses of the DL100-7-KER, the DLS10 and the SPOT-9DMI for light powers of 50 and 500 μW. Additionally the fit based on Eq. 4.2 for each frequency response is shown. The model describes the effect quite well for lower frequencies. Above a certain frequency the model deviates significantly from the measured frequency response. The fit range was increased stepwise until the model did differ more than 5% from the value at the maximum frequency of the selected range (45 kHz for the DL100-7-KER, 10 kHz for the DLS10 and 15 kHz for the SPOT9DMI). For earlier results reported in the literature (Berg-Sorensen *et al.*, 2003; Neuman and Block, 2004) the frequency range was below these critical frequencies; consequently, this effect has not been observed before. For frequencies much higher than the characteristic frequency f_{diode} the second term in Eq. 4.2 approaches zero and the term, α^2, becomes dominant. Thus Eq. 4.2 will always be able to fit a low-pass filtered system up to a certain frequency, as long as the slope of the attenuation part is $\leq$6 dB/octave.

Now we use the Lorentzian function with the expression for the low-pass effect included, to fit to the power spectral densities for the 2.67 μm trapped bead trapped in the OT apparatus discussed previously. For this 'new' Lorentzian there are four fit parameters, D and f_c describing the dynamics of the trapped bead and α and f_{diode} describing the detector response. Again hydrodynamic and aliasing corrections are included. For all spectra the fit range was 110 Hz - 15 kHz. In Fig. 4.8, curve (d) the result is shown using this correction method. The resulting key fit parameters values are given in the last column of Table. 4.2. The trap stiffness values found for each detector are in good agreement. The trap stiffness found for the DL100-7-KER in the case no correction method was used is remarkably close to (<5%) the values found using the two corrections methods, indicating the small low-pass effect of this detector. For the other two detectors the trap stiffness is strongly underestimated in case of no correction. In separate experiments the trap stiffness values found with the two correction methods were compared with another calibration technique for OT

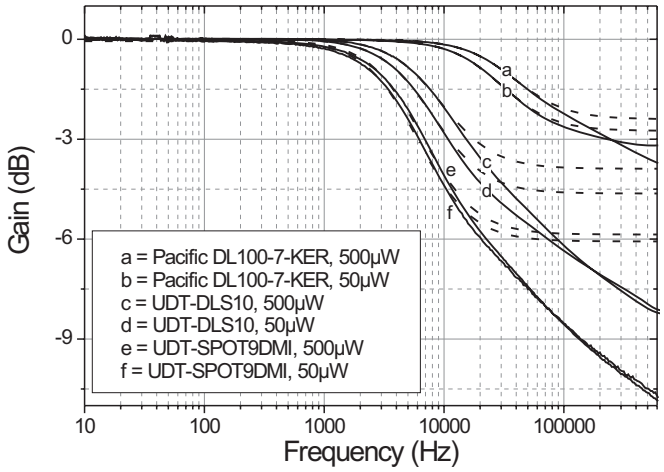

Figure 4.9. Frequency response of the DL100-7-KER, the DLS10 and the SPOT9DMI determined with the LED wobbler at 500 and 50 µW at 1070 nm. The dashed lines are the corresponding fits using Eq. 4.2. For the DLS10 the fit range was limited to 10 kHz, for the SPOT9-DMI to 15 kHz and for the DL100-7-KER to 45 kHz.

(sinusoidal driving force, Chapter 3) where the trap stiffness did not differ more than <5% from this value.

Finally we investigated the overall effect of the light power on the deduced trap stiffness using the first correction method discussed for both AFM and OT. Instead of correcting the spectra acquired at 500 µW with the frequency response of the detector at the appropriate power we used the detector response determined at 50 µW. For the DL100-7-KER we found a stiffness of 590 pN/µm instead of 577 pN/µm using the appropriate correction light power. For the DLS10 we found 654 pN/µm instead of 595 pN/µm and for the SPOT-9DMI 584 pN/µm instead of 591 pN/µm. Although the difference in the power for the correction curves was a factor of 10, we found for both the DL100-7-KER and the SPOT9DMI an acceptable change of < 3%. For the DLS10 a change of 10% was found.

4.4 Conclusions

As shown for QDs and PSDs, silicon-based detectors can become bandwidth limited already at frequencies near 5 kHz for wavelengths ≥850 nm. With the LED wobbler the low-pass effect of several detectors was characterized with high accuracy for different wavelengths, bias voltage, and light powers up to high operating frequencies, in our case limited by the bandwidth of the electronics (600 kHz).
Alternative solutions to prevent unintended low-pass filtering include the use of an InGaAs detector (for near-infrared light), for which a potential drawback can be the size of the active area, currently ≤4 mm. Another solution is the use of another or a second light source operating at a shorter wavelength (<850 nm).

Due to the limited bandwidth of silicon position detectors large errors are found in the force constant determination in AFM and OT applications. However we have shown that the power spectral density can be corrected for the frequency response of

the position detector as determined with the LED wobbler. Applying the equipartition theorem for AFM or curve-fitting a Lorentzian in OT the force constant can be determined more accurately. For variations of the light power within a factor of ten we found a variation of <3% for the force constant for the DL100-7-KER and the SPOT9-DMI. This makes acquisition of the frequency response of these two detectors for various powers redundant.
For OT an additional correction method is available by including a model for the detector low-pass effect into the Lorentzian curve-fit. However we have shown that this model partially describes the low-pass effect of the detector and is thus only applicable up to a maximum frequency range. Knowledge of the frequency response of the detector beforehand is thus required. Remarkable is the performance for the DL100-7-KER PSD in contrast to all other detectors investigated. For a wavelength of 1064 nm the detection bandwidth is still 230 kHz, which is the reason this detector is implemented in the SPOT microscope.

Chapter 5

The positional fluctuations of a trapped bead

Optical tweezers are a very suitable tool to measure forces with high accuracy on individual (bio)polymers such as DNA in a force range of typically 0-100 pN, from which the mechanical properties can be deduced. These mechanical properties are important for the resolution of the optical tweezers. Upon extending the molecule to a force level of 10-50 pN the positional fluctuations of a trapped bead are found to decrease because of the stiffness of the molecule as it is sensed by the trapped bead. When indenting a DNA molecule stretched by a force in this range with a probe, we found that the effective stiffness of the DNA molecule as sensed by the trapped bead increased, but was dependent on the total indentation. The accuracy with which we can detect proteins is dependent on the effective stiffness of the DNA molecule and dependent on the strength of the interaction forces between the probe and the proteins. Dependent on these interaction forces we calculated that proteins have to be displaced $\sim$10 nm along the direction of the DNA molecule (not moving them over the DNA) to localize them.

5.1 Introduction

To locate proteins on a single dsDNA molecule, the molecule has to be stretched close to or beyond its contour length to allow measurement of the additional forces induced by the probe. One of the most important parameters determining the minimum detection limit with which these forces can be measured is the stiffness of the DNA molecule as it is sensed by the optical tweezers. The elastic properties of a single DNA molecule and its consequences for the resolution were obtained by acquiring a force-extension curve, which is discussed first. To locate proteins a probe is scanned along the molecule while indenting it. In the last section of this chapter we focus on the consequences of the magnitude of the interaction forces between the probe and the proteins for the expected detection limit with which we can locate proteins.

5.2 Materials and methods

5.2.1 Suspending a single DNA molecule

A double-stranded λ-DNA molecule with a contour length of 16.4 μm (48.5 kbp) functionalized at its two extremities with biotin, was suspended between two streptavidin-coated 2.67 μm polystyrene beads. Both chemical protocols for making this construct and the procedure for suspending a single molecule are described in (Bennink *et al.*, 1999). The buffered solution in which a DNA molecule was stretched, was a TE-buffer supplemented with 150 mM NaCl, 0.05% BSA and 0.01% NaN_3 (pH 7.5).

5.2.2 Force-extension data acquisition

The suspended DNA molecule was stretched by moving the bead immobilized on the μ-pipette controlled by the XYZ-stage, where the data acquisition was synchronized with the applied ramp to the XYZ-stage. Due to the resolution of the DAQ-card (12-bits) the ramp was created with steps of 25 nm with the time between each step determined by the pulling speed (1-10 μm/s) as set in the software. For each step, data was acquired at a rate of 100 kHz to calculate an average value and the standard deviation. This provides the force-extension data as well as the positional fluctuations of the trapped bead during the experiment. This is the standard mode used to acquire force-extension curves.

5.3 Results

5.3.1 Forces and fluctuations upon extension

In Fig. 5.1 a typical force-extension curve for a single dsDNA is shown acquired with a trap stiffness of 268 pN/μm at a pulling speed of 4 μm/s. The force response up to a force of ∼50 pN can be described by the modified worm-like chain model as discussed in Chapter 2 (Bustamante *et al.*, 1994). At a force of 60-70 pN a plateau was observed, which is slightly dependent on the salt concentration (Smith *et al.*, 1996; Baumann *et al.*, 1997; Punkkinen *et al.*, 2005). At this plateau a transition occurred till the molecule was extended to approximately 1.7 times its contour length where the force increased further upon extension. The structure of the DNA in this force region is still not elucidated. Upon retracting, hysteresis probably due to melting (Smith *et al.*, 1996; Baumann *et al.*, 1997) was observed at extensions ranging from 18 to 25 μm until it coincides again with the stretching curve. The force plateau and the hysteresis are typical for dsDNA. Together with the reproducibility of the force-extension curve these distinct features ensured that a single molecule was trapped between the beads and stretched.

In Fig. 5.1 the standard deviation of the trapped bead position during the force-extension procedure is also plotted. This sets the minimum detection limit with which the position of the trapped bead can be obtained, which is eventually important for the

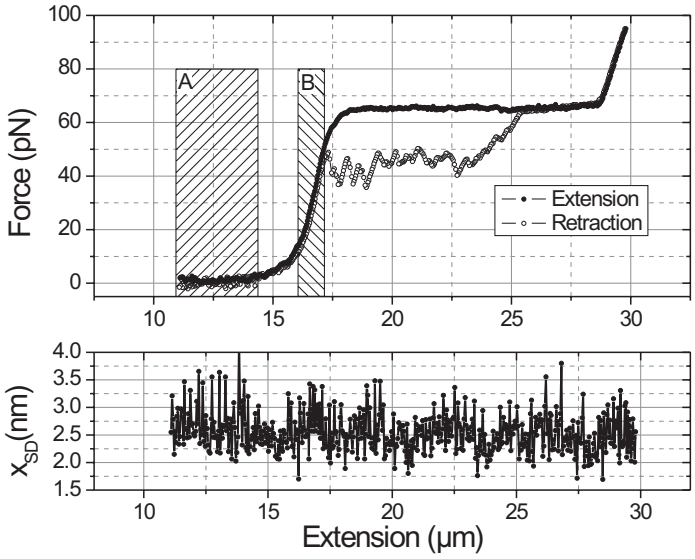

Figure 5.1. Force extension curve of a single dsDNA molecule. In addition the standard deviation of the position signal (nm) during extension of the molecule is shown. The pulling speed was 4 μm/s and the trap stiffness 268 pN/μm. Area A indicates the entropic linear regime and area B the enthalpic linear regime of the molecule.

accuracy with which proteins can be localized. In Chapter 3 the position fluctuations are expressed as a root-mean-square value where the mean value of the position was assumed zero. However when an external force is applied to the bead it is displaced. Therefore the positional fluctuations have to be expressed as a standard deviation x_{sd} that can be written as

$$x_{sd} = \sqrt{\frac{4\gamma k_b T B}{k_{eff}^2}} = \frac{\sqrt{4\gamma k_b T B}}{k_{tr} + k_{dna}} \tag{5.1}$$

where k_{eff} is the effective spring constant the bead experiences, k_{tr} the trap stiffness, and k_{dna} the stiffness of the DNA molecule. The effective stiffness k_{eff} is derived as follows

$$\begin{aligned} \frac{1}{k_A} &= \frac{1}{k_{dna}} + \frac{1}{k_{pip}} \\ k_A &= \frac{k_{dna}k_{pip}}{k_{dna} + k_{pip}} = k_{dna} \qquad (k_{pip} \gg k_{dna}) \\ k_{eff} &= k_{tr} + k_{dna} \end{aligned}$$

where the different springs in the bead-DNA-bead system are shown in Fig. 5.2. In this derivation the stiffness of the compliant linkers (the streptavidin-biotin linkers) as well as the stiffness of the pipette k_{pip} holding one of the beads were assumed rigid.

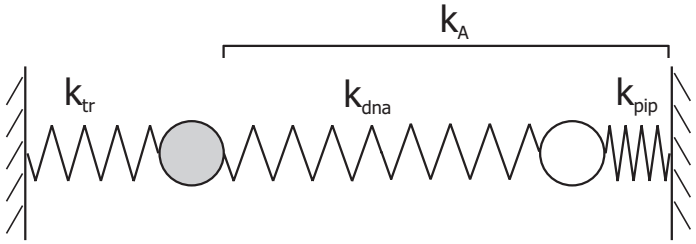

Figure 5.2. Schematic layout of the bead-DNA-bead system. Indicated are the spring constants of each component.

The stiffness of the DNA molecule k_{dna} at a certain extension x is given by the slope $(dF/dx)|_x$ of the force-extension curve. In the enthalpic regime (Area B in Fig. 5.1; 10-50 pN) the elastic response of the DNA molecule can be described by the linear stretching law (Eq. 2.3) and thus the stiffness equals $k_{dna} = S/L_0$ with S the stretching modulus and L_0 the contour length.

The force-extension curve shown in Fig. 5.1 is acquired in TE-buffer containing 50 mM NaCl resulting in a stretching modulus of ∼800 pN and a stiffness of 50 pN/μm. In experiments described in literature where dsDNA was stretched in a TE-buffer with 150 mM NaCl (pH 8.0) the stretching modulus was ∼1100 pN and thus k_{dna}=66 pN/μm (Smith *et al.*, 1996). This is consistent with literature reports where it is shown that a decreasing (monovalent) salt concentration leads to an increasing bending modulus and a decreasing stretching modulus (Baumann *et al.*, 1997; Punkkinen *et al.*, 2005).

When the DNA molecule is not stretched the fluctuations of the trapped bead are expected to be 2.4 nm for a trap stiffness k_{tr}=268 pN/μm and a detection bandwidth B of 1 kHz (based on Eq. 5.1). In the enthalpic regime a stiffness of the DNA molecule of 50 pN/μm was sensed and the standard deviation x_{sd} was expected to decrease to 2.0 nm. For extensions <15 μm a standard deviation x_{sd} of ∼2.6 nm was measured (Fig. 5.1) and for higher extensions x_{sd} is slightly decreased to ∼2.4 nm. In other DNA stretching experiments different results were found. In some cases the position fluctuations decreased upon extending the molecule and thus reflecting the expected dynamics, but in other cases the fluctuations actually increased. In an attepmpt to shed some lights on this, power spectral densities of the deflection signal of the trapped bead were acquired at different DNA extensions, but no clear explanation was found.

5.3.2 Forces and fluctuations upon indentation

Since we are able to measure the positional fluctuations, we can determine the influence of indenting or touching the molecule with a probe. To detect forces initiated by the probe the DNA molecule was stretched. As we have shown in the previous section the detection accuracy will improve when the stiffness of the molecule is the higher, which is in the enthalpic linear regime. Therefore we typically stretch a single DNA molecule to a force between 10-50 pN. The additional force F_{dna} in the molecule when

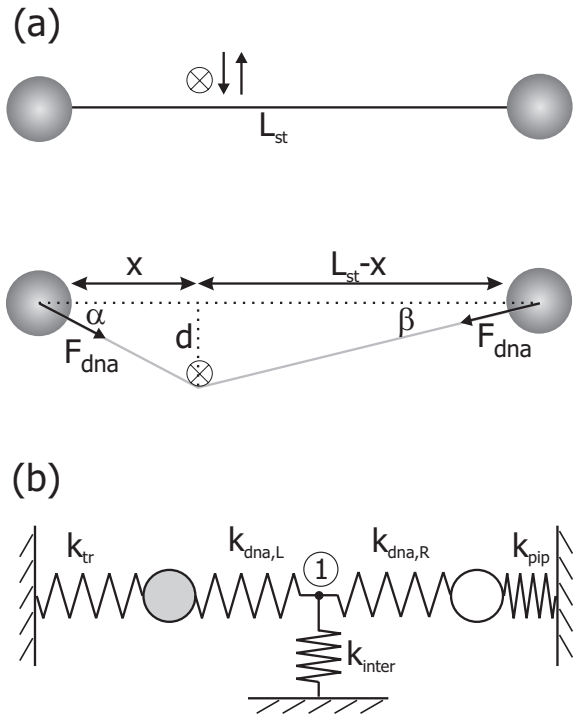

Figure 5.3. (a) Geometric representation of indenting DNA over a distance d at a certain position x along the DNA molecule. F_{dna} indicates the additional force initiated in the molecule due to this indentation. (b) The different spring constants for this experimental configuration.

a probe is indenting the molecule over a distance d at position x along the molecule, schematically depicted in Fig. 5.3(a), is

$$F_{dna} = \frac{S}{L_{st}} \left[\sqrt{d^2 + x^2} + \sqrt{(L_{st} - x)^2 + d^2} - L_{st} \right] \tag{5.2}$$

The part between the square brackets expresses the relative extension of the molecule where L_{st} indicates the length of the molecule for no indentation and x the position of the probe parallel to the DNA molecule.

When the DNA molecule is indented the force increases within the molecule resulting in a displacement of the trapped bead. To be able to detect this displacement it has to overcome the thermal fluctuations x_{sd} of the OT apparatus given by Eq. 5.1. Equating Eq. 5.1 with Eq. 5.2 the required indentation along the DNA molecule was derived for different x_{sd}. A detailed analysis is given in the Appendix. It was found that for a trap stiffness of 500 pN/μm the minimum required indentation is ∼100 nm to achieve a minimum displacement of the trapped bead of x_{sd}. Proteins are typically 1-10 nm in size and will therefore result in a displacement of the trapped bead below the detection limit x_{sd} and consequently will not be detected.

However, local displacements of the molecule generated in the axial direction will result in a much higher displacement of the trapped bead in comparison with a similar amount of indentation. Displacements in this direction are a result from the interaction between the scanning probe and the DNA molecule and proteins. These interactions consist of friction and adhesion forces. Differences in these forces when a protein is passed during a scan will lead to a change in the tension in the DNA molecule and therefore a change in the bead position. Similar as in the previous section we can estimate the required displacement of a protein caused by the interaction with the probe. Therefore we model this interaction with a Hookean spring with a stiffness parameter k_{inter}. In Fig. 5.3(b) a schematic representation of all the spring constants in the system including k_{inter} is given. The scanning probe and the μ-pipette immobilizing one of the beads are considered rigid.

When $k_{inter} = 0$ there are no interaction forces and thus no probe is sensed. In this case the effective stiffness experienced by the trapped bead is

$$k_{eff} = k_{tr} + k_{dna,tot} \tag{5.3}$$

and thus determined by the trap stiffness k_{tr} and the stiffness of the complete DNA molecule $k_{dna,tot}$ ($1/k_{dna,tot} = 1/k_{dna,L} + 1/k_{dna,R}$). For a rigid connection between the probe and the molecule $k_{inter} \gg k_{dna,R}$ and the effective stiffness is

$$k_{eff} = k_{tr} + k_{dna,L} \tag{5.4}$$

and thus dependent on the stiffness of the part of the DNA molecule in between the probe and the trapped bead. These two equations can be expressed as a function of the stretching modulus S by substituting

$$k_{dna,L} = \frac{S}{\alpha L_0} \qquad k_{dna,R} = \frac{S}{(1-\alpha)L_0} \qquad k_{dna,tot} = \frac{S}{L_0} \tag{5.5}$$

where α is the fraction of the DNA molecule considered to be at the left side of the probe.

To calculate the minimum required local displacement of point 1 indicated in Fig. 5.3(b) we assume a rigid connection between the probe and this point. A displacement x_1 of this point in the axial direction of the DNA molecule results in a displacement x_{bead} of the trapped bead according to

$$x_{bead} = x_1 \left(\frac{k_{dna,L}}{k_{tr} + k_{dna,L}} \right) \tag{5.6}$$

Equating this equation with x_{sd} in Eq. 5.1 we can write

$$x_1 = \frac{\sqrt{4\gamma k_b T B}}{k_{dna,L}} \tag{5.7}$$

that shows that the required displacement x_1 is independent of the trap stiffness. Because $k_{dna,L}$ is dependent on the length of the molecule between the probe and the

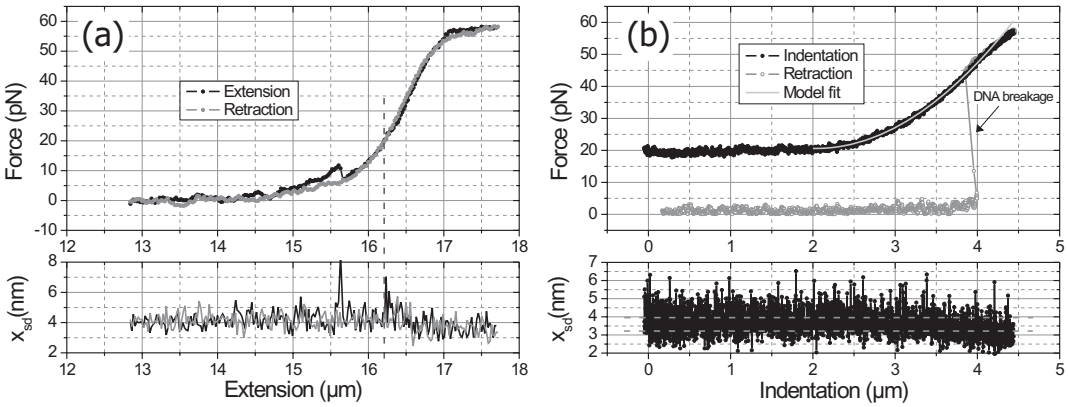

Figure 5.4. (a) Force-extension curve of a single dsDNA molecule acquired at 5 µm/s. In the lower graph the fluctuations of the bead during the acquisition is shown. To acquire a force-indentation curve (figure (b)) the molecule is stretched to 20 pN. As probe a 2 µm pipette is used. When the probe is retracted the bead-DNA-bead connection is broken as indicated in the graph.

trapped bead we can substitute $k_{dna,L} = S/(\alpha L_0)$. In the worst case scenario $\alpha = 1$ and $k_{dna,L} = k_{dna,tot}$ is the stiffness of the DNA molecule as can be calculated by the slope $(dF/dx)|x$ in the force-extension curve at the current extension. For $k_{dna,tot}$=66 pN/µm the minimum displacement x_1 has to be 12 nm. For a rigid connection in the middle of the molecule α=0.5 and the required displacement is 6 nm. The optical tweezers is thus much more sensitive for displacements of the molecule generated in the axial direction than for displacements in the transverse direction and for displacements closer to the trapped bead.

When localizing proteins the resolution will be dependent on k_{inter} since it determines the effective stiffness of the DNA molecule as sensed by the trapped bead. Experimentally we investigated the change of this effective stiffness by indenting a naked DNA molecule with a 2 µm pipette. First a force-extension curve of a DNA molecule was acquired at a speed of 5 µm/s and a trap stiffness of 295 pN/µm, shown in Fig. 5.4(a). The detection bandwidth in this case is limited to 32.4 kHz and is therefore far beyond the cut-off frequency of the optical trap. Thus $x_{sd} = \sqrt{k_b T/k_{eff}}$ was expected to be 3.7 nm when the molecule was not stretched. In the enthalpic regime a stiffness of the DNA molecule of 53 pN/µm was found and consequently we expected a standard deviation of 3.4 nm. The experimental results show a standard deviation of 4.0 nm for the unstretched DNA molecule and 3.7 nm in the enthalpic regime. Although the positional fluctuations are slightly larger the change is in the appropriate order. Notable is that once the standard deviation decreased the level remained constant for higher extensions, even for the force plateau at 60-70 pN. Despite of this plateau, indicating a transition of the DNA molecule, the bead still seems to experience an effective stiffness similar to the stiffness in the enthalpic region of the molecule (10-50 pN).

For the touching experiment the dsDNA molecule was stretched to 20 pN and

indented with the 2 μm pipette in the middle of the molecule over a range of 4.5 μm and a speed of 0.7 μm/s. During retraction the bead-DNA-bead connection was broken as indicated in the force-indentation curve in Fig. 5.4(b). Eq. 5.2 was fitted to the force-indentation curve in the range of 2-4μm. From the fit results we found a stretching modulus S of 939±6 pN with x=8.2 μm and L_0=16.4 μm set as fixed values. From these results the stiffness of the DNA molecule was 57 pN/μm according to Eq. 5.2 where we found 53 pN/μm from the force-extension curve as shown in Fig. 5.4(a) and thus both are in good agreement. The stiffness of the molecule as sensed by the trapped bead upon touching can be deduced from the fluctuations in the bead position shown also in Fig. 5.4(b). If there was an immediate fixed connection as soon as the probe touched the molecule the stiffness of the molecule would increase with a factor 2 to 116 pN/μm. In this case x_{sd} would reduce to 3.2 nm. However in Fig. 5.4(b) a gradual decrease of x_{sd} was found starting at 3.7 nm for no indentation to approximately 3.2 nm for a 2 μm indentation. The gradual decrease in x_{sd} suggests a gradual increase in k_{inter} indicating that the interaction forces are increased for increasing indentations. One plausible explanation could be an increasing contact area of the DNA molecule with the pipette.

5.4 Conclusions

Upon stretching a single dsDNA molecule the trapped bead starts to sense the stiffness of the DNA molecule. Up to ∼50 pN this stiffness is related to the slope of the force-extension curve. For an increasing DNA stiffness it was expected that the positional fluctuations of the trapped bead were decreasing. As this was indeed found for several molecules we also observed opposite results. Analysis of the power spectral densities of the bead position at different extensions did not give a clear explanation.

For proteins to be located, we found that it is most favorable to initiate displacements of the protein (including the DNA molecule) in the axial direction of the DNA molecule. A displacement in this direction will result in a much higher displacement of the trapped bead in comparison with a similar amount of displacement of the molecule in the perpendicular direction (i.e. indentation). The required displacement to overcome the (thermal) positional fluctuations of the trapped bead is a function only of the effective stiffness of the DNA molecule. From touching experiments with a 2 μm pipette we found that this effective stiffness is increasing when the molecule is touched by a probe, but is strongly dependent on the magnitude of the interaction forces that consist of friction, adhesion and electrostatic forces. For the experiment with the 2 μm pipette the indentation in the middle of the molecule had to be increased to ∼2 μm until the expected decrease in the positional fluctuations of the trapped bead was achieved for which we could assume a rigid connection between the probe and the molecule. For the localization of proteins in the worst case scenario where the stiffness of the molecule is not affected by the probe a local displacement in the order of 10 nm has to be generated.

Chapter 6

Experiments

In this chapter we present the first experimental results obtained with the SPOT-microscope. For the localization of proteins it is desirable that there is a strong difference in the interaction force of the scanning probe with the naked DNA and with proteins. The friction force between a pipette with a tip diameter of 170 nm and a naked DNA molecule was determined for different indentations. The typical friction force was found to be $<$1 pN. The first localization results were obtained for a 450 nm poly-L-lysine coated bead connected to a DNA molecule, using a μ-pipette with a tip diameter of 2 μm as probe or a MWNT with a diameter of 50-100 nm. The high interaction forces of the pipette with the 450 nm occurred over a range of 1.5 μm. For the MWNT this range was in the order of 0.5 μm similar to the bead size.
As a final step towards the localization of individual proteins we used a single DNA molecule with digoxigenin incorporated over a range of 90 nm in approximately the middle of the molecule. Scanning with an anti-digoxigenin coated pipette we were able to localize these sites due to the high binding affinity between this antibody-antigen pair. The range over which the interaction was measured was typically $\sim$150 nm.

6.1 Introduction

As discussed in the previous chapter the interaction forces, consisting of friction and adhesion forces, are crucial for the localization of proteins since the forces resulting from topography will be too small. A strong contrast between the interactions of the probe with the naked DNA and proteins is desirable since this difference in initiated force has to overcome the positional fluctuations of the trapped bead. To have an indication of the magnitude of the interaction forces between the probe and a single naked DNA molecule, the DNA was scanned with a 170 nm pipette at several indentations, which we will discuss first in the experimental section. Next localization experiments acquired for 450 nm poly-L-lysine (PLL) coated beads coupled to a DNA molecule based on electrostatic interactions are presented. As probe we used a μ-pipette with a diameter of 2 μm as well as a MWNT, to investigate their influence on the localization accuracy and the initiated interaction forces.

As a final step towards protein localization we focus on the localization of ∼20 digoxigenin (DIG) molecules that are bound to single DNA molecules over a range of ∼90 nm at approximately the middle of the DNA molecule. Using an anti-digoxigenin (α-DIG) coated μ-pipette we located the DIG molecules based on their strong binding affinity.

6.2 Materials and Methods

6.2.1 PLL-coating of beads

10 μl of carboxylated (COOH) polystyrene beads at a concentration of 2% (450 nm, Polysciences,Warrington, PA, USA) were suspended in 1 ml TE-buffer (pH 7.5) and centrifuged (30 minutes, 20 krpm). After removal of the supernatant the beads were resuspended in 1 ml 0.1% poly-L-lysine (PLL) in a HEPES buffer (pH 7.5) and were continuously rotated at room temperature overnight. The beads were then centrifuged again and resuspended in 1 ml TE-buffer. This solution was kept as a stock solution and stored at 4 ^{o}C. The final concentration of the beads in this stock solution was $\sim 10^7$ beads/ml. To obtain the solution as used in the experiments, 20 μl of the stock solution was diluted in 1 ml TE-buffer.

6.2.2 Connecting a 450 nm bead to a single DNA molecule

A single dsDNA molecule was connected between two streptavidin-coated polystyrene beads (Fig. 6.1(a)) following the procedure described by Bennink *et al.* (1999). A force-extension curve was recorded to verify if a single DNA molecule was stretched. To increase the electrostatic interactions between the positively charged 450 nm PLL-coated bead and the negatively charged DNA molecule the TE-buffer contained a salt concentration of 50 mM NaCl instead of 150 mM as previously discussed. A continuous flow was maintained in the flow cell to keep the DNA from coiling when blocking the optical trap (Fig. 6.1(b)). After introducing the 450 nm beads solution for ∼10 seconds a single bead was caught with the optical trap (Fig. 6.1(c)) and the bead solution was switched back to the TE buffer, ensuring no additional beads entered the optical trap. Next the 450 nm bead was brought in contact to the middle of the molecule (Fig. 6.1(d)). A connection between the bead and the molecule was affirmed when the floating bead followed the movements of the trapped 450 nm bead (Fig. 6.1(e)). Next the trap was blocked again with the continuous flow keeping the molecule from coiling (Fig. 6.1(f)). Next we injected the scanning probe into the flow cell and brought it in close proximity ($\leq$10 μm) with the DNA molecule (Fig. 6.1(g)). Finally the free 2.67 μm bead was trapped again such that the construct was ready for the scanning experiments (Fig. 6.1(g)).

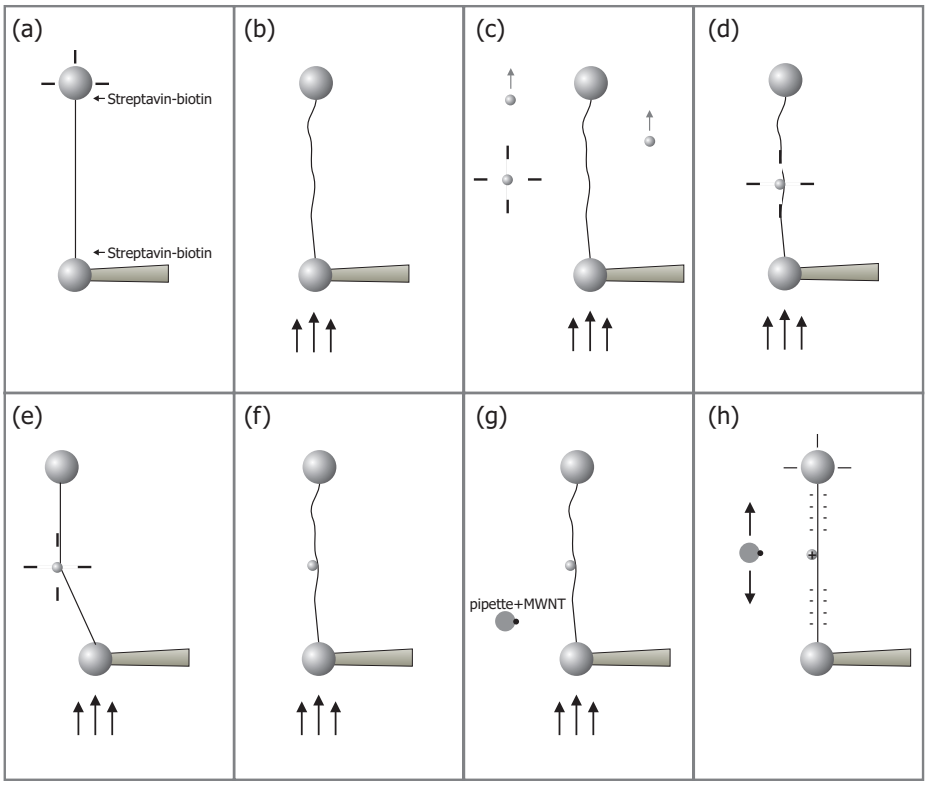

Figure 6.1. Schematic representation of the procedure used to connect a 450 nm poly-L-lysine (PLL) coated bead to a single dsDNA molecule based on electrostatic interactions.

6.2.3 Spot images

Here we introduce the method of representing the acquired data with the SPOT-microscope. Labview-written SPM software, primarily designed for AFM and near-field scanning optical microscopy (NSOM) controlled the position of the scanning probe and made the probe carry out a 1 dimensional scan in the axial directionaxis of the DNA molecule as indicated in Fig. 6.1(h) while simultaneously recording the deflection of the trapped bead. The position of the probe perpendicular to the DNA was manually controlled by applying an offset voltage to a separate piezo stack. The acquired detector signals are presented in a 2 dimensional image, which we call the SPOT-image from this point on. The vertical axis of these SPOT images corresponds to the position along the DNA molecule and the horizontal direction of the SPOT images corresponds to the number of the acquired line trace. As the probe is scanning back and forth two SPOT images are created. One image contains all the traces and the other image contains all the corresponding retraces. In this chapter we only show the trace SPOT-images unless otherwise indicated.

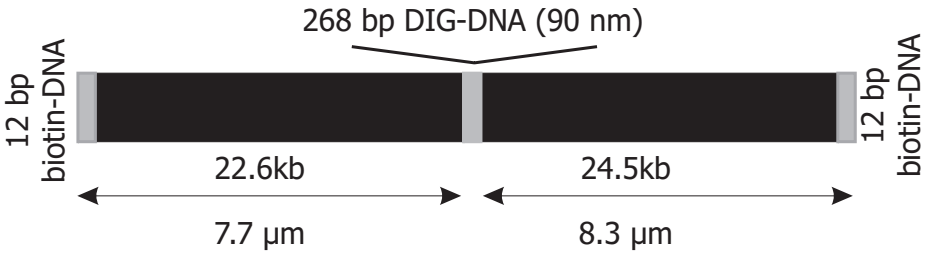

Figure 6.2. The DIG-DNA construct. The 12 bp overhang at both ends of a λ-DNA is filled in with 12 nucleotides of which 2 are functionalized with biotin. In approximately the middle of the molecule there is a 268 bp fragment including DIG molecules in a ratio 1:20, resulting in $\sim$13 DIG molecules available over a range of 90 nm. The contour length of the complete construct is 16.1 µm.

6.2.4 Hysteresis of the piezo-tube

A piezo-tube was used to scan the probe back and forth, while a piezo stack was used to independently control the indentation of the molecule. Piezo tubes exhibit hysteresis which makes independent calibration of the probe position necessary. Since the hysteresis is a function of the scan speed (in Volts) and the scan range, the actual position as function of the applied voltage was recorded with these predefined settings. The actual position of the tube was determined with a LED mounted to the end of the tube in combination with a position detector (PSD, DL100-7-KER) mounted to the optical table. To convert the PSD signal from Volts to microns optical microscope images of a µ-pipette clamped to the piezo tube were obtained as a function of the applied voltage in a DC measurement. The position of the probe was determined applying a centroid algorithm on the microscopy images.

6.2.5 DIG-functionalized DNA

Bacteriophage λ-DNA was labeled with biotinylated-dATP (Gibco-BRL) and biotinylated-dUTP (Sigma) by using Klenow fragments (Sigma). The labeled DNA was purified by a Centricon-100 spin column. The purified DNA was digested with two enzymes, SacI (NEB) and XbaI (NEB) to create two long fragments, one (22.6 kbp) with an SacI overhang and one (24.5 kbp) with an XbaI overhang. These fragments were purified by electro-elution (Bio-trap, Chromtech, Cheshire, UK). A 391 bp double-stranded DNA fragment labeled with digoxigenin was created by PCR using digoxigenin labeled dUTPs (Roche). Since both dUTP and dTTP binds to dATP some of the dTTPs were replaced for dig-dUTP. The 391 bp fragment was incubated with dig-dUTP and dTTP (ratio digdUTP: dTTP was 1:20) and dATP, dGTP, dCTP, and Klenow DNA polymerase for PCR. One in 20 dTTPs was replaced by a labeled dUTP. The 391 bp fragment was digested with SacI and XbaI to create a 268 bp fragment with a SacI overhang at one end and an XbaI overhang at the other end. Finally the fragment was purified by electro-elution. The two long fragments (22.6 kb and 24.5) were mixed together with the 268 bp fragment at a ratio 1:1:20 for annealing. The

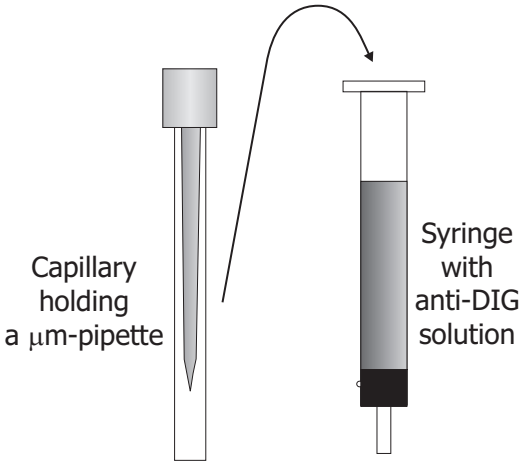

Figure 6.3. Method used to coat a pipette with α-DIG. To keep volumes small the pipette was inserted into a capillary held at its back-end by a rubber cap. Subsequently the capillary was injected in a 1 ml syringe containing a TE-buffer with 100 μg/ml α-DIG. After the capillary with the pipette was filled, it was closed at its open end with another rubber cap and stored at 4^{o}C until use.

mixture was heated and cooled down slowly and finally ligated with T4 DNA ligase (NEB) at 16^{o}C. A schematic structure of the resulting DNA molecules is shown in Fig. 6.2 where the length of the different regions are indicated.

6.2.6 α-DIG functionalized pipettes

For the preparation of α-DIG coated pipettes small volumes are essential to prevent the use of large amounts of antibody. Glass capillaries with an inner diameter of 1.5 mm were cleaned by placing them 1 hour in a 65% HNO_3 solution. Subsequently they were rinsed several times with Milli-Q and finally dried using nitrogen. Freshly pulled μ-pipettes (1-2 μm tip diameter) were silanized with TMSDMA (Chapter 2) and inserted into the capillaries. A small rubber cap placed at the end of the capillary held the pipette at its back-end as indicated in Fig. 6.3.

From a 1 ml syringe (BD Plastipak, Franklin Lakes, NJ, USA) the rubber cap was taken off from the plunger. Subsequently we placed it upside down in the syringe tube, creating a small but long container. 200 μl TE-buffer with 100 μg/ml α-DIG was injected in this. Inserting the capillary with the μ-pipette in this container the capillary was filled with the α-DIG solution due to capillary forces. After filling, the capillaries were taken out and closed at its open end with another rubber cap and stored at 4^{o}C. Shortly before the experiment an α-DIG coated pipette was taken out of the capillary and rinsed several times with TE-buffer. Next it was mounted into the microscope and directly injected into the flow cell.

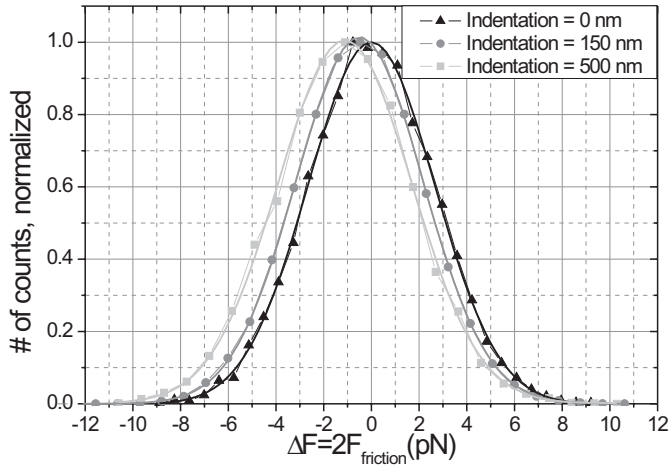

Figure 6.4. Histogram of the friction force values between a 170 nm pipette and a single DNA molecule within a scan range of 1.25 μm derived from 50 line traces. Histograms are shown for three indentations.

6.3 Experimental results

6.3.1 Friction forces between a probe and naked DNA

In the first experiment we scanned an uncoated pipette with a tip diameter of 200 nm (TIP01TW1F-L, WPI, Sarasota, FL, USA) back and forth along a single DNA molecule stretched with a tension of 30 pN. The force was recorded in the case the probe was moving away (trace) from the trapped bead and for the probe moving towards the bead (retrace). Subtracting traces and their corresponding retraces yielded the friction forces multiplied by a factor of 2 ($2F_{fric} = F_{trace} - F_{retrace}$).

Macroscopically the friction force between two solids moving with respect to each other is dependent on the normal force N and the dynamic friction coefficient μ_s according to Coulomb's law (Bowden and Tabor, 1950).

$$F = \mu_s N \tag{6.1}$$

Here the normal force is a function of the indentation d (Eq. 5.2) and the position of the probe with respect to the trapped bead. Therefore recordings were obtained for different indentations: 0, 150, and 500 nm with a total scan range of 5 μm and a scan speed of 50 μm/s, which was the typical speed used in the scanning experiments. We positioned the probe manually such that its range was in the center of the DNA molecule. To minimize the influence of the probe position on the normal force a range of 1.25 μm from the obtained data around the center position of the probe was analyzed. For each indentation 50 (re)traces were analyzed. After subtracting the trace and retraces the resulting force values ($2F_{fric}$) were plotted in a histogram and fitted with a Gaussian to calculate the mean friction force for the corresponding indentation, as shown in Fig. 6.4(a). For no indentation the mean friction force as determined by the Gaussian fit was 0.00 pN. At an indentation of approximately 150

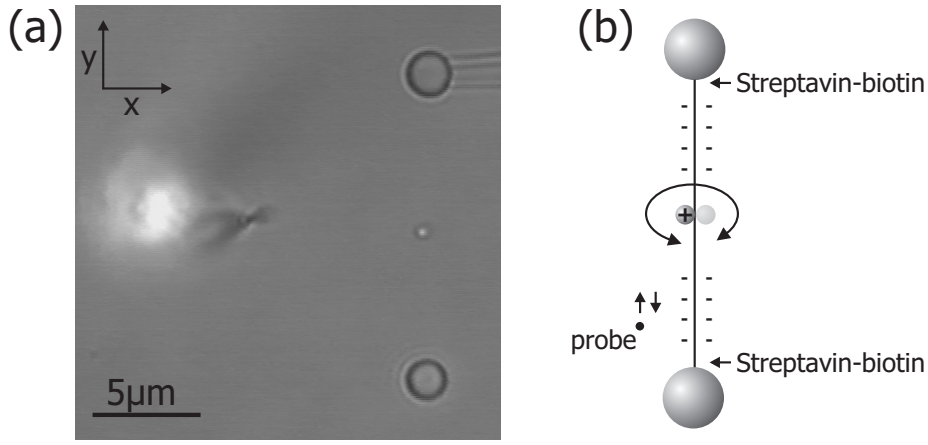

Figure 6.5. (a) An optical microscope image of the two 2.67 µm beads suspending a single λ-DNA molecule. A 450 nm PLL-coated bead was connected to the middle of the molecule based on electrostatic interactions. A multi-walled carbon nanotube (MWNT) connected to a silanized µ-pipette was used as probe. (b) A schematic overview of the system. The DNA molecule was stretched in between 10-55 pN. Assuming the DNA to be a rod and not torsionally constraint the bead can rotate freely around the axis of the DNA molecule.

nm the mean friction force was 0.24 pN and at 500 nm 0.55 pN. The values found are corrected for an offset attributed to the drag force induced by the moving pipette. The offset values at the three indentations were determined for the same system without a suspended DNA molecule and found nearly constant with a value of approximately 0.08 pN.

6.3.2 Localizing a 450 nm bead on a DNA molecule

To localize a protein or, as we discuss in this section, a 450 nm bead it is important that the interaction forces between the probe and the bead are larger than the interaction forces between the probe and the naked DNA and furthermore that this difference is large enough to overcome the positional fluctuations of bead in the optical trap, as discussed in the previous chapter. These fluctuations expressed as a force, F_{sd}, can be derived from Eq. 5.1 as

$$F_{sd} = k_{tr} x_{sd} = \frac{k_{tr}}{k_{tr} + k_{dna,eff}} \sqrt{4\gamma k_b T B} \tag{6.2}$$

where $k_{dna,eff}$ is the effective stiffness of the DNA molecule as sensed by the trap. The smallest force that can be detected is thus $\leq \sqrt{4\gamma k_b T B} \approx 0.64$ pN.

A 450 nm bead coupled to a single DNA molecule was scanned with a µ-pipette and a MWNT as a probe, where for the latter one an optical image is shown in Fig. 6.5(a). In Fig. 6.5(b) a schematic representation of the bead-DNA-bead system is shown. Considering the DNA molecule to be not torsionally constrained the bead can

freely rotate around the axis of the DNA molecule. Before discussing the localization of a 450 nm bead with one of the two probes we first give an indication of the typical binding force between the 450 nm bead and the DNA molecule based on electrostatic interactions.

Binding forces between the 450 nm bead and DNA

From the procedure necessary to couple a single 450 nm bead to a naked stretched DNA molecule, an indication of the binding force between the bead and the DNA molecule was derived. When touching the DNA molecule with the 450 nm bead we subsequently moved it around to affirm a connection as schematically depicted in Fig. 6.1(e). In most of the cases (>80%) we were able to pull the 450 nm bead out of the trap by moving the DNA molecule away. In Chapter 3 we found a linear detection range of 0.10 μm for these beads limited by the escape force. Although a maximum trap stiffness of 334 pN/μm was found for the results discussed in Chapter 3, the maximum trap stiffness for the experiments discussed in this chapter was found to be ∼600 pN/μm. Since we were still able to pull the beads out of the trap the binding force between a single bead and the DNA molecule originating from the electrostatic interactions is >50 pN.

Localizing the 450 nm bead with a μ-pipette

Fig. 6.6 is a SPOT-image containing the traces acquired by scanning a pipette with a tip diameter of 2 μm over a range of 8.2 μm at a speed of 50 μm/s. In the lower graph the position of the probe perpendicular to the DNA molecule is given. The DNA molecule was stretched to ∼25 pN with a trap stiffness of 501 pN/μm. Note that it is not possible to determine the actual indentation of the DNA molecule, since it is unknown at which point the probe touched the molecule. Two areas are pointed out in the SPOT-image where the bead is clearly observed. In the dark section before area 1 the probe was approaching the DNA molecule and even indenting the molecule where slight interaction forces were visible. However retracting the probe ∼30 nm resulted in a clear localization of the bead indicated as area 1. In between area 1 and 2 the probe was retracted and repositioned resulting in an observed shift of the bead.

In Fig. 6.7(a) an individual line trace of the SPOT-image is shown for both areas as indicated in Fig. 6.6. Within each area we extracted line traces with force peaks higher than 30 pN. The averaged result of these line traces are also shown in Fig. 6.7(a), again for both areas. From the onset of the signal in the individual line traces it was clear that there was no induced movement of the bead over the DNA molecule. The fact that in several individual line traces the typical force plateau for dsDNA is visible indicates a binding force of at least 65 pN between the bead and the DNA molecule. The strong interaction forces originate from both topography and from electrostatic interactions between the probe and the bead since the borosilicate pipette is negatively charged. In Fig. 6.7(b) a histogram is shown for the maximum force observed in the line traces for both area 1 and 2 after these traces were selected by a threshold of 30 pN. The mean maximum force was 68 pN in area 1 and 66 pN in area 2.

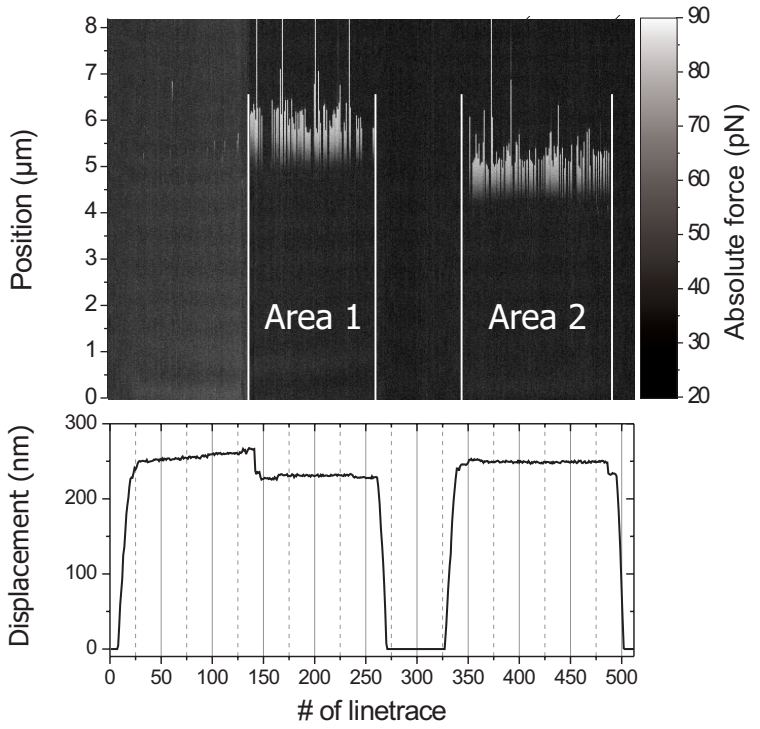

Figure 6.6. A 'SPOT-image' of a 450 nm bead connected to a single DNA molecule. The y-axis indicates the position of the probe where the trapped bead is located at the bottom side of the image and the immobilized bead at the upper side. The x-axis indicates the number of the line trace acquired. The signal plotted is the force in the DNA molecule during scanning. Only the trace image is shown corresponding to the probe moving away from the trapped bead. In the lower graph the displacement of the probe perpendicular to the DNA is pointed out.

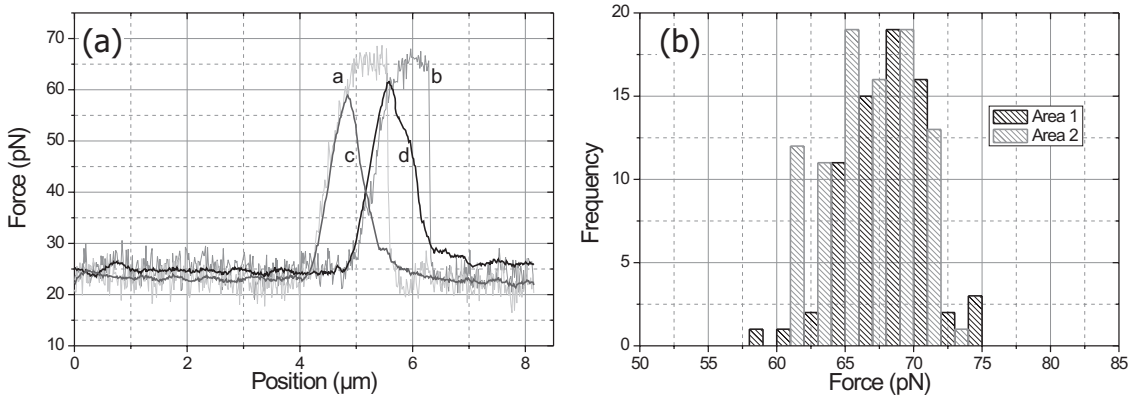

Figure 6.7. (a) Individual (curve a and b) and averaged (curve c and d) line traces for the two areas as indicated in Fig. 6.6. (b) Histogram of the maximum force observed in each line trace in the two areas that was selected by a threshold of 30 pN.

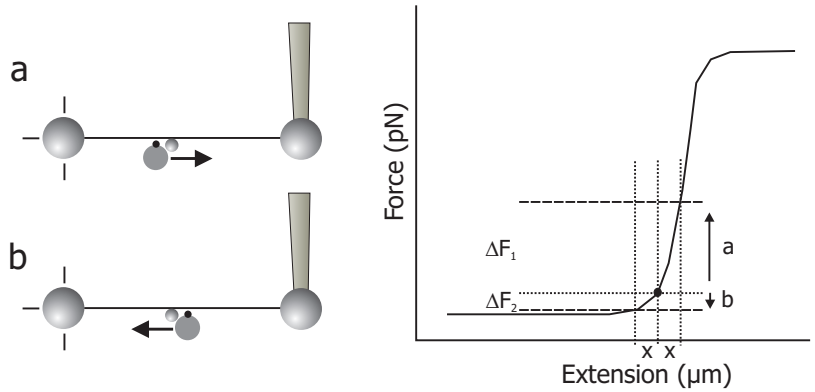

Figure 6.8. Schematic representation indicating the influence of the scanning direction on the measured force. In situation (a) the probe is scanning in a direction away from the trapped bead. Generating a displacement x of the trapped bead when the probe passes the 450 nm bead this results in an observed force difference ΔF_1. Scanning in the opposite direction (situation (b)) while initiating the same displacement x of the trapped bead this results in a force change ΔF_2.

In the retrace images the bead was not visible for which we do not have an explanation. The difference between the trace and retrace images is the scanning direction, which influences the response of the trapped bead. In Fig. 6.8 the influence of the scanning direction is schematically explained. Consider a DNA molecule that is stretched to a certain force F indicated with the black dot in the force-extension curve. Assume that if the probe is scanning in a direction away from the trapped bead (situation (a)) it initiates an additional extension x of the molecule resulting in a force increase ΔF_1 due to its interaction with the 450 nm bead. Based on symmetry the same force increase will be generated in the opposite scanning direction, but this force increase is experienced by the bead immobilized on the μ-pipette. The part of the DNA molecule between the probe and the trapped bead will be relaxed by a distance x and therefore a force decrease ΔF_2 (situation (b)). As can be seen there is a difference between the initiated force changes, which is dependent on the local slope of the force-extension curve. In general the force change for the retraces is smaller than for the traces. In addition the measured force cannot become smaller than 0 pN limiting the maximum achievable force change in the retraces by the stretching level of the molecule. Since the molecule in the experiment was stretched to 25 pN a similar force decrease was expected for the retraces. Rotation of the bead is not thought to be an explanation since for the trace image the bead is localized in area 1 for 76% of the time and 90% in area 2 if we consider the dark line traces in these two areas to be a situation where the 450 nm bead was located at the other side of the DNA molecule.

The disadvantage of the strong interaction forces between the pipette and the 450 nm is that it makes it difficult to detect multiple beads connected to the molecule. As can be seen from Fig. 6.7(a) the individual line trace shows an increase in force over

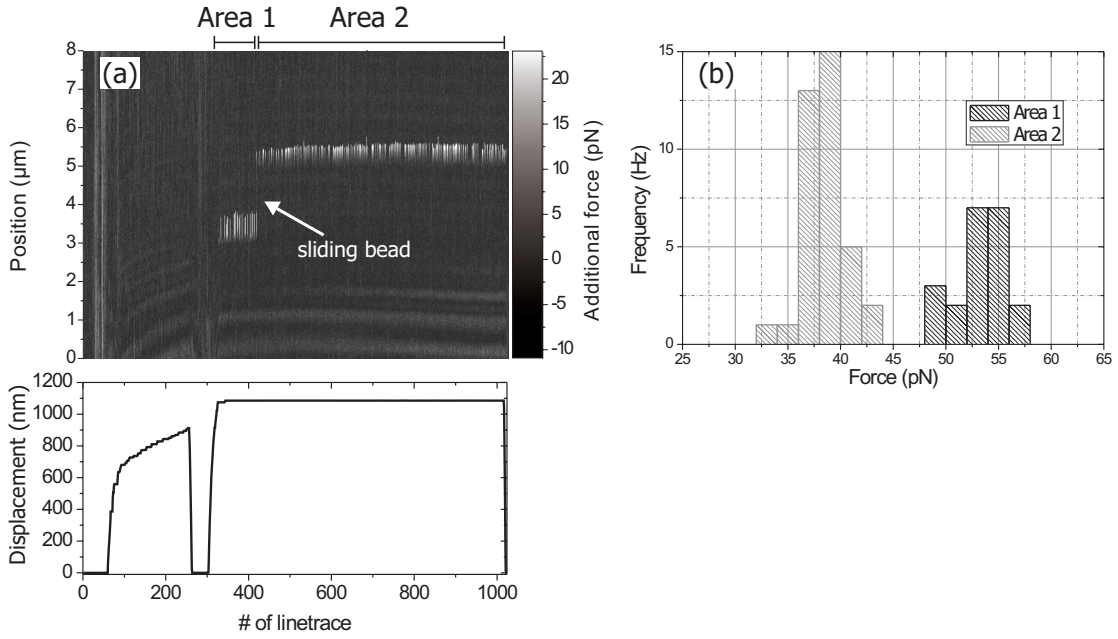

Figure 6.9. (a) Trace image of a 450 nm poly-L-lysine coated polystyrene bead on a single suspended dsDNA molecule acquired with the SPOT. During the experiment the bead slided, indicated with the arrow, a few microns to a new position. The areas before and after this sliding are called area 1 and 2. (b) Histogram of the maximum force observed in each line trace in the two areas.

a range of ∼1.5 µm. This means that if a second bead was located within this range it most likely was not detected. In the case for localizing multiple particles on a DNA molecule a trade-off has to be made between the magnitude of the interaction forces and its consequences for the resolution and the limitations it can bring for observing multiple particles.

Localizing the 450 nm bead with a MWNT

In this section we discuss the localization of a 450 nm bead with a MWNT as probe instead of a µ-pipette. A 450 nm bead was coupled to a DNA molecule after which the molecule was stretched to a force of 20 pN with a trap stiffness of 574 pN/µm. The trace SPOT-image acquired for this system is shown in Fig. 6.9(a). The signal visualized here was DC-filtered to enable electronic amplification, preventing limitations in the resolution due to digitization of the analog signals. In the lower graph the position of the probe perpendicular to the DNA molecule is given. In the first part of the SPOT image the probe approached the DNA molecule until the bead appeared in the SPOT image. At this point the indentation of the DNA molecule was kept constant. As can be seen the bead moved once a few microns over the DNA molecule to a new position during the experiment indicated with an arrow in Fig. 6.9. The 'dark states' in area 1 and 2 during visualization of the bead are attributed to a

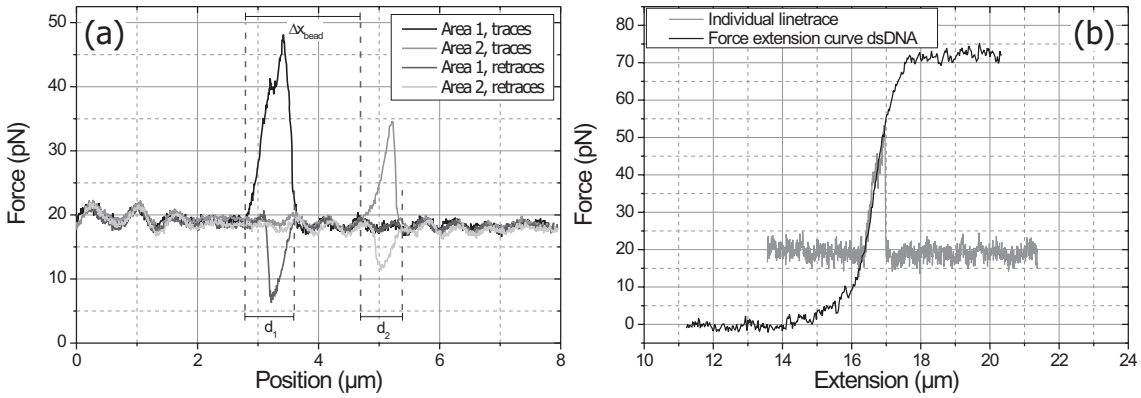

Figure 6.10. (a) Averages of the extracted lines from the trace and retrace images for area 1 and 2. (b) Comparison of an individual line trace in area 1 (see Fig. 6.10) and the actual force extension curve of the dsDNA molecule.

rotation of the bead. In the lower part of the image where the probe was the closest to the trapped bead, interference is visible caused by backscattering from the pipette holding the probe. In Fig. 6.9(b) a histogram is shown for the maximum force observed in each line trace for area 1 and 2 indicated in the SPOT image. In area 2 the average maximum force is 39 pN and somewhat lower than in area 1 where an average maximum force of 54 pN was found. In comparison with the localization results of the 450 nm bead obtained with the µ-pipette the mean maximum force was found lower. A smaller diameter of the probe can lead to stronger interactions based on topography, but also to lower interactions due to a smaller contact area. Furthermore the electrostatic interactions are expected to be smaller for the carbon nanotube since it is not negatively charged. For these experiments rotation of the bead seems not to be an issue since for area 1 the bead is observed 75% of the time and for area 2 82%, which is in the same order as found for the µ-pipette experiment.

Fig. 6.10(a) also presents the averages of the retraces for area 1 and 2. We will call the point at which the probe touches the bead resulting in a sudden increase in force, the initiation point. The distance between the initiation points in the trace and the corresponding retrace, indicated in Fig. 6.10(a) as d_1 and d_2, equals the sum of the diameter of the bead and the probe. For this experiment we found for d_1 $\sim$800$\pm$100 nm and for d_2 $\sim$700$\pm$100 nm, where we expected 500-550 nm (bead diameter + MWNT diameter). Since in this case we are considering line averages an explanation for the difference could be a small displacement of the bead during imaging or drift of the probe with respect to the bead-DNA-bead system. Analyzing individual traces and their related retraces the size was $\sim$600$\pm$100 nm (d_1), closer to the expected value. Comparison of the traces and retraces provides thus valuable positional information even though the distances over which interaction take place are large. Note that for these scanning experiments the average maximum force for the retraces was indeed smaller than for the traces as expected and discussed in the previous section.

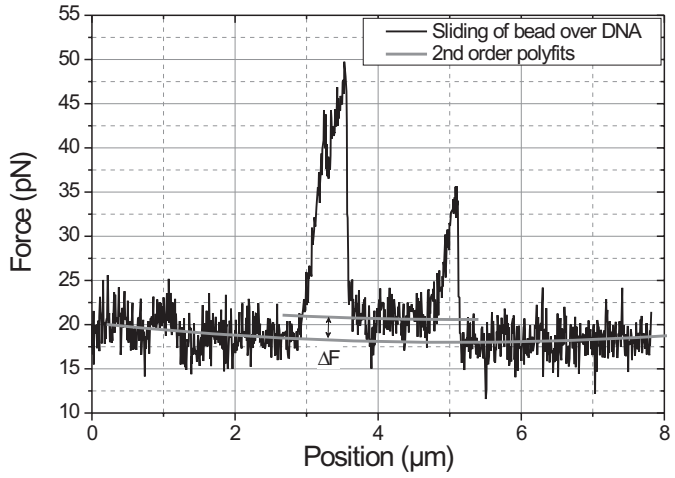

Figure 6.11. Line trace where the 450 nm bead slided over the DNA molecule for 1.9±0.1µm to a new position. A 2nd order polynomial fit was used to obtain ΔF indicating the force required to move this bead over the molecule.

The large bead displacement observed during the experiment and indicated in Fig. 6.9 with the arrow, can be deduced from the line traces. In Fig. 6.10(a) this distance is indicated as Δx_{bead} and found to be 1.9±0.1 µm. The line trace in which the bead moved over the DNA molecule to a new position is shown in Fig. 6.11. From this trace the same positional shift of 1.9±0.1 µm was found. The additional force required to move the bead over the DNA molecule was derived by fitting a 2nd order polynomial to the part of the curve where the probe was sliding over the naked DNA. Using the same fit parameter values and fitting only the offset value in the region where the bead was sliding over the DNA we calculated the additional force ΔF as the difference in the offset values resulting in 2.6±0.2 pN.

In a next step we analyzed the bright field images acquired with a CCD-camera during the experiment at a frame rate of 25 Hz. Applying a particle tracking method, based on cross-correlating a template image of the bead, the position of the 450 nm bead was determined for each individual frame. In Fig. 6.9 the resulting x and y positions of the bead are shown. Again the shift of the bead over the DNA molecule (in the y-direction) is clearly visible. From the mean y-position before and after the shift of the bead again a displacement of 1.9±0.1 µm was found, identical to that as determined from the SPOT-images. From the x-position of the bead the moment of indentation at about frame number 2500 can be clearly seen. The shift in x-position was ∼300 nm calculated from the mean positions that equals the indentation of the DNA molecule.

Assuming that the bead rotates randomly around the DNA molecule the bead will be detected mostly at its outer positions when observed at an angle perpendicular to the rotation axis in Fig. 6.12. But for a random rotation the distribution was also expected to be symmetric, but as can be seen for the frames (0-2000) there is a preference for the position around 1.9 µm instead of 2.2 µm (79% versus respectively 21%). This means that the bead was actually directed mostly towards the probe,

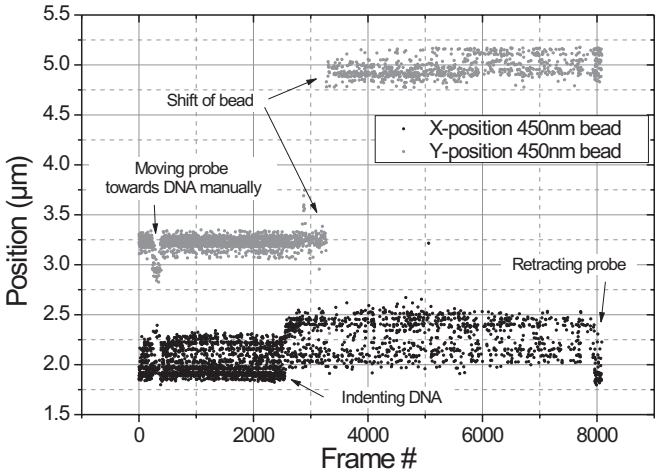

Figure 6.12. X (black dots) and Y position (red dots) of the 450nm bead during the complete experiment determined using a template tracking algorithm.

which was unexpected since the DNA was not torsionally constrained. When we indented the DNA molecule, the distribution was shifted and furthermore the bead is slightly more often (61%) found at the 'other side' of the DNA molecule.

The side excursions $R_\perp$ of a single DNA molecule for large tensions (10-55 pN) was derived by Marko and Siggia (1995) and can be written as

$$R_\perp = \sqrt{\frac{k_b T L}{F}} \tag{6.3}$$

where the molecule was considered as a string, suggesting the presence of vibration modes in the molecule. Consequently $R_\perp$ is 58 nm in the middle of the molecule for a tension of 20 pN. In our experiment we coupled a small bead to the molecule affecting the time behavior of the side excursions. For the DNA molecule pulled taut and neglecting its transverse thermal fluctuations ($R_\perp$), the maximum displacement of the bead due to rotation around the DNA molecule equals its diameter. From Fig. 6.12(a) it can be seen that the x-position was confined to a band of ∼500 nm, which is in accordance with the summation of the diameter of the bead and the transverse fluctuations of the DNA molecule. For the y-position a variation of 90 nm was found before indentation. During indentation the variation was broadened to ∼300 nm where presumably the initiated bead displacements in the axial direction of the molecule by the probe was the dominant factor.

In another scanning experiment with the same construct the bead slided more frequently over the DNA, but with shorter distances and for a longer period of time as shown in Fig. 6.13. In addition the centroid data (Fig. 6.13(b)) is shown. The intermediate black region in the SPOT image was caused by a temporarily retraction of the probe. This experiment illustrates the possibility of the SPOT microscope to follow or induce dynamics. However this does not allow averaging of multiple line traces to obtain a higher resolution in the position determination of the 450 nm bead.

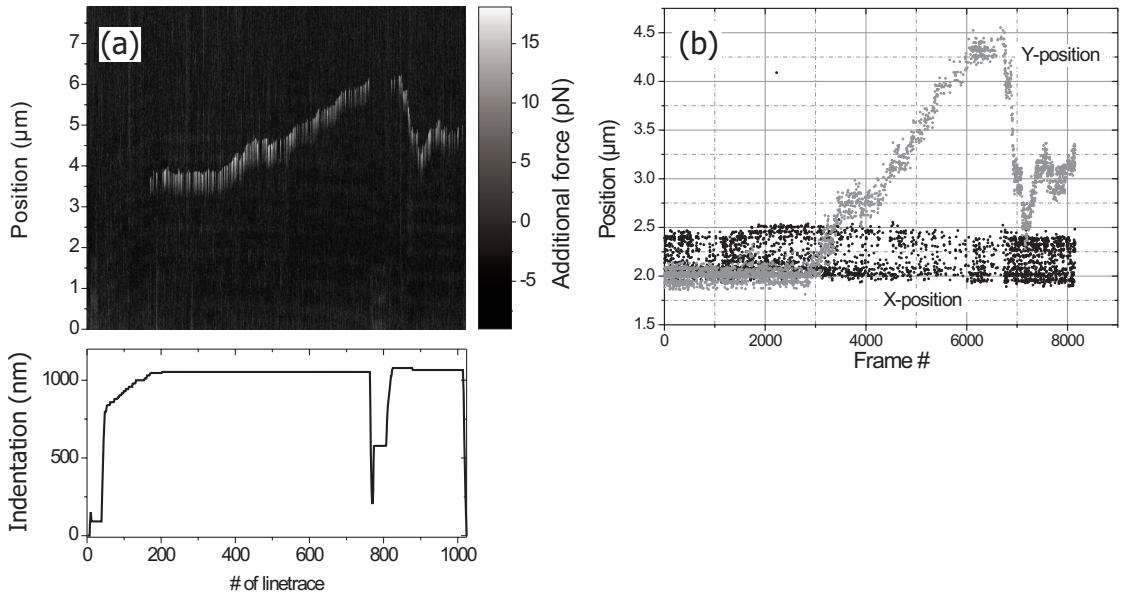

Figure 6.13. (a) SPOT image of a 450 nm bead on a single suspended DNA molecule. During imaging the bead slided over the DNA molecule. (b) X (black dots) and Y position (grey dots) of the 450nm bead during the complete experiment determined using a template tracking algorithm.

6.3.3 Localizing DIG-sites on a single DNA molecule

Now that we have shown that 450 nm beads can be localized we want to go one step further. As a step towards single protein localization we prepared a DNA construct with approximately 13 DIG molecules spread over a range of 90 nm around the middle of the molecule. To localize these DIG-molecules a µ-pipette with a tip diameter of 2 µm was coated with α-DIG to achieve a large interaction between the probe and the sample, since DIG forms a strong noncovalent bond with its antibody α-DIG consisting of van der Waals, hydrogen and ionic bonds.

A single DIG-DNA molecule was suspended between two beads and stretched to 25 pN. It was scanned with an α-DIG coated pipette over a range of 6.0 µm around the middle of the molecule at a speed of 50 µm/s. Upon passing the DIG-sites (268 bp = 91 nm) α-DIG molecules will bind. Dependent on the binding strength and loading rate (in this case $k_{eff} \cdot$ 50 µm/s $\approx$3-4 $\cdot 10^3$ pN/s) the bindings will be disrupted if the tension in the molecule is strong enough. In Fig. 6.14(a) a 3D representation is shown where consecutive force traces are plotted next to each other. In one axis the position along the DNA is plotted, while in the orthogonal axis the number of the line scan is plotted. In the z-direction the additional force is plotted. Clear stick-slip motion is visible in the area where the DIG sites are located. The signal visualized here was DC-filtered to enable electronic amplification to prevent limitations in the resolution due to digitization of the analog signals. Consequently the offset force of 25 pN is not observed. In Fig. 6.14(b) several individual traces and retraces are shown

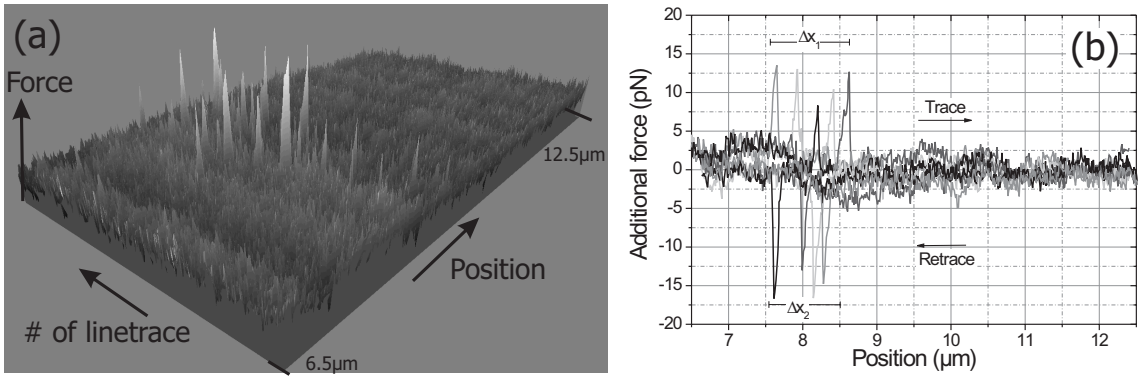

Figure 6.14. SPOT image acquired by scanning along a DNA molecule with a few DIG-sites located in the middle of the molecule with an α-DIG coated µ-pipette. Some of the individual line traces and retraces are plotted showing a stick-slip behavior caused by binding of α-DIG molecules to DIG-sites.

indicating the stick-slope motion within an area $\Delta x_1 \approx \Delta x_2 \approx 1$ µm caused by α-DIG/DIG binding. The size of the area within which the stick-slip motion is visible, is a convolution of the contact area of the pipette and the area in which the DIG-sites are localized. Furthermore the relatively large area of Δx_1 and Δx_2 makes it not possible to draw any conclusions on the orientation of the DNA molecule in between the two beads. Dependent on the orientation of the molecule there is a different DNA length in between the probe and the trapped bead, which can be 7.7 µm or 8.3 µm.

The mean value of the maximum amplitude for all the stick-slip motion shown in the trace image was found to be 11 pN. With an offset of 25 pN the average rupture force is ∼36 pN where no conclusions can be drawn if we have single or multiple bonds that are sensed. Several groups have measured the binding forces of ligand-receptor pairs using AFM and OT. Mostly the streptavidin-biotin pair has been investigated, which is one of the strongest noncovalent bonds. (Florin *et al.*, 1994; Lee *et al.*, 1994; Hinterdorfer *et al.*, 1996; Evans and Ritchie, 1997; Merkel *et al.*, 1999; Lo *et al.*, 2001; Ota *et al.*, 2005) In these studies it was found that the rupture force is slightly dependent on the loading rate. For streptavidin-biotin the individual rupture force was approximately 150 pN for a loading rate of 10^4 pN/s. For a lower loading rate a decrease in rupture force was observed. For α-DIG-DIG the binding affinity is lower and therefore a lower rupture force is expected (Chevalier *et al.*, 1997).

6.3.4 Localization accuracy

In the previously discussed experiments we used probes with different diameters and functionalization to localize 450 nm beads and DIG molecules. These few experiments are not sufficient to extract statistically relevant conclusions on the influence of indentation, probe diameter, and buffer conditions on the localization accuracy and the interactions between the probe and the sample. Here we derive an estimation of the localization accuracy and provide a sense for its dependence on the interaction forces. In this estimation we assumed an infinitesimally thin and rigid probe, i.e. the ideal probe.

In the localization of the 450 nm bead with the pipette and the MWNT, the most important difference in the detected signals was the 'rupture force'. This force, 66 pN wfor a μ-pipette probe and 39-54 pN for the MWNT, gives an indication of the interaction strength between the probe and the 450 nm bead. Related to the strength of the interactions is the change in effective stiffness of the DNA molecule as sensed by the optical trap (discussed in Chapter 5), due to a connection between the probe and the 450 nm bead.

For the scanning experiments the change in the effective stiffness of the DNA molecule was determined by measuring the slope of the linetraces at the point where the probe touched the 450 nm bead and the slope of the force extension curve of the naked DNA molecule at the same tension. For the μ-pipette probe the change in effective stiffness was a factor of 1.9 and for the MWNT this change was 1.3. The accuracy with which the position of the 450 nm bead can be determined is dependent on the positional fluctuations of the trapped bead and therefore on the stiffness of the DNA molecule. For the experiments shown the detection bandwidth B was 32.4 kHz far beyond the corner-frequency of the Lorentzian describing the response of the trapped bead. Based on Eq. 3.12 the force fluctuations can be expressed as $F_{sd} = k_{tr}x_{sd} = k_{tr}\sqrt{k_bT/(k_{tr}+k_{dna})}$ (where the subscript 'rms' is replaced by 'sd' indicating a standard deviation). Experimentally these force fluctuations (expressed as a standard deviation) are in the order of 2 pN, which can be derived from the individual linetraces plotted in Fig. 6.7(a) for the pipette and Fig. 6.10(b) for the MWNT, outside the region where the 450 nm beads were detected.

To detect a 450 nm bead the force increase at the initiation point has to be larger than these fluctuations. The required displacement of the 450 nm bead (still fixed to the molecule) and thus the localization accuracy therefore can be expressed as $F_{sd}/k_{dna,eff}$. Assuming a stiffness of the naked DNA molecule of 66 pN/μm (Smith *et al.*, 1996) the localization accuracy with the pipette is in the order of $2/(1.9 \cdot 66)$=16 nm and the accuracy with the MWNT $2/(1.3 \cdot 66)$=23 nm.

For the α-DIG/DIG experiment a similar derivation can be done. In this experiment the change in effective stiffness of the DNA molecule as sensed by the optical trap was a factor of 1.7, which results in an accuracy of 18 nm.

6.4 Conclusions

For localization of proteins it is positive that the friction forces found between the pipette (170 nm tip diameter) and a naked DNA molecule were <1 pN. This is advantageous for the localization of proteins since it is dependent on the difference of the probe interaction with the naked DNA and the probe interaction with proteins. This difference must be high enough to overcome the positional fluctuations of the trapped bead.

As a first model system for the SPOT-microscope we localized a 450 nm bead coupled to a DNA molecule where we used both a μ-pipette and a MWNT as scanning probe. The interaction forces for the pipette were found to be 68 pN therefore reaching the force plateau of the molecule. This high interaction force made the 450 nm bead move with a total range (the interaction range) of typically 1.5 μm corresponding to an extension of the part of the DNA molecule in between this bead and the optically trapped bead. Furthermore these forces resulted in an increase of the effective stiffness of the DNA molecule with a factor of 1.9 where the bead was approximately connected to the middle of the molecule. For the MWNT the interaction forces were found to be slightly lower, in the range of 40-50 pN resulting in an interaction range in the order of 0.5 μm and a change in effective stiffness of the DNA molecule with a factor of 1.3. A lower interaction range is preferable when multiple beads or proteins have to be detected. In the experiments with the MWNT we observed also a positional shift 1.9±0.1 μm of the bead, confirmed by video microscopy.

As a final step towards protein localization we localized DIG-sites with an α-DIG coated pipette (2 μm diameter) taking advantage of the strong binding affinity of this antibody-antigen pair. This strong affinity resulted in a high interaction force of the probe with the DIG molecules that were located over a range of 90 nm close to the middle of the DNA molecule. Due to convolution of this range with the size of the μm pipette these interactions were observed over a range of ∼1 μm. The mean maximum interaction force was found to be 36 pN, where the effective stiffness of the DNA molecule increased with a factor of 1.7. The typical range over which each interaction occurred was ∼150 nm.

In general the localization accuracy is dependent on the fluctuations of the trapped bead and the effective stiffness as sensed by the optical trap as was already expected from Chapter 5. Since we were able to do only a few experiments, it was not possible to obtain sufficient statistics. Based on the assumption of a infinitesimally thin and rigid probe we estimated the localization accuracy to be in the order of 15-20 nm.

Chapter 7

Conclusions and Outlook

This chapter summarizes the main conclusions of this thesis and offers suggestions for instrumental improvements. An outlook on future applications of the SPOT-microscope is provided, giving a glance at the capabilities of the microscope and the information that can obtained with respect to other single-molecule techniques in the field of molecular biophysics.

7.1 Final conclusions

We have designed and constructed the SPOT-microscope, a combination of scanning probe microscopy and optical tweezers. A single λ-DNA molecule was attached at each end to 2.67 μm polystyrene beads. One of the beads was immobilized on a μ-pipette and the other was held in the optical trap. A multi-walled carbon nanotube attached to a borosilicate μ-pipette, was used as a scanning probe. The DNA molecule was pulled taut and touched by the probe that was scanned back and forth. The induced forces resulting from the probe/DNA and probe/bead (450 nm) interactions, were measured by the optical trap.

Because of the proximity of the scanning probe to the optical trap it was not possible to use the light transmitted through the bead as a force signal as is common in a standard transmission-based OT. Therefore we had to build a reflection-based OT apparatus. In this process it was found that the linear detection range of the position detector was strongly dependent on the type of detector for beads larger than 1.4 μm. Using a quadrant detector the linear detection range was found to be 0.25 μm for 2.50 μm beads, whereas with the position sensitive detector a larger range of 0.57 μm was achieved. This difference was caused by the shape of the reflection pattern as it appeared on the detector.

Another issue that needed to be dealt with was the reduced amount of light on the detector. In an OT apparatus nearly all the laser light is refracted through the trapped bead, whereas only a small part ($\sim$0.01%) is reflected. For trapping a 1-2.50 μm bead with a laser power of 550 mW at the objective, the reflected light power at

the position detector was in the order of 100-500 μW. Despite this low intensity, the noise in the trap was still limited by the thermal motion of the trapped bead (0.5-3.0 μm in diameter) and not by the shot noise of the detector or other types of noise. For some beads 1/f noise was detected in the power spectral density function of the deflection signal attributed to rotational movements of the trapped bead. We have shown that the reflection-based OT apparatus is sensitive for rotational movements due to surface imperfections of the bead and the presence of small 'dirt' particles resulting in a slight asymmetric backscattered beam profile.

Furthermore we characterized the low-pass effect of silicon-based position detectors with a two-LED wobbler system, as function of wavelength, applied bias voltage and total light power up to 600 kHz. In AFM and OT applications the low-pass effect of the commonly used silicon detectors leads to serious errors in the force constant determination of the probe. We have shown that this low-pass effect can be compensated for using the frequency response of the detector as determined with the LED-wobbler.

As a first model system for the SPOT-microscope we localized 450 nm beads coupled to a DNA molecule where we used both a pipette with a tip diameter of 2 μm and a MWNT (40-90 nm diameter) as scanning probe. The main differences found for these two probes was the magnitude of the interaction forces, 68 pN for the pipette and 40-50 pN for the MWNT that resulted in a different interaction range, 1.5 μm for the pipette and 0.5 μm for the MWNT.
We also localized DIG-sites with an α-DIG coated pipette (2 μm diameter), utilizing the strong binding affinity of this antibody-antigen pair. This strong affinity resulted in a high interaction force of the probe with the DIG molecules ($\sim$20) that were located over a range of 90 nm approximately in the middle of the DNA molecule. Due to the convolution of this range and the size of the μ-pipette the onset of the force in different scans was spread over a range of approximately 1 μm. The mean maximum interaction force was found to be 36 pN after which a force drop was visible.

In general the localization accuracy is dependent on the fluctuations of the trapped bead and the effective stiffness as sensed by the optical trap. We showed that the change in effective stiffness of the DNA molecule as sensed by the optical trap was related to the rupture force, which is an indication for the strength of the interactions between the probe and the sample. Since we were able to do only a few experiments, it was not possible to obtain sufficient statistics, but based on the assumption of a infinitesimally thin and rigid probe we estimated a localization accuracy in the order of 15-20 nm.

7.2 Improvements

7.2.1 Instrumental improvements

An inherent problem in single-molecule experiments is the low throughput. Especially in the SPOT-microscope many steps are required before the actual scanning experiment can be performed. One of the time-limiting factors is the preparation of the scanning probe and subsequently its injection into the flow cell. The binding strength between the MWNT and the pipette was not always sufficient to withstand the transfer of the probe from air into the flow cell that was filled with an aqueous buffer. The surface tension at the water-air interface located at the entry-hole in the flow cell was in many cases strong enough to flip or even pull off the MWNT from the pipette. To allow continuity we generally prepared several probes such that there was at least one that can be used as probe. Once a MWNT made the transfer from air to water it was found that the binding strength between the MWNT and the pipette was always strong enough to be used as scanning probe. Improvements in the scanning probe design can be in the functionalization of nanotubes such that they can be covalently coupled to a pipette (Hafner *et al.*, 2001; Zhang *et al.*, 2003) or the use of UV glue to fix the MWNT to the pipette in a similar way as discussed for the canti(c)lever in Chapter 2.

Furthermore scaling down the dimensions of the scanning probe is desired for improving the resolution. A possibility would be to use SWNTs, which have a diameter of 1-1.5 nm. A problem is their attachment to the pipette that is used as a handle. Manual attachment of a SWNT to a pipette requires a SEM for visualization together with an accurate positioning system for moving the tip of the pipette with respect to the nanotube (Nishijima *et al.*, 1999). A more efficient and parallel approach is the use of chemical vapor deposition (CVD) to directly grow SWNTs on the pipette. In this procedure nanometer-sized metallic catalyst particles are used as initiation centers. Carbon is absorbed on the metallic particles. When this carbon precipitates, it nucleates a nanotube with a similar diameter as the catalyst particle. This procedure allows the production of numerous scanning probes at the same time (Hafner *et al.*, 1998, 2001).
Instead of using nanotubes one can develop probes in a similar way as AFM cantilevers. Using lithography techniques one can create edges with a curvature in the order of 10 nm. Producing tips in this way one has to bear in mind the required dimensions of the probe and the handles necessary to connect it to a pipette. As shown in Chapter 2 UV glue can be used to provide this connection, however it was also shown that the size of the handles, the lever in the case of a canti(c)lever, cannot be too large otherwise heating as a result of illumination with the laser can be a problem.

As shown in Chapter 3 the reflection-based OT apparatus is sensitive for rotations of the trapped bead. Irregularities on the surface of the 2.67 μm beads were observed when they were imaged in a scanning electron microscope (SEM). Use of other beads not having these irregularities will reduce the rotational sensitivity of the optical trap

and therefore reduce the 1/f-noise visible in the power spectral density of the deflection signal.
Furthermore the positional fluctuations of the trapped bead is a function of the effective stiffness of the DNA molecule. Using shorter DNA molecules the accuracy with which a protein can be detected is improved, but a trade-off has to be made between this improvement and the possibility of the use of shorter molecules from a practical point of view. If the pipette becomes too close to the trapped bead, the bead can be pushed out of the trap or the pipette influences the force measurement. A safe distance between the probe and each of the two beads is in the order of 3 μm. Shorter molecules will therefore strongly limit the scan range.
The implementation of a second optical trap also has some advantages. This provide the ability to cross-correlate both detector signals from the two beads. By tracking the statistical correlation between movement of both beads events that may not be visible in the position data of each bead can be detected (Mehta *et al.*, 1997). In addition, two traps allow the bead-DNA-bead system to be moved around freely. In this case an integrated probe is an option, which will greatly reduce the time needed for setting up the experiment.

7.2.2 Exploring the optimal conditions for SPOT-imaging

A pre-requisite for localizing proteins on a DNA molecule in the SPOT-microscope is that the DNA molecule is stretched. In this thesis we mentioned that the molecule should be stretched to the enthalpic linear regime of 10-50 pN. In this regime the effective stiffness of the molecule as sensed by the trap reached its maximum value, resulting in the highest achievable localization accuracy. However, a more detailed study should be carried out to determine the minimum required force for localization, which not necessarily has to be in the 10-50 pN range.

To study DNA-protein interactions in their most native state, we want to start with a minimal tension in the molecule. In a proceeding step the DNA-protein interactions can be studied at different levels of tension. In the case improvements are necessary first improvements on the level of instrumentation have to be made, such that for instance buffer conditions as the salt concentrations and pH are kept unaltered, preserving the native state of the DNA-protein interactions.

7.3 Outlook

The SPOT-microscope was built in order to localize individual proteins while interacting with a single DNA molecule and to acquire information of the influence of tension in the DNA molecule on the functional and dynamic properties of the protein. Furthermore the advantage of the SPOT-microscope is that since no surface is needed as a support, three dimensional diffusive processes are not obstructed except by the presence of the probe and the two beads suspending the DNA molecule, which

creates an environment that better resembles in vivo conditions. For future applications we want to focus on these advantages of the SPOT-microscope with respect to other single-molecule techniques and therefore want to study DNA-protein complexes where parameters such as force, diffusion and position play an important role. In the next sections we discuss some possible future experiments.

7.3.1 DNA-protein interaction studies

RNA polymerase

RNA polymerase (RNAP) is a protein that transcribes DNA into messengerRNA (mRNA). During transcription that is initiated at specific promoter DNA sequences, RNAP translocates along DNA while following its helical pitch. To synthesize RNA the presence of NTPs (ribonucleoside triphosphates) and ATP is required, and controlling the concentrations can function as a tool to control the transcription rate. The transcription process is reversible, which means that RNAP may backtrack along the DNA. Finally RNAP will preferentially release its RNA transcript at specific terminator DNA sequences.

From crystallography studies the size of *E.coli* RNAP is in the order of 10x10x16 nm and is thus a relative large protein (Darst *et al.*, 1989). From a recent OT study it was found that RNAP moves over the DNA template with base-pair steps (Abbondanzieri *et al.*, 2005). Furthermore AFM studies were carried out to make a distinction between the diffusion and transcription by RNAP over a DNA molecule (Guthold *et al.*, 1999). For non-specific interactions the RNAP was sliding over the DNA performing a one-dimensional random-walk. During transcription the RNAP was observed to processively thread the DNA template at rates of 1.5 bp/s. A similar study was achieved by combining OT with a total internal reflection fluorescence microscope (TIRF) (Harada *et al.*, 1999). Another AFM study concerned the bending of promotor DNA by RNAP (Rivetti *et al.*, 1999), where it was suggested that during transcription initiation the promotor DNA wraps around the RNAP over an angle of nearly 300 ^{o}.

In the SPOT-microscope we are able to deduce DNA-RNAP interaction parameters as the transcription rate as a function of the tension in the DNA, where we do not apply a force to the RNAP as was the case in the OT study of Abbondanzieri *et al.* (2005). Furthermore this allows to detection of unwinding events of the promotor DNA by the RNAP complex leading to elongation of the DNA molecule in the order of 60 nm Revyakin *et al.* (2004), which is an important step in the transcription initiation process. In general structural changes in the RNAP-DNA complex at different stages of the transcription process can be related to the position of this complex. In addition a multi-protein system complex can be studied where for instance promotor sites with physically separated domains on the DNA need to be brought together by proteins.

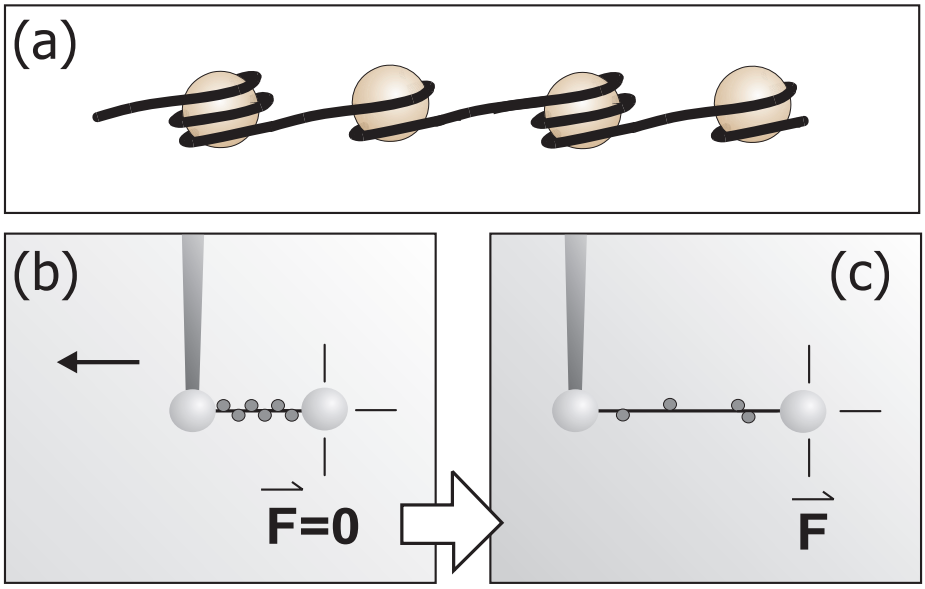

Figure 7.1. (a) A nucleosomal array ('bead-on-a-string structure'). (b) The formation of nucleosomes is allowed by exerting no tension to the DNA molecule. (c) Several nucleosomes are disrupted by increasing the tension.

Chromatin

Within a human cell the 2 meter genome has to undergo an enormous compaction in length of a factor 10^5 to fit in the cell nucleus. The first step in this compaction process is the formation of nucleosomes. These complexes, ∼11 nm in size are octamers of 4 different histone proteins around which DNA is wrapping itself ∼1.7 times (146 bp) leading to a compaction in length as is depicted in Fig. 7.1(a) (Kornberg and Lorch, 1999). These nucleosomal fibers are compacted further into a higher order assembly known as the 30-nm fiber (Carruthers and Hansen, 2000). A fundamental issue in biology is how this highly compacted chromatin is accessible for proteins allowing processes as transcription, recombination, and replication. This means that the nucleosome has to undergo certain conformational changes to allow these processes that need access to the DNA template.

Although the crystal structure of the nucleosomal particles is well known (Luger *et al.*, 1997; Harp *et al.*, 2000) not much is known about the dynamics of nucleosomes. AFM studies were performed to reveal the number of wraps of DNA around a nucleosomal particle (Nikova *et al.*, 2004) and the internucleosomal distance (Yodh *et al.*, 2002). A distribution of ∼1 wrap and ∼2 wraps of DNA corresponds to ∼25 nm and ∼50 nm of bound DNA length. From the internucleosomal distances it was found that nucleosomes are spaced along the DNA at certain distances, with the length of interconnecting, linker DNA varying according to the cell or tissue type. From OT studies the bound DNA length associated with 1 or 2 wraps was also derived by forcing unwrapping of the nucleosomes and measuring the associated length increase of ∼27

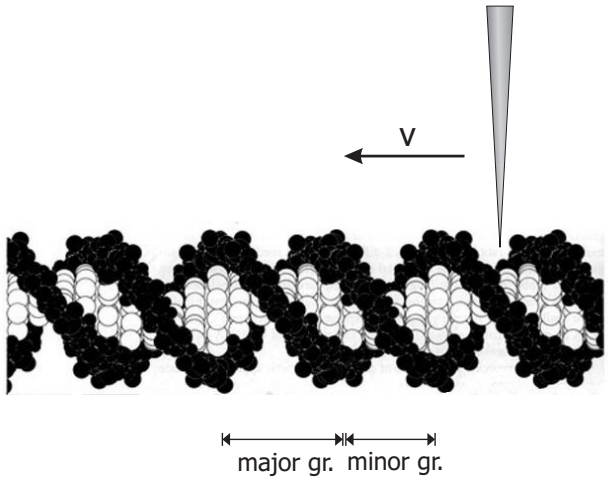

Figure 7.2. The sound of DNA. Scanning at a constant speed with a probe that partially penetrates into the major and minor groove (in the order of 1 nm) induces vibrations in the longitudinal direction of the molecule. These vibrations are characterized by a distinct frequency that is a function of the scan speed and the width of the grooves. Consequently the frequency will shift upon extension or retraction.

nm (Brower-Toland *et al.*, 2002) and ∼65 nm (Bennink *et al.*, 2001). Recently fluorescence resonance energy transfer (FRET) was applied to assess fast conformational fluctuations in nucleosomes (Tomschik *et al.*, 2005).

With the SPOT-microscope we can apply tension to force the unwrapping of nucleosomes while simultaneously measuring their position and thus the internucleosomal distance schematically presented in Fig. 7.1(b) and (c). Consequently we can determine which nucleosomes are unwrapped and determine if there is a preference in unwrapping nucleosomes with 1 wrap or 2 wraps. As a next step the requirements of further compaction of the bead-on-a-string structure can be studied as function of histone concentration and the presence of for instant the high mobility group (HMG) proteins that are the most abundant group of non-histone proteins. These proteins serve as architectural elements which affect the structure of both the DNA and the chromatin fiber. Structural alterations caused by HMG proteins facilitate a variety of DNA-dependent processes occurring in the context of chromatin (Bustin and Reeves, 1996; Catez *et al.*, 2003).

7.3.2 The sound of DNA

Besides studying the interactions between DNA and proteins the SPOT-microscope should be capable of determining the helical structure of DNA under various tensions. If we have a scanning probe thin enough to penetrate partially into the major and minor groove the widths of these grooves can be felt. Scanning with a constant speed v over a DNA molecule as indicated in Fig. 7.2, vibrations are generated with a pronounced frequency dependent on the scanning speed and the width of the major and minor groove. These frequencies appear in the power spectral density function

of the deflection signal of the trapped bead. To be able to detect the generated frequencies the scan speed should be chosen low enough such that the frequencies appear below the corner-frequency of the frequency spectrum of the trapped bead. Dependent on the tension within the molecule it is expected that the width of the grooves is altered and resulting in a frequency shift. In this way the unwinding of the helical structure of a dsDNA molecule during extension can be accurately characterized.

Still unknown is the exact structure of dsDNA when it is overstretched, subjected to forces of 65 pN or more. Various models for the structure of this so-called S-form have been proposed, but verification by experimental methods still awaits (Leger *et al.*, 1999; Rouzina and Bloomfield, 2001; Konrad and Bolonick, 1996; Kosikov *et al.*, 1999). One of the ideas is that the bases in the S-DNA conformation are pointed outside. The availability of these bases can be verified with the SPOT-microscope by coating the probe such that it binds to these bases. A large increase in interaction force will then be observed when the molecule is stretched beyond 65 pN.

Bibliography

Abbondanzieri E. A., Greenleaf W. J., Shaevitz J. W., Landick R., and Block S. M., "Direct observation of base-pair stepping by RNA polymerase", *Nature*, **438**(7067), 460–465. 2005.

Akita S., Nishijima H., Nakayama Y., Tokumasu F., and Takeyasu K., "Carbon nanotube tips for a scanning probe microscope: their fabrication and properties", *J. Phys. D - Appl. Phys.*, **32**(9), 1044–1048. 1999.

Albrecht T. R., and Quate C. F., "Atomic resolution imaging of a non-conductor by atomic force microscopy", *J. Appl. Phys.*, **62**(7), 2599–2602. 1987.

Anselmi C., Bocchinfuso G., De Santis P., Savino M., and Scipioni A., "Dual role of DNA intrinsic curvature and flexibility in determining nucleosome stability", *J. Molec. Biol.*, **286**(5), 1293–1301. 1999.

Ashkin A., *Phys. Rev. Lett.*, **24**, 156. 1970.

Ashkin A., "Forces of a Single-Beam Gradient Laser Trap on a Dielectric Sphere in the Ray Optics Regime", *Bioph. J.*, **61**(2), 569–582. 1992.

Ashkin A., Dziedzic J.M., Bjorkholm J.E., and Chu S., "Observation of a single-beam gradient force optical trap for dielectric particles", *Opt. Lett.*, **11**(5), 288–290. 1986.

Ashkin A., Dziedzic J. M., and Yamane T., "Optical trapping and manipulation of single cells using infrared laser beams", *Nature*, **330**(6150), 769–71. 1987.

Ashkin A., and Dziedzic J.M., "Optical Levitation by Radiation Pressure", *Appl. Phys. Lett.*, **19**(8), 283–285. 1971.

Ashkin A., and Dziedzic J. M., "Optical trapping and manipulation of viruses and bacteria", *Science*, **235**(4795), 1517–20. 1987.

Bahatyrova S., Frese R. N., van der Werf K. O., Otto C., Hunter C. N., and Olsen J. D., "Flexibility and size heterogeneity of the LH1 light harvesting complex revealed by atomic force microscopy: functional significance for bacterial photosynthesis", *J. Biol. Chem.*, **279**(20), 21327–33. 2004^a.

Bahatyrova S., Frese R. N., Siebert C. A., Olsen J. D., van der Werf K. O., van Grondelle R., Niederman R. A., Bullough P. A., Otto C., and Hunter C. N., "The native architecture of a photosynthetic membrane", *Nature*, **430**(7003), 1058–1062. 2004^b.

Baumann C. G., Smith S. B., Bloomfield V. A., and Bustamante C., "Ionic effects on the elasticity of single DNA molecules", *PNAS*, **94**(12), 6185–90. 1997.

Bennink M. L., *Force spectroscopy of single DNA-protein complexes: An optical tweezers study*, Ph.D. thesis, University of Twente, Enschede. 2000.

Bennink M. L., Scharer O. D., Kanaar R., Sakata-Sogawa K., Schins J. M., Kanger J. S., de Grooth B. G., and Greve J., "Single-molecule manipulation of double-stranded DNA using optical tweezers: interaction studies of DNA with RecA and YOYO-1", *Cytometry*, **36**(3), 200–8. 1999.

Bennink M. L., Leuba S. H., Leno G. H., Zlatanova J., de Grooth B. G., and Greve J., "Unfolding individual nucleosomes by stretching single chromatin fibers with optical tweezers", *Nat. Struct. Biol.*, **8**(7), 606–610. 2001.

Bennink M. L., Nikova D. N., van der Werf K. O., and Greve J., "Dynamic imaging of single DNA-protein interactions using atomic force microscopy", *Anal. Chim. Act.*, **479**(1), 3–15. 2003.

Berg-Sorensen K., Oddershede L., Florin E. L., and Flyvbjerg H., "Unintended filtering in a typical photodiode detection system for optical tweezers", *J. Appl. Phys.*, **93**(6), 3167–3176. 2003.

Berg-Sorensen K., and Flyvbjerg H., "Power spectrum analysis for optical tweezers", *Rev. Sci. Instr.*, **75**(3), 594–612. 2004.

Binnig G, Rohrer H., Gerber Ch, and Weibel E, "Surface studies by scanning tunneling microscopy", *Phys. Rev. Lett.*, **49**(1), 57–61. 1982^a.

Binnig G, Rohrer H., Gerber Ch, and Weibel E, "Tunneling through a controllable vacuum gap", *Appl. Phys. Lett.*, **40**, 178–180. 1982^b.

Binnig G, Quate C. F., and Gerber Ch, "Atomic force microscopy", *Phys. Rev. Lett.*, **56**(9), 930–933. 1986.

Block S. M., Goldstein L. S., and Schnapp B. J., "Bead movement by single kinesin molecules studied with optical tweezers", *Nature*, **348**(6299), 348–52. 1990.

van den Bos A., Heskamp I., Siekman M., Abelmann L., and Lodder C., "The CantiClever: a dedicated probe for magnetic force microscopy", *Ieee Transactions on Magnetics*, **38**(5), 2441–2443. 2002.

Bouchiat C., Wang M. D., Allemand J. F., Strick T., Block S. M., and Croquette V., "Estimating the persistence length of a worm-like chain molecule from force-extension measurements", *Bioph. J.*, **76**(1), 409–413. 1999.

Bowden F.P., and Tabor D., *Friction and Lubrication of Solids: Part 1*. New York: Oxford University Press. 1950.

Brower-Toland B. D., Smith C. L., Yeh R. C., Lis J. T., Peterson C. L., and Wang M. D., "Mechanical disruption of individual nucleosomes reveals a reversible multistage release of DNA", *PNAS*, **99**(4), 1960–1965. 2002.

Bustamante C., Marko J. F., Siggia E. D., and Smith S., "Entropic elasticity of lambda-phage DNA", *Science*, **265**(5178), 1599–600. 1994.

Bustamante C., and Keller D., "Scanning Force Microscopy in Biology", *Phys. Today*, **48**(12), 32–38. 1995.

Bustin M., and Reeves R., "High-mobility-group chromosomal proteins: architectural components that facilitate chromatin function", *Prog. Nucl. Ac. Res. Mol. Biol.*, **54**, 35–100. 1996.

Carruthers L. M., and Hansen J. C., "The core histone N termini function independently of linker histones during chromatin condensation", *J. Biol. Chem.*, **275**(47), 37285–90. 2000.

Catez F., Lim J. H., Hock R., Postnikov Y. V., and Bustin M., "HMGN dynamics and chromatin function", *Biochem. Cell Biol.*, **81**(3), 113–22. 2003.

Chevalier J., Yi J., Michel O., and Tang X. M., "Biotin and digoxigenin as labels for light and electron microscopy in situ hybridization probes: where do we stand?", *J. Histochem. Cytochem.*, **45**(4), 481–91. 1997.

Chu S., Bjorkholm J. E., Ashkin A., and Cable A., "Experimental observation of optically trapped atoms", *Phys. Rev. Lett.*, **57**(3), 314–317. 1986.

Cluzel P., Lebrun A., Heller C., Lavery R., Viovy J. L., Chatenay D., and Caron F., "DNA: an extensible molecule", *Science*, **271**(5250), 792–4. 1996.

Cui Y., and Bustamante C., "Pulling a single chromatin fiber reveals the forces that maintain its higher-order structure", *PNAS*, **97**(1), 127–32. 2000.

Dai H. J., Hafner J. H., Rinzler A. G., Colbert D. T., and Smalley R. E., "Nanotubes as nanoprobes in scanning probe microscopy", *Nature*, **384**(6605), 147–150. 1996.

Darst S. A., Kubalek E. W., and Kornberg R. D., "Three-dimensional structure of Escherichia coli RNA polymerase holoenzyme determined by electron crystallography", *Nature*, **340**(6236), 730–2. 1989.

Darwin C.R., *The origin of species*. Vol. 11, New York: P.F. Collier & Son. 1909.

Davenport R. J., Wuite G. J. L., Landick R., and Bustamante C., "Single-molecule study of transcriptional pausing and arrest by E-coli RNA polymerase", *Science*, **287**(5462), 2497–2500. 2000.

Drake B., Prater C. B., Weisenhorn A. L., Gould S. A. C., Albrecht T. R., Quate C. F., Cannell D. S., Hansma H. G., and Hansma P. K., "Imaging Crystals, Polymers, and Processes in Water with the Atomic Force Microscope", *Science*, **243**(4898), 1586–1589. 1989.

Dunn R. C., "Near-field scanning optical microscopy", *Chem. Rev.*, **99**(10), 2891–928. 1999.

Evans E., and Ritchie K., "Dynamic strength of molecular adhesion bonds", *Biophys. J.*, **72**(4), 1541–55. 1997.

Finer J. T., Simmons R. M., and Spudich J. A., "Single myosin molecule mechanics: piconewton forces and nanometre steps", *Nature*, **368**(6467), 113–9. 1994.

Florin E. L., Moy V. T., and Gaub H. E., "Adhesion forces between individual ligand-receptor pairs", *Science*, **264**(5157), 415–7. 1994.

Ghislain L. P., Switz N. A., and Webb W. W., "Measurement of Small Forces Using an Optical Trap", *Rev. Sci. Instr.*, **65**(9), 2762–2768. 1994.

Gittes F., and Schmidt C. F., "Thermal noise limitations on micromechanical experiments", *Eur. Bioph. J. Biophys. Lett.*, **27**(1), 75–81. 1998.

Guthold M., Zhu X., Rivetti C., Yang G., Thomson N. H., Kasas S., Hansma H. G., Smith B., Hansma P. K., and Bustamante C., "Direct observation of one-dimensional diffusion and transcription by Escherichia coli RNA polymerase", *Biophys. J.*, **77**(4), 2284–94. 1999.

Hafner J. H., Bronikowski M. J., Azamian B. R., Nikolaev P., Rinzler A. G., Colbert D. T., Smith K. A., and Smalley R. E., "Catalytic growth of single-wall carbon nanotubes from metal particles", *Chem. Phys. Lett.*, **296**(1-2), 195–202. 1998.

Hafner J. H., Cheung C. L., Woolley A. T., and Lieber C. M., "Structural and functional imaging with carbon nanotube AFM probes", *Progr. Biophys. Molec. Biol.*, **77**(1), 73–110. 2001.

Hansma P. K., Cleveland J. P., Radmacher M., Walters D. A., Hillner P. E., Bezanilla M., Fritz M., Vie D., Hansma H. G., Prater C. B., Massie J., Fukunaga L., Gurley J., and Elings V., "Tapping Mode Atomic-Force Microscopy in Liquids", *Appl. Phys. Lett.*, **64**(13), 1738–1740. 1994.

Harada Y., Funatsu T., Murakami K., Nonoyama Y., Ishihama A., and Yanagida T., "Single-molecule imaging of RNA polymerase-DNA interactions in real time", *Biophys. J.*, **76**(2), 709–15. 1999.

Harp J. M., Hanson B. L., Timm D. E., and Bunick G. J., "Asymmetries in the nucleosome core particle at 2.5 A resolution", *Acta Crystallogr. D Biol. Crystallogr.*, **56 Pt 12**, 1513–34. 2000.

Hegner M., Smith S. B., and Bustamante C., "Polymerization and mechanical properties of single RecA-DNA filaments", *PNAS*, **96**(18), 10109–10114. 1999.

Hinterdorfer P., Baumgartner W., Gruber H. J., Schilcher K., and Schindler H., "Detection and localization of individual antibody-antigen recognition events by atomic force microscopy", *PNAS*, **93**(8), 3477–3481. 1996.

Huisstede J. H. G., van der Werf K. O., Bennink M. L., and Subramaniam V., "Force detection in optical tweezers using backscattered light", *Opt. Expr.*, **13**(4), 1113–1123. 2005.

Huisstede J. H. G., van Rooijen B. D., van der Werf K. O., Bennink M. L., and Subramaniam V., "Dependence of silicon position-detector bandwidth on wavelength, power, and bias", *Opt. Lett.*, **31**(5), 610–612. 2006.

Kassies R., van der Werf K. O., Lenferink A., Hunter C. N., Olsen J. D., Subramaniam V., and Otto C., "Combined AFM and confocal fluorescence microscope for applications in bio-nanotechnology", *J. Microsc.*, **217**(Pt 1), 109–16. 2005.

Kellermayer M. S. Z., and Bustamante C., "Folding-unfolding transitions in single titin molecules characterized with laser tweezers (vol 276, pg 1112, 1997)", *Science*, **277**(5329), 1117–1117. 1997.

Kojima H., Muto E., Higuchi H., and Yanagida T., "Mechanics of single kinesin molecules measured by optical trapping nanometry", *Biophys. J.*, **73**(4), 2012–22. 1997.

Konrad M. W., and Bolonick J. I., "Molecular dynamics simulation of DNA stretching is consistent with the tension observed for extension and strand separation and predicts a novel ladder structure", *J. Am. Chem. Soc.*, **118**(45), 10989–10994. 1996.

Kornberg R. D., and Lorch Y., "Twenty-five years of the nucleosome, fundamental particle of the eukaryote chromosome", *Cell*, **98**(3), 285–94. 1999.

Kosikov K. M., Gorin A. A., Zhurkin V. B., and Olson W. K., "DNA stretching and compression: large-scale simulations of double helical structures", *J Mol Biol*, **289**(5), 1301–26. 1999.

Krishnan A., Dujardin E., Ebbesen T. W., Yianilos P. N., and Treacy M. M. J., "Young's modulus of single-walled nanotubes", *Phys. Rev. B*, **58**(20), 14013–14019. 1998.

La Porta A., and Wang M. D., "Optical torque wrench: Angular trapping, rotation, and torque detection of quartz microparticles", *Phys. Rev. Lett.*, **92**(19), –. 2004.

Landau L.D., Lifshiftz E.M., and Sykes J. B., *Theory of elasticity*. 3rd edn., Oxford: Butterworth-Heinemann. 1986.

Landau L.D., and Lifshiftz E.M., *Fluid mechanics*. 2nd edn., Oxford: Pergamon Press. 1987.

Lang M. J., and Block S. M., "Resource letter: LBOT-1: Laser-based optical tweezers", *Am. J. Phys.*, **71**(3), 201–215. 2003.

Lee G. U., Kidwell D. A., and Colton R. J., "Sensing Discrete Streptavidin Biotin Interactions with Atomic-Force Microscopy", *Langmuir*, **10**(2), 354–357. 1994.

Leger J. F., Romano G., Sarkar A., Robert J., Bourdieu L., Chatenay D., and Marko J. F., "Structural transitions of a twisted and stretched DNA molecule", *Phys. Rev. Lett.*, **83**(5), 1066–1069. 1999.

Leuba S. H., Bennink M. L., and Zlatanova J., "Single-molecule analysis of chromatin", *Methods Enzymol*, **376**, 73–105. 2004.

Liphardt J., Onoa B., Smith S. B., Tinoco I. Jr, and Bustamante C., "Reversible unfolding of single RNA molecules by mechanical force", *Science*, **292**(5517), 733–7. 2001.

Lo Y. S., Zhu Y. J., and Beebe T. P., "Loading-rate dependence of individual ligand-receptor bond-rupture forces studied by atomic force microscopy", *Langmuir*, **17**(12), 3741–3748. 2001.

Lu J. P., "Elastic properties of carbon nanotubes and nanoropes", *Phys. Rev. Lett.*, **79**(7), 1297–1300. 1997.

Luger K., Mader A. W., Richmond R. K., Sargent D. F., and Richmond T. J., "Crystal structure of the nucleosome core particle at 2.8 A resolution", *Nature*, **389**(6648), 251–60. 1997.

Marko J. F., and Siggia E. D., "Stretching DNA", *Macromolecules*, **28**(26), 8759–8770. 1995.

Marszalek P. E., Lu H., Li H., Carrion-Vazquez M., Oberhauser A. F., Schulten K., and Fernandez J. M., "Mechanical unfolding intermediates in titin modules", *Nature*, **402**(6757), 100–3. 1999.

Marti O, Drake B, and Hansma P.K., "Atomic force microscopy of liquid covered surfaces: atomic resolution images", *Appl. Phys. Lett.*, **51**(7), 486–486. 1987.

Martin Y., and Wickramasinghe H.K., "Magnetic imaging by force microscopy with 1000-A resolution", *Appl. Phys. Lett.*, **50**(20), 1455–1457. 1987.

Mehta A. D., Finer J. T., and Spudich J. A., "Detection of single-molecule interactions using correlated thermal diffusion", *PNAS*, **94**(15), 7927–7931. 1997.

Mehta A. D., Rief M., Spudich J. A., Smith D. A., and Simmons R. M., "Single-molecule biomechanics with optical methods", *Science*, **283**(5408), 1689–1695. 1999.

Merkel R., Nassoy P., Leung A., Ritchie K., and Evans E., "Energy landscapes of receptor-ligand bonds explored with dynamic force spectroscopy", *Nature*, **397**(6714), 50–3. 1999.

Meyer G., and Amer N. M., "Novel Optical Approach to Atomic Force Microscopy", *Appl. Phys. Lett.*, **53**(12), 1045–1047. 1988.

Neuman K. C., and Block S. M., "Optical trapping", *Rev. Sci. Instr.*, **75**(9), 2787–2809. 2004.

Nikova D. N., Pope L. H., Bennink M. L., van Leijenhorst-Groener K. A., van der Werf K., and Greve J., "Unexpected binding motifs for subnucleosomal particles revealed by atomic force microscopy", *Biophys. J.*, **87**(6), 4135–45. 2004.

Nishijima H., Kamo S., Akita S., Nakayama Y., Hohmura K. I., Yoshimura S. H., and Takeyasu K., "Carbon-nanotube tips for scanning probe microscopy: Preparation by a controlled process and observation of deoxyribonucleic acid", *Appl. Phys. Lett.*, **74**(26), 4061–4063. 1999.

van Noort S. J., van der Werf K. O., Eker A. P., Wyman C., de Grooth B. G., van Hulst N. F., and Greve J., "Direct visualization of dynamic protein-DNA interactions with a dedicated atomic force microscope", *Biophys. J.*, **74**(6), 2840–9. 1998.

Odijk T., "Stiff Chains and Filaments under Tension", *Macromolecules*, **28**(20), 7016–7018. 1995.

Oesterhelt F., Oesterhelt D., Pfeiffer M., Engel A., Gaub H. E., and Muller D. J., "Unfolding pathways of individual bacteriorhodopsins", *Science*, **288**(5463), 143–146. 2000.

Ota T., Sugiura T., and Kawata S., "Rupture force measurement of biotin-streptavidin bonds using optical trapping", *Appl. Phys. Lett.*, **87**(4), –. 2005.

Peterman E. J. G., van Dijk M. A., Kapitein L. C., and Schmidt C. F., "Extending the bandwidth of optical-tweezers interferometry", *Rev. Sci. Instr.*, **74**(7), 3246–3249. 2003.

Pope L. H., Bennink M. L., and Greve J., "Optical tweezers stretching of chromatin", *J. Muscle Res. Cell. Motil.*, **23**(5-6), 397–407. 2002.

Pope L. H., Bennink M. L., van Leijenhorst-Groener K. A., Nikova D., Greve J., and Marko J. F., "Single chromatin fiber stretching reveals physically distinct populations of disassembly events", *Biophys. J.*, **88**(5), 3572–83. 2005.

Punkkinen O., Hansen P. L., Miao L., and Vattulainen I., "DNA overstretching transition: ionic strength effects", *Biophys. J.*, **89**(2), 967–78. 2005.

Putman C. A. J., Vanderwerf K. O., Degrooth B. G., Vanhulst N. F., and Greve J., "Tapping Mode Atomic-Force Microscopy in Liquid", *Appl. Phys. Lett.*, **64**(18), 2454–2456. 1994.

Reif F., *Fundamentals of statistical and thermal physics*. New York: McGraw-Hill. 1965.

Revyakin A., Ebright R. H., and Strick T. R., "Promoter unwinding and promoter clearance by RNA polymerase: detection by single-molecule DNA nanomanipulation", *Proc Natl Acad Sci U S A*, **101**(14), 4776–80. 2004.

Rief M., Gautel M., Oesterhelt F., Fernandez J. M., and Gaub H. E., "Reversible unfolding of individual titin immunoglobulin domains by AFM", *Science*, **276**(5315), 1109–1112. 1997.

Rivetti C., Guthold M., and Bustamante C., "Scanning force microscopy of DNA deposited onto mica: Equilibration versus kinetic trapping studied by statistical polymer chain analysis", *J. Molec. Biol.*, **264**(5), 919–932. 1996.

Rivetti C., Guthold M., and Bustamante C., "Wrapping of DNA around the E.coli RNA polymerase open promoter complex", *Embo. J.*, **18**(16), 4464–75. 1999.

Romano G., Sacconi L., Capitanio M., and Pavone F. S., "Force and torque measurements using magnetic micro beads for single molecule biophysics", *Opt. Comm.*, **215**(4-6), 323–331. 2003.

Roosen G., "Optical levitation of spheres", *Can. J. Phys.*, **57**, 1260–1279. 1979.

Roosen G., and Imbert C., "Optical levitation my means of 2 horizontal laser beams - theoretical and experimental study", *Physics. Lett.*, **59A**, 6–8. 1976.

Rouzina I., and Bloomfield V. A., "Force-induced melting of the DNA double helix - 1. Thermodynamic analysis", *Bioph. J.*, **80**(2), 882–893. 2001.

Shivashankar G. V., Feingold M., Krichevsky O., and Libchaber A., "RecA polymerization on double-stranded DNA by using single-molecule manipulation: the role of ATP hydrolysis", *PNAS*, **96**(14), 7916–21. 1999.

Simmons R. M., Finer J. T., Chu S., and Spudich J. A., "Quantitative measurements of force and displacement using an optical trap", *Bioph. J.*, **70**(4), 1813–1822. 1996.

Smith P. J. S., Hammar K., Porterfield D. M., Sanger R. H., and Trimarchi J. R., "Self-referencing, non-invasive, ion selective electrode for single cell detection of trans-plasma membrane calcium flux", *Micr. Res. Techn.*, **46**(6), 398–417. 1999.

Smith S. B., Cui Y. J., and Bustamante C., "Overstretching B-DNA: The elastic response of individual double-stranded and single-stranded DNA molecules", *Science*, **271**(5250), 795–799. 1996.

Stevens R., Nguyen C., Cassell A., Delzeit L., Meyyappan M., and Han J., "Improved fabrication approach for carbon nanotube probe devices", *Appl. Phys. Lett.*, **77**(21), 3453–3455. 2000.

Strick T. R., Allemand J. F., Bensimon D., Bensimon A., and Croquette V., "The elasticity of a single supercoiled DNA molecule", *Science*, **271**(5257), 1835–7. 1996.

Strick T. R., Allemand J. F., Bensimon D., and Croquette V., "Behavior of supercoiled DNA", *Bioph. J.*, **74**(4), 2016–2028. 1998.

Svoboda K., Schmidt C. F., Schnapp B. J., and Block S. M., "Direct observation of kinesin stepping by optical trapping interferometry", *Nature*, **365**(6448), 721–7. 1993.

Svoboda K., and Block S. M., "Biological Applications of Optical Forces", *Ann. Rev. Bioph. Biomol. Struct.*, **23**, 247–285. 1994.

Tomschik M., Zheng H., van Holde K., Zlatanova J., and Leuba S. H., "Fast, long-range, reversible conformational fluctuations in nucleosomes revealed by single-pair fluorescence resonance energy transfer", *PNAS*, **102**(9), 3278–83. 2005.

Wang M. D., Yin H., Landick R., Gelles J., and Block S. M., "Stretching DNA with optical tweezers", *Biophys. J.*, **72**(3), 1335–46. 1997.

Wang M. D., Schnitzer M. J., Yin H., Landick R., Gelles J., and Block S. M., "Force and velocity measured for single molecules of RNA polymerase", *Science*, **282**(5390), 902–7. 1998.

Wensink H., Jansen H. V., Berenschot J. W., and Elwenspoek M. C., "Mask materials for powder blasting", *J. Micromech. Microeng.*, **10**(2), 175–180. 2000.

van der Werf K.O., Putman C.A.J., de Grooth B.G., Segerink F.B., Schipper E.H., van Hulst N.F., and Greve J., "Compact standalone atomic force microscope", *Rev. Sci. Instr.*, **64**(10), 2892. 1993.

Wohland T., Rosin A., and Stelzer E. H. K., "Theoretical determination of the influence of the polarization on forces exerted by optical tweezers", *Optik*, **102**(4), 181–190. 1996.

Wong E. W., Sheehan P. E., and Lieber C. M., "Nanobeam mechanics: Elasticity, strength, and toughness of nanorods and nanotubes", *Science*, **277**(5334), 1971–1975. 1997.

Wuite G. J. L., Davenport R. J., Rappaport A., and Bustamante C., "An integrated laser trap/flow control video microscope for the study of single biomolecules", *Bioph. J.*, **79**(2), 1155–1167. 2000.

Yin H., Wang M. D., Svoboda K., Landick R., Block S. M., and Gelles J., "Transcription against an applied force", *Science*, **270**(5242), 1653–7. 1995.

Yodh J. G., Woodbury N., Shlyakhtenko L. S., Lyubchenko Y. L., and Lohr D., "Mapping nucleosome locations on the 208-12 by AFM provides clear evidence for cooperativity in array occupation", *Biochem.*, **41**(11), 3565–74. 2002.

Zhang N. Y., Xie J. N., Guers M., and Varadan V. K., "Chemical bonding of multiwalled carbon nanotubes to SU-8 via ultrasonic irradiation", *Smart Mater. Struct.*, **12**(2), 260–263. 2003.

Appendix

Corrections for the power spectrum method

Hydrodynamic corrections to the power spectral density

The derivation of the Lorentzian describing the power spectral density of a bead in an optical trap is based upon Stokes' law ($F_{dr} = 6\pi\eta r_{bead} v$) that assumes a constant velocity v. However, the oscillations of a trapped bead create a velocity field around it, where the present motion of the fluid depends on the past motion of the body due to solvent inertia. As a result the friction is frequency dependent. The analytical solution of the Navier-Stokes equation for the motion of a sphere in a viscous solvent is well known (Landau and Lifshiftz, 1987; Peterman *et al.*, 2003; Berg-Sorensen and Flyvbjerg, 2004) and given by

$$F_{fric} = -\gamma_0(1 + \frac{r_{bead}}{\delta})\dot{x} - (3\pi\rho r^2\delta + \frac{2}{3}\pi\rho r_{bead}^3)\ddot{x} \tag{1}$$

with δ the characteristic penetration indicating the exponential decrease of the fluids velocity field. The radius of the bead is expressed by r_{bead}, γ_0 is the friction coefficient of Stokes' law and ρ is the density of water at room temperature. The penetration depth δ can be expressed as

$$\delta(f) = \sqrt{\frac{\eta}{\pi\rho f}} \tag{2}$$

with η the viscosity (water: 10^{-3} N s/m^2) and ρ the density (water: 1.0 g/cm^3) of the solvent. For these corrections the power spectral density can be rewritten as

$$S_{hydro} = \frac{(D/\pi^2)[1 + (f/f_\delta)^{1/2}]}{(f_c - f^{3/2}/f_\delta^{1/2} - f^2/f_m)^2 + (f + f^{3/2}/f_\delta^{1/2})^2} \tag{3}$$

where f_m indicates the time it takes for friction to dissipate the kinetic energy of the sphere and the fluid it entrains. The flow pattern around the sphere is parameterized by f_δ. These two parameters are described as

$$f_\delta = \left(\frac{\delta}{r_{bead}}\right)^2 f = \frac{\rho}{\pi\eta r_{bead}^2} \qquad f_m = \frac{\gamma_0}{2\pi m^*} = \frac{\gamma_0}{3\pi m} \tag{4}$$

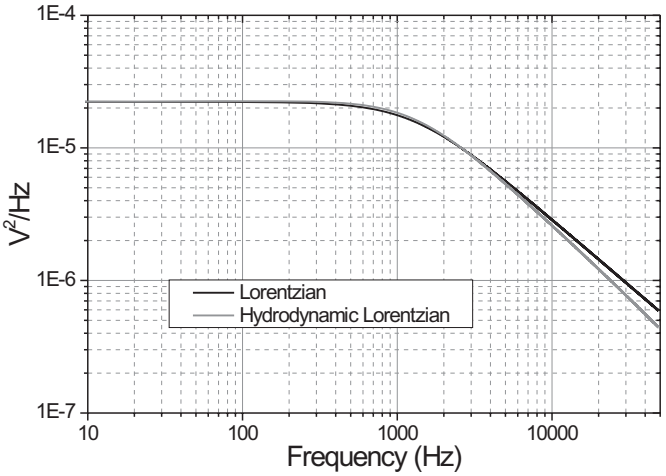

Figure 1. Theoretical curve of the Lorentzian function described by Eq. 3.11 and the hydrodynamic Lorentzian for a 2.60 μm bead and a trap stiffness of 200 pN/μm indicating the influence of the frequency dependence of the friction.

with

$$m^* = m + \frac{2\pi\rho r_{bead}}{3} = \frac{3}{2}m \tag{5}$$

The hydrodynamic version of the power spectral density S_{hydro} contains the same fitting parameters f_c and D as the Lorentzian given by Eq. 3.11, but differs from it at frequencies $\gtrsim$1 kHz. In Fig. 1 the theoretical Lorentzian for a trap stiffness of 200 pN/μm is plotted together with the hydrodynamic Lorentzian indicating the influence of the frequency dependent friction force. Due to the frequency dependent friction force the response is slightly reduced at frequencies above approximately 1 kHz in comparison with the Lorentzian based on Stokes' law.

Electronic low-pass filters and aliasing

Using a finite sampling frequency f_{sample} analog signals will suffer from aliasing. Frequencies above $f_{sample}/2$ turn up as lower frequencies in the sampled signal. To prevent aliasing a so-called anti-aliasing filter is used to limit the detection bandwidth B below $f_{sample}/2$. Dependent on the roll-off frequency f_{3dB} of this filter it effects the Lorentzian. Assuming a first-order filter the power at a certain frequency is reduced according to

$$\frac{S(f)}{S_x(f)} = \frac{1}{1 + (f/f_{3dB})^2} \tag{6}$$

which can be used to account for filtering.

Low-pass filters are not ideal and therefore one has to account for aliasing by replacing the Lorentzian S_x (or S_{hydro}) with

$$S_{alias}(f) = \sum_{n=-\infty}^{n=+\infty} S_x(f + n \cdot f_{sample}) \tag{7}$$

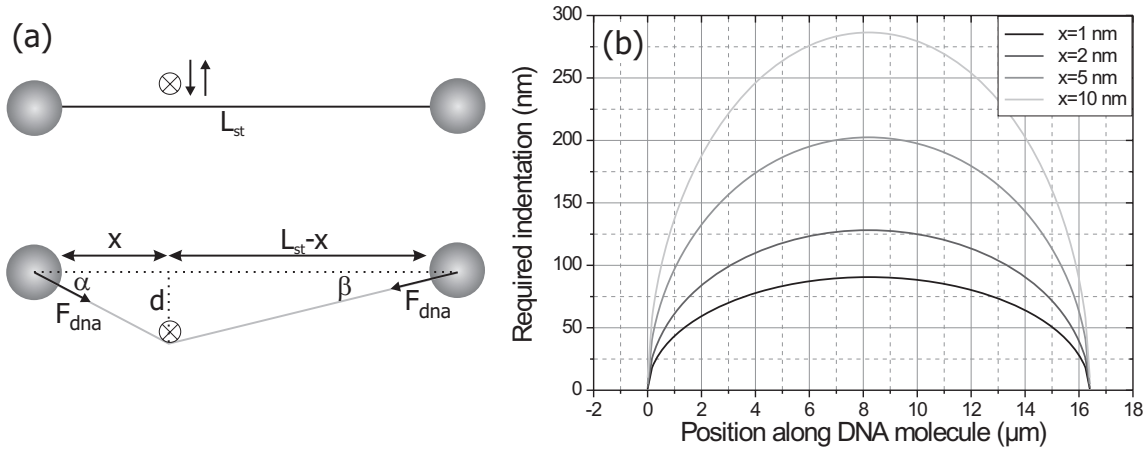

Figure 2. (a) Geometric representation of indenting DNA over a distance d at a certain position x along the DNA molecule. F_{dna} indicates the additional force initiated in the molecule due to this indentation. (b) The required indentation at different positions x along the DNA molecule to result in a displacement Δx of the trapped bead.

where in practice a summation from $-10, +10$ is sufficient (Berg-Sorensen and Flyvbjerg, 2004).

Scanning DNA

With the SPOT microscope we ultimately want to localize proteins on a stretched DNA molecule. To detect forces initiated by the probe the DNA molecule has to be stretched to a predefined force level, typically in between 10-50 pN. To estimate the minimum detectable size of a particle on the DNA molecule only considering topography we derived the influence of indenting the DNA molecule over a distance d at position x along the molecule, schematically depicted in Fig. 2(a).

Assuming a Hookean spring behavior (Eq. 2.3), the additional force F_{dna} generated by an indentation d can be expressed as

$$F_{dna} = \frac{S}{L_{st}} \left[\sqrt{d^2 + x^2} + \sqrt{(L_{st} - x)^2 + d^2} - L_{st} \right] \tag{8}$$

The part between the square brackets expresses the absolute extension of the molecule where L_{st} indicates the length of the molecule for no indentation and x the position of the probe parallel to the DNA molecule.
When the DNA molecule is indented the force within the molecule increases, resulting in a displacement of the trapped bead. To be able to detect this displacement it has to overcome the resolution x_{sd} of the OT apparatus given by Eq. 5.1. Substituting this equation in Eq. 8 using $F_{dna} = k_{tr} \cdot x_{sd}$ we can calculate the required indentation assuming a force constant of 1087 pN for dsDNA (Smith *et al.*, 1996). In Fig. 2(b) the required indentation is shown for various Δx. For a 2.67 µm bead, a bandwidth of 1 kHz and a trap stiffness of 100 pN/µm, x_{sd} is approximately 4 nm whereas for

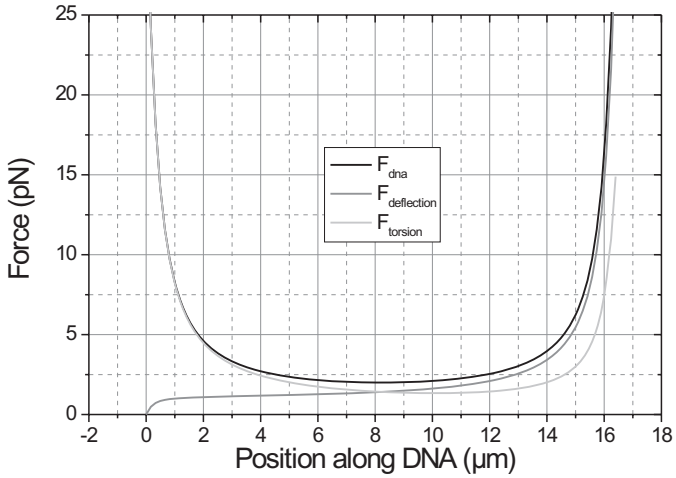

Figure 3. The additional force F_{dna} and the decomposed forces F_{defl} and F_{tors} along a stretched DNA molecule for a constant indentation of 500 nm. In this derivation the molecule is stretched to 10-50 pN where we assumed S=1087 pN and L_0=16.4 µm.

a trap stiffness of 500 pN/µm x_{sd} is 1 nm. For the latter trap stiffness, achievable in our microscope, the minimum required indentation is ∼100 nm.

When scanned with a constant indentation as is done in the described experiments, the force within the DNA molecule can be decomposed in two orthogonal forces measured as a deflection (the tension in the axial direction of the DNA molecule when it is not indented) and a torsion, according to

$$F_{deflection} = F_{dna} \cdot \cos\alpha \qquad F_{torsion} = F_{dna} \cdot \sin\alpha \tag{9}$$

where F_{dna} is given by Eq. 5.2 and α is the induced angle due to indentation as indicated in Fig. 2.

In Fig. 3 the total additional force in the DNA molecule, F_{dna}, and the decomposed forces F_{deflec} and F_{tors} are shown for a constant indentation of 500 nm along the whole molecule. In this derivation the molecule was stretched to 10-50 pN where we assumed S=1087 pN and L_0=16.4 µm. The total tension in the molecule strongly increases when the probe approaches one of the beads holding the ends of the DNA molecule. To maintain a constant tension in the molecule, the total force signal has to be used in a feedback loop to control the indentation applied with the probe. Without feedback the tension varies approximately 1-2 pN in a range from 4 to 12 µm for an indentation of 500 nm. In practice forces have to be generated in the axial direction of the DNA molecule, such that indentations in the order of ¡100 nm are sufficient, resulting in even smaller variations in tension.

Glossary of Symbols and Abbreviations

Abbreviation	Description
AFM	atomic force microscope
B	bending constant ($\mathrm{N} \cdot \mathrm{m}^2$)
bp	basepair
CCD	charge-coupled device
CNT	carbon nanotube
CVD	chemical vapor deposition
DAQ	data acquisition
DNA	deoxyribose nucleic acid
DIG	digoxigenin
ds	double-stranded
IMAQ	image acquisition
IR	infra-red
k_b	Boltzmanns constant ($1.38 \cdot 10^{-23}$ $\mathrm{m}^2\mathrm{kg/Ks}^2$)
kb	kilo basepairs
LH	ligh harvesting
L_p	persistence length (nm)
MFM	magnetic force microscope
mRNA	messenger RNA
MWNT	multi-walled carbon nanotube
NA	numerical aperture
NSOM	near-field scanning optical microscope
OT	optical tweezers
PCR	polymerase chain reaction
PLL	poly-L-lysine
PSD	position sensitive detector
QD	quadrant detector
rpm	rotations per minute
rms	root-mean-square
RNA	ribonucleic acid

Abbreviation	Description
sd	standard deviation
SEM	scanning electron microscope
SPOT	scanning probe optical tweezers
SPM	scanning probe microscopy
STM	scanning tunneling microscope
ss	single-stranded
SWNT	single-walled carbon nanotube
UV	ultra-violet
α-DIG	anti-digoxigenin

Summary

DNA contains the genetic instructions specifying the biological development of all cellular forms of life. DNA is transcribed to produce messengerRNA, which in turn is translated by ribosomes into proteins that are the "the machinery of life". These proteins perform a crucial role in many processes within the living cell. Understanding interactions between these molecules is enhanced by single molecule force spectroscopy and imaging techniques that yield new information such as the structure of these molecules, the stoichiometry in which they form complexes, the forces that hold them together and the mechanical and dynamic behavior of individual molecules and complexes thereof. With conventional techniques these properties are masked in the ensemble average.

A single molecule force spectroscopy technique that allows mechanically stretching of a single DNA molecule while simultaneously measuring the forces acting on the molecule is optical tweezers (OT). This technique is capable of holding small micron-sized spherical particles in the focus of a strongly convergent light beam, as demonstrated in the late eighties by Ashkin *et al.* (1986). A displacement of these spherical beads within the focus can be related to the force required to initiate this positional shift. The beads form a perfect handle for fixing the ends of a single DNA molecule, allowing the molecule to be stretched, from which the mechanical properties such as the Young's modulus and the persistence length of the molecule can be deduced.

Nowadays the technique is mostly applied to study DNA-protein interactions in which structural changes and mechanical properties are altered or displacements of the molecule are generated. Important information that is not obtained by OT is the positional information about the DNA-binding proteins. The main goal of the work described in this thesis is to construct a microscope in which OT and scanning probe microscopy (SPM) are combined, to be able to localize proteins while simultaneously controlling the tension within the DNA molecule. This apparatus enables the study of the effect of tension in the molecule on the functional properties of DNA-binding proteins. An advantage of the 'Scanning Probe Optical Tweezers', i.e. SPOT-microscope, is that the DNA-protein interactions are not obstructed by the presence of a supporting surface as is the case for imaging using conventional SPM techniques.

The SPOT-microscope consists of a reflection-based OT apparatus in combination

with a MWNT probe fixed to a glass μ-pipette. This probe was injected through an entry-hole into a flow cell in which a single DNA molecule was suspended between two 2.6 μm polystyrene beads, one of them immobilized on a μ-pipette integrated in the flow cell and one held by the optical trap. To allow the probe to get close to the optical trap and the DNA molecule, the backscattered trapping laser light from the trapped bead was used for force detection as opposed to the transmitted light as used in most optical tweezers instruments. In the development of the reflection-based OT apparatus we found that the use of a position sensitive detector for measuring the deflection of the backscattered laser light resulted in a linear detection range of 0.57 μm for 2.5 μm beads, a factor of 2 higher than obtained with a quadrant detector.

Furthermore the frequency response of the detector plays a crucial role in the trap stiffness calibration, which is essential in force spectroscopy. It is obtained by fitting a Lorentzian function to the power spectral density of the deflection signal. Due to the transparency of silicon for near-infrared light (>850 nm) the detection bandwidth was limited. Several detectors were characterized as a function of the wavelength, applied bias voltage and total light power, using a two-LED wobbler system. In AFM and OT applications the low-pass effect of the commonly used silicon detectors leads to serious errors in the force constant determination of the probe. We have shown that this low-pass effect can be compensated for using the frequency response of the detector as determined with the LED-wobbler.

Scanning back and forth with a pipette with an ending diameter of 2 μm and a MWNT (40-90 nm) as probe, we were able to localize single 450 nm beads coupled to the middle of the DNA molecule. The main differences found for these two probes was the magnitude of the interaction forces, 68 pN for the pipette and 40-50 pN for the MWNT that resulted in a different interaction range, 1.5 μm for the pipette and 0.5 μm for the MWNT.

We also localized DIG-sites with an α-DIG coated pipette (2 μm diameter), using the strong binding affinity of this antibody-antigen pair. This strong affinity resulted in a high interaction force of the probe with the DIG molecules ($\sim$13) that were located over a range of 90 nm approximately in the middle of the DNA molecule. Due to the convolution of this range and the size of the μ-pipette the onset of the force in different scans was spread over a range of approximately 1 μm.

We have shown that the SPOT-microscope is capable of 'feeling' individual beads and small molecules on a single DNA molecule. The next step is to really localize individual proteins, where the interaction force between the probe and the proteins will play a crucial role. Instrumental improvements such as further development of the scanning probe and the detection scheme are possible ways to achieve the full potential of the SPOT-microscope.

Samenvatting

DNA bevat de genetische instructies die de biologische ontwikkeling bepaald van alle cellulaire vormen van het leven. De sequentie van DNA wordt weggeschreven naar messengerRNA, waarna deze code door ribosomen wordt vertaald naar eiwitten, die de machines van het leven zijn. Deze eiwitten vervullen een cruciale rol in de vele processen in een levende cel. Het begrip van interacties tussen deze moleculen is verbeterd door kracht spectroscopie op enkele moleculen en het visualiseren van deze moleculen met behulp van optische technieken. Deze technieken geven ons inzicht in de structuur van de moleculen, de stoichiometrie waarin complexen worden gevormd, de krachten die ze bij elkaar houden en het mechanische en dynamische gedrag van individuele moleculen en complexen daarvan. Deze informatie gaat verloren in algemene technieken waar naar de gemiddelde eigenschappen wordt gekeken.

Een krachtmicroscoop dat in staat is om enkele DNA moleculen te strekken en simultaan de uitgeoefende krachten op dit molecuul te meten is de 'Optical Tweezers (OT)', oftewel het 'optisch pincet'. Deze techniek kan kleine ronde microdeeltjes vasthouden in het brandpunt van een sterk gefocusseerde lichtbundel, gedemonstreerd in de eind jaren tachtig door Ashkin *et al.* (1986). Een verplaatsing van zo'n bolletje in het brandpunt, kan worden gerelateerd aan de benodigde kracht. Tevens kunnen deze bolletjes gebruikt worden om beide uiteinden van een DNA molecuul vast te houden. Hierdoor kan het molecuul uitgerekt worden, zodat de mechanische eigenschappen zoals de Young's modulus en de 'persistence length' kunnen worden afgeleid.

Tegenwoordig wordt de techniek vooral toegepast om structurele veranderingen en veranderingen in mechanische eigenschappen door DNA-eiwit interacties te bepalen. Belangrijke informatie dat echter gemist wordt, is de positie van deze DNA-bindende eiwitten. Het doel van het werk dat beschreven staat in dit proefschrift is dan ook het bouwen van een combinatie-microscoop van OT met 'scanning probe microscopy (SPM)' om zodoende eiwitten te kunnen lokaliseren waarbij tegelijkertijd de kracht in het DNA molecuul wordt gecontroleerd. Met deze microscoop kan dan het effect van de kracht in het molecuul op de functionele eigenschappen van een DNA-bindend eiwit bestudeerd worden. Een voordeel van deze 'Scanning Probe Optical Tweezers' oftewel de SPOT-microscoop, is dat DNA-eiwit interacties niet worden belemmerd door de aanwezigheid van een oppervlak, wat wel het geval is in standaard SPM technieken.

De SPOT-microscoop bestaat uit een op reflectie gebaseerde OT opstelling in combinatie met een probe, in dit geval een carbon-nanotube (MWNT) gefixeerd aan een glazen micro-pipette. Deze probe wordt geïnjecteerd door een opening in een

stromings kanaal waarin het DNA molecuul is gestrekt tussen 2 polystyreen bolletjes met een diameter van 2.6 μm. Eén bolletje wordt vastgehouden door een pipette, geïntegreerd in het stromingskanaal, de ander wordt vastgehouden door het optische pincet. Om kracht detectie mogelijk te maken is het laser licht , gereflecteerd door dit bolletje, gebruikt als detectie signaal, noodzakelijk in verband met de aanwezigheid van de probe dat het doorgelaten licht blokkeerd. Tijdens de ontwikkeling van de reflectie gebaseerde OT microscoop bleek dat het gebruik van een 'position sensitive detector' resulteerde in een lineair detectie bereik van 0.57 μm voor 2.5 μm bolletjes. Bij het gebruik van een 'quadrant detector' was deze range een factor 2 kleiner.

De overdrachtsfunctie van een detector, bekeken in het frequentie-domein, speelt een cruciale rol in de bepaling van de veerconstante van het optische pincet, dat essentieel is in krachtspectroscopie. Deze veerconstante wordt bepaald door de 'power-spectral density' van het detectie signaal zo goed mogelijk te fitten met een Lorentz-functie. De transparantie van silicium voor het nabije-infrarood (>850 nm) zorgt er echter voor dat de detectie bandbreedte wordt beperkt. Met behulp van een 2 LED-systeem is de overdrachtsfunctie gekarakteriseerd voor verschillende detectoren als functie van de golflengte, het bias voltage en de totale licht intensiteit. Zowel in 'atomic force miscope (AFM)' als in OT applicaties leidt deze bandbreedte beperking tot serieuze fouten in de bepaling van de veerconstante. We hebben laten zien dat voor de bandbreedte beperking gecorrigeerd kan worden, door gebruik te maken van de overdrachtsfunctie van de detector zoals die is bepaald met het 2 LED-systeem.

Het was mogelijk om een enkel 450 nm bolletje, bevestigd in het midden van een DNA molecuul, te lokaliseren door met een pipette (2 μm in diameter) of een MWNT (40-90 nm) langs het DNA te bewegen. Het belangrijkste verschil tussen beide probes, was de grootte in de interactie kracht tussen het 450 nm bolletje en de probe. Voor de pipette was de maximale kracht 68 pN en voor de MWNT 40-50 pN, wat tevens resulteerde in verschillen in de afstand waarover deze interacties plaatsvonden, namelijk 1.5 μm voor de pipette en 0.5 μm voor de MWNT.

Tevens waren we in staat om digoxigenin (DIG) moleculen te lokaliseren met een anti-DIG gefunctionaliseerde pipette (2 μm diameter), gebruik makende van de sterke affiniteit tussen dit antibody-antigen paar. Deze affiniteit zorgde voor een hoge interactie kracht tussen de probe en de DIG moleculen (∼13), die zich over een afstand van 90 nm in het midden van het DNA bevonden. Door convolutie van deze afstand met de grootte van de μ-pipette waren de interacties tussen de probe en deze moleculen verspreid over een afstand van ongeveer 1 μm.

We hebben laten zien dat de SPOT-microscoop in staat is om enkele bolletjes en kleine moleculen te 'voelen' op een enkel DNA molecuul. De volgende stap is het realiseren van het lokaliseren van enkele eiwitten, waar de interactie krachten tussen de probe en deze eiwitten van enorm belang zal zijn. Instrumentele verbeteringen, zoals het verder ontwikkelen van de probe en het krachtsdetectie schema, zijn eventuele wegen om alle potentie uit de SPOT-microscoop te halen.

Nawoord

Tja, dit is het dan. Na een onderzoeksperiode van 4 jaar zijn dit de laatste afrondingen van mijn proefschrift. Het resultaat van 4 jaar onderzoek waar ik met een goed en tevreden gevoel op terugkijk. Tevens wordt hiermee ook een periode van een aantal maanden van veel schrijven afgerond. Een moeilijke maar ook leuke periode. Bij het doorkijken van al mijn journaals van de afgelopen jaren, kom je dingen tegen waarbij je denkt: "Dat is waar ook, dat heb ik ook ooit nog eens geprobeerd."

Doelstelling was om een hybride microscoop te bouwen, bestaande uit Optical Tweezers, oftewel een 'optisch pincet', en een micromechanische sensor/actuator dat het mogelijk zou moeten maken om een enkel DNA molecuul te strekken om vervolgens de positie van enkele eiwitten op dit molecuul te bepalen door het af te tasten. Het was een uitdagend project dat lang niet altijd vanzelf ging. Een project met vele aspecten op het experimentele vlak. Het bouwen van een opstelling, de ontwikkeling van een probe, het schrijven van software en natuurlijk het uitvoeren van de experimenten waar het uiteindelijk allemaal om gaat. En dat laatste was wel eens frustrerend. Experimenten die vele stappen vereisten voordat het daadwerkelijke experiment kon worden uitgevoerd. En dan is de kans wel erg groot dat er natuurlijk iets misgaat. Maar als het dan eindelijk toch een keer gelukt, weet je waar je het voor doet. Al met al een ontzettend leerzame periode dat ik absoluut niet had willen missen.

Via deze weg wil ik dan ook iedereen bedanken die dit project mogelijk hebben gemaakt. Maar in het bijzonder wil ik hier toch een aantal mensen uitlichten:

Allereerst Martin, bedankt voor je enthousiasme waarmee je me ondersteund hebt. De kritische noten en zeer nuttige discussies hebben me ontzettend gestimuleerd en is zeker ten goed gekomen aan de kwaliteit van dit proefschrift en de verschillende artikelen.
Vinod, ondanks dat ik je pas de laatste twee jaar van mijn onderzoek heb mee mogen maken, bedankt dat je er mede voor gezorgd hebt om verschillende publicaties de deur uit te krijgen en de interesse in mijn project.
Voor de technische ondersteuning wil ik Kees ontzettend bedanken. Het was fijn om jouw gedrevenheid en pragmatische manier van aanpak te mogen beleven.

Kirsten, misschien wel vaak het ondergeschoven paard, maar zonder jouw ondersteuning op het biochemische vlak had ik niet de resultaten bereikt zoals die er nu liggen. Bedankt!
Roel, ondanks dat je al een jaar weg bent, alsnog bedankt voor de fijne gesprekken en gezelligheid.
Alle volleyballers: Aufried, Henny, Henk-Jan, Tycho, Martijn, Sjoerd, Joris en alle anderen die door de jaren heen hebben meegespeeld en nog steeds mee spelen.
Ine, voor de goede gesprekken en het gezelschap in Long Beach. Volgens mij dacht echt iedereen dat moeder en zoon daar rond liepen. Hoezo rood haar.....!!?
Frans, bedankt voor je (technische) ondersteuning. Altijd bereid om te helpen met van alles en nog wat.
Iedereen bij mij op de kamer voor de gezelligheid: Bart, Chandrashekhar, Tomasz, Alma en Maryana.
Sylvia, voordat ik jouw vergeet... (geintje). Bedankt voor jouw aandacht en leuke, altijd even vrolijke gesprekken.

Tenslotte wil ik iedereen binnen BPE (BioPhysical Engineering) die ik niet persoonlijk bij naam heb genoemd, ontzettend bedanken voor de gezellige sfeer binnen de groep. Ik heb altijd met veel plezier gewerkt in de groep, mede dankzij jullie.

Jurgen

Publications

Papers

Huisstede J. H. G., van der Werf K. O., Bennink M. L., and Subramaniam V., "Force detection in optical tweezers using backscattered light", *Opt. Expr.*, **13**(4), 1113–1123. 2005.

Huisstede J. H. G., van Rooijen B. D., van der Werf K. O., Bennink M. L., and Subramaniam V., "Dependence of silicon position-detector bandwidth on wavelength, power, and bias", *Opt. Lett.*, **31**(5), 610–612. 2006.

Huisstede J. H. G., van der Werf K. O., Bennink M. L., and Subramaniam V., "Force constant calibration corrections for silicon position detectors in the near-infrared", submitted.

Huisstede J. H. G., van der Werf K. O., Bennink M. L., and Subramaniam V., "Combining optical tweezers and scanning probe microscopy to study DNA-protein interactions", submitted.

Huisstede J. H. G., van der Werf K. O., Bennink M. L., and Subramaniam V., "Localizing a 450nm bead on a single suspended DNA molecule using a scanning probe optical tweezers", in preparation.

Conference and meeting contributions

Huisstede, J.H.G., Bennink, M.L., Greve, J., "DNA-protein interaction studies using optical tweezers and micromechanical tools", *Annual Dutch Scanning Probe Day*, Leiden. (poster) 2002.

Huisstede, J.H.G., Bennink, M.L., Greve, J., "DNA-protein interaction studies using optical tweezers and micromechanical tools", *Annual Dutch Meeting on Molecular and Cellular Biophysics*, Lunteren. (poster) 2003.

Huisstede, J.H.G., Bennink, M.L., Greve, J., "Investigation of DNA-protein interaction using optical tweezers and micro mechanical tools", *SMST meeting*, Enschede. (oral presentation) 2004.

Huisstede, J.H.G., Werf, K.O. van der, Bennink, M.L., Subramaniam, V., "Combining scanning probe technology and Optical Tweezers to probe single proteins on a freely suspended DNA molecule", *Nanoscale 2 Conference (Veeco)*, Grenoble. (poster) 2004.

Huisstede, J.H.G., Werf, K.O. van der, Bennink, M.L., Subramaniam, V., "Combining scanning probe technology and optical tweezers to probe individual proteins on a freely suspended DNA molecule", *ALW/FOM/VvBBMT meeting on Molecular and Cellular Biophysics*, Lunteren. (poster) 2004.

Huisstede, J.H.G., Werf, K.O. van der, Bennink, M.L., Subramaniam, V., "Tickling DNA with Optical Tweezers and nanoscale tip probes", *BFT and MTP Meeting*, Enschede. (oral presentation) 2004.

Huisstede, J.H.G., Werf, K.O. van der, Bennink, M.L., Subramaniam, V., "Tickling DNA with Optical Tweezers and nanoscale tip probes", *BFT and SMCT Meeting*, Enschede. (oral presentation) 2004.

Huisstede, J.H.G., Werf, K.O. van der, Bennink, M.L., Subramaniam, V., "Combining scanning probe technology and optical tweezers to probe single proteins on a freely suspended DNA molecule", *Biophysical Society Meeting*, Long Beach, CA, USA. (poster) 2005.

Huisstede, J.H.G., Werf, K.O. van der, Bennink, M.L., Subramaniam, V., "Tickling DNA with Optical Tweezers and nanoscale tip probes", *BFT and MPI (Göttingen) Meeting*, Enschede. (oral presentation) 2005.

Huisstede, J.H.G., Werf, K.O. van der, Bennink, M.L., Subramaniam, V., "Combining optical tweezers with scanning probes", *KNAW Meeting*, Amsterdam. (oral presentation) 2005.

Huisstede, J.H.G., Werf, K.O. van der, Bennink, M.L., Subramaniam, V., "Combining optical tweezers with scanning probes", *Annual meeting MESA+ Institute for nanotechnology*, Enschede. (oral presentation) 2005.

Huisstede, J.H.G., Werf, K.O. van der, Bennink, M.L., Subramaniam, V., "Investigation of DNA-protein interactions using optical tweezers and micromechanical tools", *Annual Dutch Meeting on Molecular and Cellular Biophysics*, Lunteren. (poster) 2005.

Rooijen, B.D., Huisstede, J.H.G., Werf, K.O. van der, Bennink, M.L., Subramaniam, V., "Position sensitive detector bandwidth dependence on wavelength, power and bias", *Annual Dutch Meeting on Molecular and Cellular Biophysics*, Lunteren. (poster) 2005.

Rooijen, B.D., Huisstede, J.H.G., Werf, K.O. van der, Bennink, M.L., Subramaniam, V., "Position sensitive detector bandwidth dependence on wavelength, power and bias", *Annual Dutch Scanning Probe Day*, Eindhoven. (poster) 2005.

Huisstede, J.H.G., Werf, K.O. van der, Bennink, M.L., Subramaniam, V., "Combining optical tweezers with scanning probes", *Annual Dutch Scanning Probe Day*, Eindhoven. (oral presentation) 2005.

Huisstede, J.H.G., Werf, K.O. van der, Bennink, M.L., Subramaniam, V., "Scanning Probe Optical Tweezers: A new tool to study DNA-protein interactions", *Biophysical Society Meeting*, Salt Lake City, UT, USA. (oral presentation) 2006.